SEPTEMBER 1959 VOLUME 5 (1959) No. 3

GREGG M. SINCLAIR LIBRARY
UNIVERSITY OF HAWAII
8-7-63

NUCLEAR INSTRUMENTS & METHODS

A JOURNAL ON ACCELERATORS, INSTRUMENTATION AND TECHNIQUES IN NUCLEAR PHYSICS

EDITOR: K. SIEGBAHN - UPPSALA

CONTENTS

DAVID S. ROBERTSON and DAVID ELLIOTT, Magnetic losses in cores of various shapes 133
W. PARKER, An apparatus for the vacuum deposition of radio active materials 142
R. MEUNIER et J. TEIGER, Circuit de coïncidence rapide à trois diodes 148
JORGE ROSENBLATT, Design of alternating gradient quadrupole lenses 152
T. FAZZINI, G. FIDECARO and H. PAUL, A synchro-cyclotron pulse simulator for testing electronic circuits 156
ROBERT W. BIRGE, ROBERT E. LANOU JR., MARIAN N. WHITEHEAD and HANS COURANT, A new use of counter control in cloud chamber operation 161
J. THIRION et J. SAUDINOS, Aimants de focalisation et d'analyse du cyclotron de Saclay . . 165
J. SÉGUINOT, M. SCHÉRER et J. TEIGER, Efficacité et dispersion du temps de collection de la lumière d'un détecteur de Čérenkov à parois réflechissantes 170
SYLVAN RUBIN, Surface analysis by charged particle spectroscopy 177
P. SZABÓ, On the optimum dimensions of collimators for neutron diffraction 184
S. SUWA, J. SANADA, T. KARASAWA, A. SUZUKI, H. OGAWA, H. YAMAGUCHI, Y. SAJI, S. KIKUCHI, H. KUMAGAI, I. HAYASHI, K. MATSUDA and K. NISIMURA, Efficient beam extraction from a synchro-cyclotron at $n = 1$ 189
W. LOHMANN, Apparatus for the development of nuclear emulsion plates 194
S. BJØRNHOLM, PH. DAM, H. NORDBY and N. O. ROY POULSEN, A method for the preparation of cyclotron targets of rare-earth oxides by electrophoresis 196
A. W. PRYOR and A. G. KLEIN, (Letter to the Editor) Modification to: Statistical design basis for fast scaling systems (Nuclear Instruments 4 (1959) 1) 199
Erratum 199
Book Reviews 200

NORTH-HOLLAND PUBLISHING COMPANY - AMSTERDAM

NUCLEAR INSTRUMENTS AND METHODS

A journal on accelerators, instrumentation and techniques in nuclear physics

EDITOR: K. SIEGBAHN, UPPSALA

EDITORIAL BOARD:

J. B. ADAMS (CERN)
F. A. ALSINA (Buenos Aires)
E. AMALDI (Rome)
H. L. ANDERSON (Chicago)
K. T. BAINBRIDGE (Cambridge, Mass.)
C. J. BAKKER (CERN)
P. R. BELL (Oak Ridge)
R. E. BELL (Montreal)
A. BERTHELOT (Saclay)
H. BRINKMAN (Groningen)
E. H. COOKE-YARBOROUGH (Harwell)
S. DE BENEDETTI (Pittsburgh)
M. DE HEMPTINNE (Louvain)
A. DE-SHALIT (Rehovoth)
M. DEUTSCH (Cambridge, Mass.)
S. DU TOIT (Pretoria)
B. S. DŽELEPOV (Leningrad)
W. GENTNER (Heidelberg)
P. C. GUGELOT (Amsterdam)
H. HALBAN (Paris)
O. HAXEL (Heidelberg)
P. HUBER (Basel)
D. J. HUGHES (Brookhaven)
S. KIKUCHI (Tokyo)
J. KOCH (Copenhagen)
M. S. KOZODAEV (Moscow)
S. LIVINGSTON (Cambridge, Mass.)
E. M. MCMILLAN (Berkeley)
M. G. MEŠČERJAKOV (Moscow)
P. B. MOON (Birmingham)
M. L. OLIPHANT (Canberra)
W. PAUL (Bonn)
A. S. RAO (Bombay)
G. SALVINI (Rome)
P. SAVIĆ (Belgrade)
P. SCHERRER (Zürich)
CH. SCHMELZER (CERN)
H. W. B. SKINNER (Liverpool)
R. TANGEN (Oslo)
D. TAYLOR (Northhampton)
V. I. VEKSLER (Moscow)
O. WERNHOLM (Stockholm)
G. VON DARDEL (CERN)
R. R. WILSON (Cornell)
S. D. WINTER (Saclay)

INSTRUCTIONS FOR CONTRIBUTORS

Contributions may be sent to the Editor, Professor K. Siegbahn, Institute of Physics, University of Uppsala, Sweden, either directly or through the intermediation of one of the members of the Editorial Board. Contributions may be written in English, French or German but should always, except for very short papers, be supplied with a brief abstract in English. Figures should be in inked original drawings or glossy prints and they should be sufficiently large. Contributors should make sure that important details in drawings and photographs will show up clearly in the diminished copy used by the publisher.

Books for review should be sent to Professor Siegbahn.

Objective and descriptive material on endeavours and product developments from the industry for the section "Spotlight on Industry" should be sent directly to the publishers, North-Holland Publishing Company, P.O. Box 103, Amsterdam.

Nuclear Instruments and Methods is published monthly. The subscription price of a volume of 360 pages is $ 17.00 (130 s), postage free.

Subscriptions should be sent to the publishers, North-Holland Publishing Company, P.O.Box 103, Amsterdam or to any subscription-agent.

No part of this issue may be reproduced in any form, by print, photoprint, microfilm or any other means without written permission from the publisher. Reprints, photoprints or microfilms are obtainable at cost from the publisher.

PHILIPS

equipment for Nuclear Physics and Atomic Energy

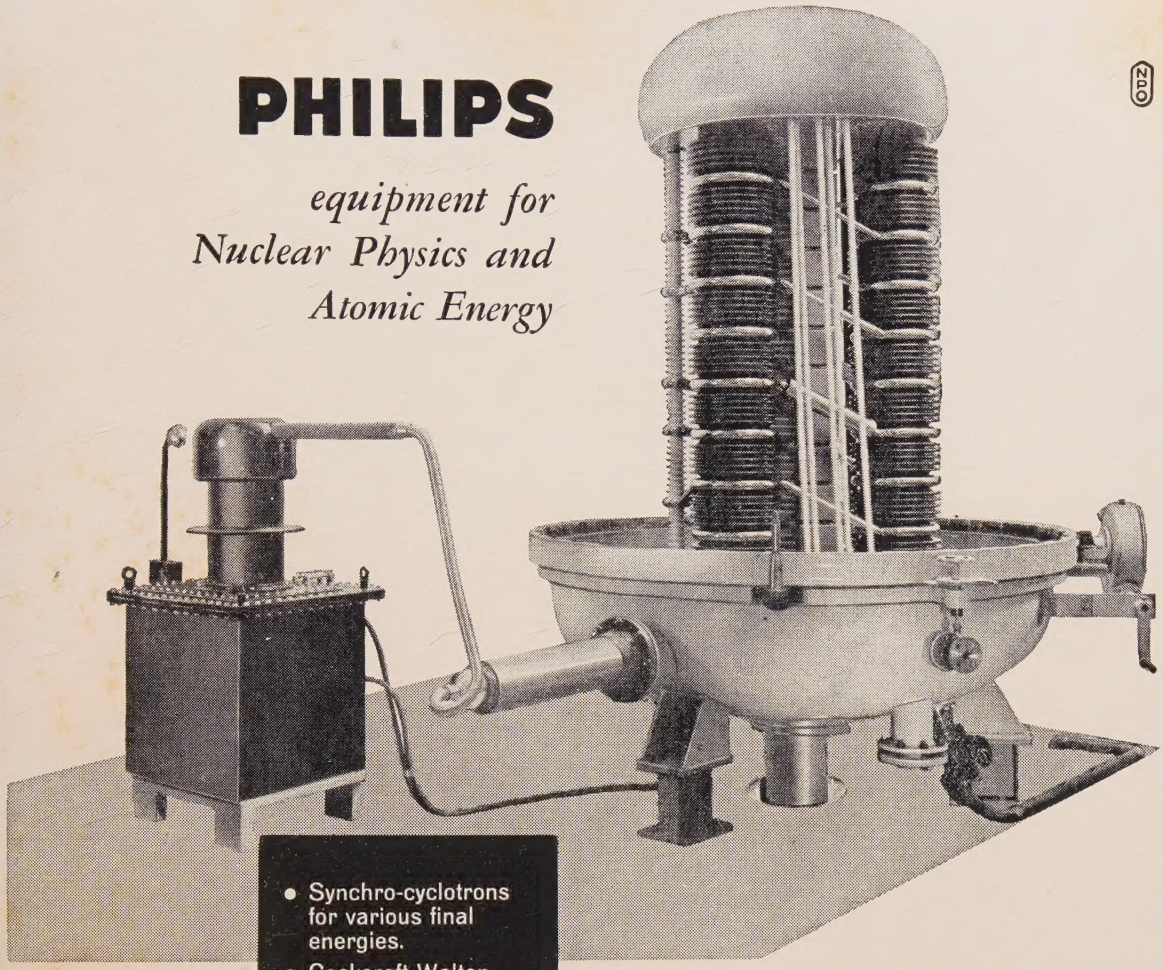

- Synchro-cyclotrons for various final energies.
- Cockcroft-Walton accelerators.
- Generators for very high d.c. voltages.
- Linear electron accelerators.
- Reactor control instrumentation.
- Radiation measuring and detection equipment.
- Civil defence instruments.
- Area monitoring instrumentation.
- Geiger counter tubes.
- Photomultipliers.
- Radio-active isotopes.
- Air & gas liquefiers.
- Vacuum measuring equipment.

This electron-accelerator of the pressurized Cockcroft-Walton type will be used for electron irradiation of solids. The continuous output of the machine is 3 mA at 1400 KeV. This output can be used either for direct electron irradiation whereby the beam is scanned over an electron window, or for the production of X-rays for which a special tungsten target has been developed.

Full information on this machine and its application in radiation chemistry, etc. will gladly be supplied.

PHILIPS

PHILIPS

Nuclear Equipment

For further information please apply to one of the following addresses:

N.V. PHILIPS' GLOEILAMPENFABRIEKEN, Scientific Equipment Department, Eindhoven-Holland
RESEARCH & CONTROL INSTRUMENTS LTD., Instrument House, 207/215, King's Cross Road, London WC1
PHILIPS ELECTRONICS INC., Instruments Division, 750, South Fulton Avenue, Mount Vernon N.Y. U.S.A.

Elcor inc.
1225 W. BROAD ST.,
FALLS CHURCH, VA.

MODEL A 309
CURRENT INDICATOR AND INTEGRATOR

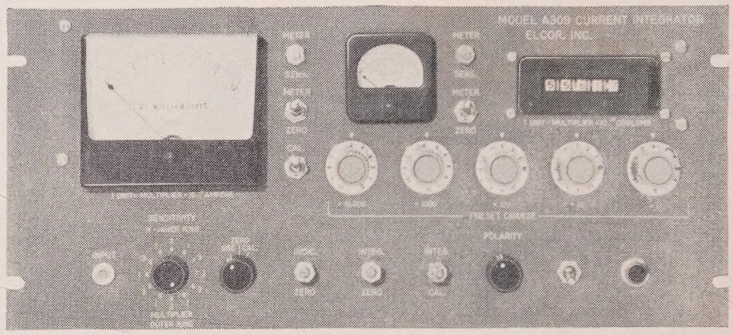

MODEL A 309 A

FEATURES

- Wide current range: 1 x 10^{-3} to 3 x 10^{-9} amp. in 12 switch settings.
- High accuracy: 1% of full scale.
- Internal calibrating current source to check proper operation.
- Front panel switch allows instrument to be used with current of either polarity.
- Pre-setting feature provides means of safeguarding against overexposure.
- Developed especially for use with Van de Graaff and other high-voltage accelerators.
- Permits many experiments with particle accelerators that would otherwise be difficult or impossible.
- Register readout gives digital accuracy on charge measurement.

The versatility and accuracy of two instruments in one!

1. Measures currents from 1 milliampere to 3 milli-microamperes.
2. Integrates input current and registers accumulated charge.

GENERAL DESCRIPTION—The Model A309 Current Indicator and Integrator is a sensitive current indicator that also measures the total charge collected in a given length of time. Developed especially for use with high-voltage particle accelerators such as the Van de Graaff generator, the instrument is also ideally suited for other applications requiring the measurement of accumulated charge or the integration of a variable current.

The full-scale sensitivity of the instrument can be varied from 1 milliampere to 3 milli-microamperes in twelve ranges. For convenience in checking the performance and accuracy of the instrument, an internal calibrating current source is provided for each range. The accumulated charge is indicated on a 5-decimal digit register. Any number up to 99,999 can be preset into the instrument, and upon reaching the corresponding charge a relay closes to actuate a warning device or control auxiliary equipment. In applications where X-rays are being generated, this feature affords protection against accidental over-exposure.

Input current of either polarity can be measured and integrated, and a front panel switch enables the instrument to be immediately changed from one polarity to the other. Advanced circuit techniques have been employed to achieve low input impedance, negligible drift, and a high overall accuracy and reliability.

Two models are available with the same specifications except for the method of presetting. In the Model A309A the presetting means consists of five front-panel switches. Presetting in the Model A309B is accomplished by manual adjustment of five presetting wheels that are accessible through the hinged cover of the register used in this model.

SPECIFICATIONS

1. Input current for full-scale meter deflection — 1 x 10^{-3} to 3 x 10^{-9} ampere in twelve switch settings.
2. Polarity of input current — positive or negative, controlled by front-panel switch.
3. Current indicating means — 4½" meter.
4. Charge indicating means — 5-decimal-digit register and 2½" meter
5. Maximum charge indicating capacity — 99,999 units.
   Note: Each unit is equal to one coulomb multiplied by the numerical value of the full-scale current.
6. Maximum integrating time — 28 hours.
7. Integrating rate for full-scale current — 1 unit per second.
8. Method of presetting:
   Model A309A — five front-panel switches.
   Model A309B — five presetting wheels in register.
9. Accuracy (Indicating and integrating accuracy, based on full-scale current) — 1%.
10. Maximum drift — .01% per hour.
11. Maximum input voltage for full-scale current — 2 millivolts.
12. Minimum signal-source impedance for 1% accuracy — 1 ohm divided by numerical value of full-scale current.
13. Calibration — Internal reference current provided for each current range.
14. Power Input — 110–125 volts, 50-60 cps.
15. Dimensions — 19" wide x 8¾" high x 13¼" deep.
16. Mounting — standard 19" relay rack.
17. Weight — approximately 25 lbs.
18. Price: Model A309A — $1674.00.
    Model A309B — $1524.00.

ELCOR,—INC. • 1225 W. BROAD STREET • FALLS CHURCH, VA.
Telephone JEfferson 2-7718
A subsidiary of Fairfax Manufacturing Co., Inc.
Bulletin No. 24-1258

256 THE TMC 256-CHANNEL PULSE ANALYSIS SYSTEM

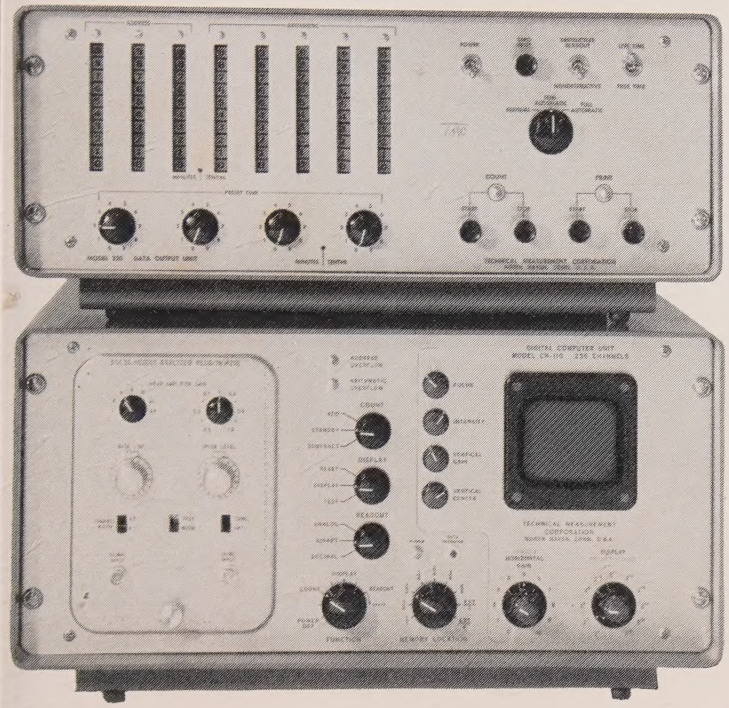

#220 DATA HANDLING UNIT usable as an active timer, event counter and readout device ... effective or actual counting times may be selected from 0.1 to 999.9 minutes in 0.1 min. steps ... manual, semi- or fully automatic operation, destructive and non-destructive readout.

TIME-OF-FLIGHT MEASUREMENT #211 plug-in ... built-in delay of 0,1,2,3 times address cycle ... choice of 9 channel lengths from 0.25 to 64 μs. ... automatic channel advance

PULSE HEIGHT ANALYSIS — #210 plug-in ... built-in linear amplifier, pulse generator ... 10-74 μs. dead time ... ±0.5% linearity

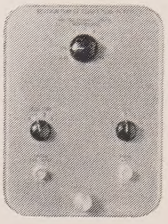

The Model CN-110 digital computer assembly ... only 8¾" high ... weighs 30 lbs. with plug-in ... operates on 25 watts

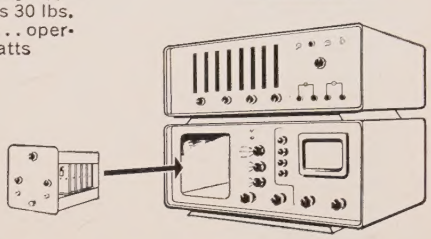

ONE BENCH-TOP INSTRUMENT...

Becomes a different pulse analyzer every time you change the logic

PULSED NEUTRON MEASUREMENT — #212 plug-in ... analysis channel lengths from 10 to 2560 μs. ... 10 μs. storage time ... (a high speed arithmetic scaler is supplied with the CN-110 at no extra charge when the 212 unit is purchased with it)

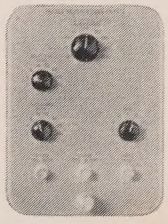

With just one CN-110 in your laboratory you have 256 channels of the pulse analysis you need — whether it's pulse height, time-of-flight, pulsed neutron or a special program. When you plug in the logic network, the instrument becomes a ready-to-use analysis system for that program. And you can change them in the time it takes to loosen a thumbscrew. Total weight is only 30 lbs., all circuits are transistorized — making this today's most versatile, compact pulse analyzer for research, field work or regular laboratory use. *They are now in production and deliveries are being made.*

THE BASIC UNIT IS A COMPLETE DIGITAL COMPUTER with all the circuitry for a 256-channel magnetic core memory and has the advantages of completely enclosed, plug-in memory ... choice of memory sub-groups ... pushbutton data transfer ... instantly selected analog, binary or digital readout.

FOR DATA HANDLING, a readout instrument has been designed specifically for use with the CN-110. The compact #220 data handling unit can be used as a live-timer during data gathering and as a readout system afterward. The #220 can be used with various types of paper tape printing and punching instruments.

Other readout devices that you can use with the CN-110 include strip chart and X-Y recorders, magnetic computer tape, punched paper cards.

Write for the new 6-page bulletin which contains complete details of the CN-110 and all accessories.

TECHNICAL MEASUREMENT CORPORATION TMC 441 WASHINGTON AVE., NORTH HAVEN, CONN.

SCINTILLATION SPECTROMETRY

NON-OVERLOADING LINEAR PULSE AMPLIFIER NE 5202:

with 5 microsecond recovery for 100 times overload. Designed for scintillation spectrometry and pulse height analysis studies, this amplifier features high gain (50.000), high gain stability (better than 0.25% per week), good linearity, low noise (less than 40 microvolts at input), excellent overload characteristics, and operation at high duty cycles. Rise time 0.2 microseconds and integral linearity 0.15%. Preamplifier NE 5202A also available. Based on the double delay line differentiated Fairstein system, it consists of three high gain feedback groups, a white cathode follower output.

SINGLE CHANNEL PULSE HEIGHT SELECTOR NE 5102:

Resolving time 1.2 microsecs; 3–140 volts operating range with energy zero drift less than 0.05 volts per day; 0 to 10 volt gate width with less than 0.01 volts per day drift; maximum counting rate, 2×10^5 c.p.s.

E.H.T. SUPPLY UNIT NE 5302:

E.H.T. SUPPLY UNIT NE 5303:

with minimum of noise and ripple; output stability 0.01%; low noise and ripple—less than 1 mV RMS; output voltage continuously variable from 500–1,800 V; output current 5mA.

As NE 5302, but with output voltage range from 1000–5000V.

SHIELDED SCINTILLATION HEAD UNITS NE 5501 & 5502:

containing white cathode follower preamplifiers with noise level of 25 microvolts; photomultipliers of 1" or 2" can be accommodated; for general use or for C14 and Tritium investigations with special rotary light locking device.

Other Units available:

Precision Ratemeter NE 5401 with eight ranges and six time constants Scanning scintillation spectrometer NE 8601.
Multi-channel scintillation spectrometer NE 8201 for industrial tracer investigations.
Scintillometers for geophysical exploration.

C^{14} and H^3 counting unit NE 8301.
Moisture and density gauge NE 8401.

Exclusive concessionaire for C.D.C./Bendix 100-channel Transistorized Kicksorter in Great Britain.

Sole agent for Harshaw Sodium Iodide Crystals in the United Kingdom.

For full detail of the above and of our SCINTILLATION PHOSPHOR PRODUCTS (plastics, liquids, loaded liquids, crystals, gels, neutron detectors, and chemicals) write to

NUCLEAR ENTERPRISES (G.B.) LTD.

SIGHTHILL, EDINBURGH, 11, SCOTLAND — TEL.: CRA 5262

Associate Company: Nuclear Interprises Ltd.
1750 Pembina Highway, Winnipeg, Canada

EKAF type 11501
Precision
High Voltage Supply

Stable operation of photomultipliers is only possible when the applied voltage is extremely constant and well regulated. Only then pulse shifting across the amplifier - often the cause of poor spectrometer readings - is eliminated.

The EKAF type 11501 High Voltage Supply, with its regulation of 0,005% for a 10% line-voltage change, is suited even where severe requirements should be met.

One of the outstanding features of this instrument is the output-setting by three calibrated controls, allowing for an output range from 500 V to 1700 V in steps of 100,10 and 1 V, with an accuracy of 1%, permitting accurate resetting of the desired output.

The maximum output of 6 mA permits the simultaneous use of more than one photomultiplier. The low internal resistance ensures a stable output-voltage under varying load conditions.

Brief specifications:

range:	**500–1700 V, d.c., in steps of 100,10 and 1 V**
polarity:	**positive or negative**
line regulation:	**0,005% for 10% change**
ripple:	**< 5 mV**
output:	**max. 6 mA**
internal resistance:	**ca 50 Ω**

EKAF

ELEKTRONISCH-KERNFYSISCHE
APPARATENFABRIEK N.V.

Sales Office: 74, Laan Copes van Cattenburch,
The Hague, Holland,
Phone 070-630977

Société d'Applications Industrielles de la Physique
S.A.I.P.
38, rue Gabriel Crié - MALAKOFF (Seine)

NUCLEAR PHYSICS

RECORDING SCINTILLATION SPECTROMETER "SPI 3"

- Resolution 8 to 10% at 0.661 MeV
- Non-saturable amplifier
- Stability: better than 1 Volt per day
- Linearity of the electronic equipment: better than 1%
- Detection starting from 5 KV
- Control oscilloscope
- 3 Scanning speeds
- Meci Speedomax recorder

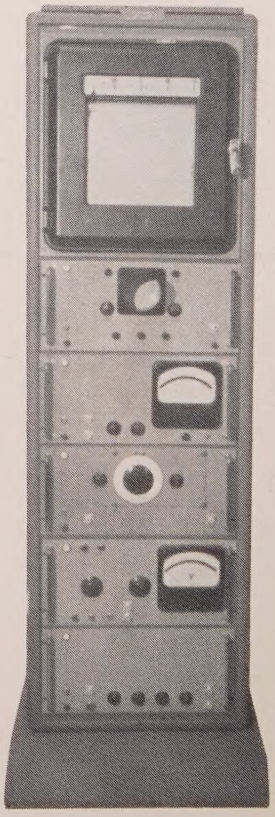

SCINTILLATION SPECTROMETER "SPE 3"

Same performance as "SPI 3"
Threshold variations are controlled by a 10-turn helipot.

OTHER PRODUCTS:

Single-channel kicksorters
Scalers
50-Channel Kicksorter "SA 50"
Proportional counters
Circulation counters
Pressurised ionisation chambers
Linear amplifiers
Vibrating condensator type D.C. amplifiers
Automatic sampling dispensers.

AGENTS:

BELGIUM: DRUA, 205 Avenue Van Volxem, BRUSSELS
DENMARK: LANGEBAEK & SON, Trondhjemsgade 9, COPENHAGEN
NETHERLANDS: ENRAF-EVERSHED, Van Leeuwenhoeksingel 69, DELFT
ITALY: AMPERE, Via Felice Casati 8, MILAN
FINLAND: ISOTEKNO, 13 A Mikontaku, HELSINKI
JAPAN: RIKEI TRADING C°, Kosato Building, 12-4 Chome Shiba Tamura-Cho Minato-Ku, TOKYO
SWITZERLAND: A. MAGAT, 28, rue de Vermont, GENEVA
U.S.A.: LEVIANT, 239 Broadway, N.Y. 7., NEW YORK

arco APPLIED RADIATION news

The first of a new generation of high power linear accelerators

High beam power at 10 Mev and beyond from ARCO L-band Linac

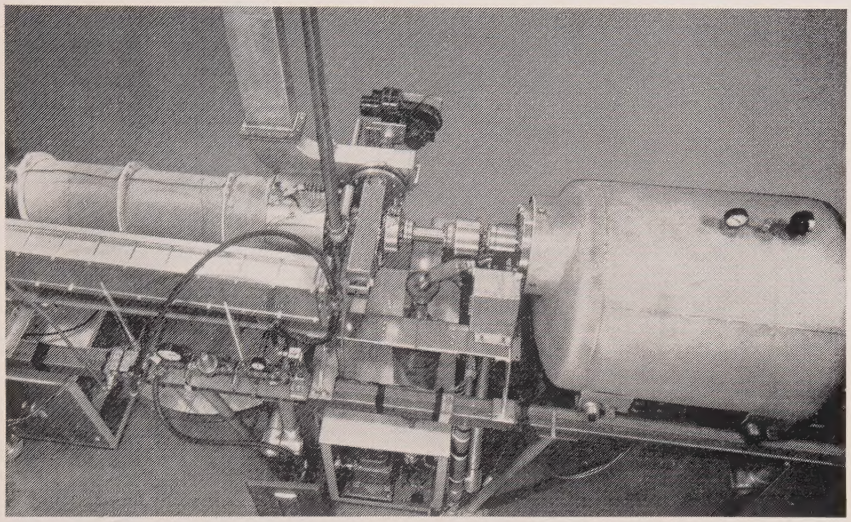

The ARCO L-band accelerator may be seen in actual operation at ARCO's Walnut Creek, California plant. Come and see it perform.

A new theoretical concept, developed by ARCO physicists, now proved beyond question.

First use of the lower L-band frequencies; higher power at lower cost.

A sweeping redesign of accelerating waveguide structures, radical with respect to conventional approaches.

Dependable Litton Industries L-band klystrons and other high-reliability production model components.

Accumulated experience of the world's largest designer-builder of electron linear accelerators.

Above are the basic ingredients which produced the new high energy, high power ARCO L-band linac—available now for unique experimentation or investigation, or practical, low cost per kw-hr radiation processing.

Data produced during exhaustive theoretical design and experimental testing on the first ARCO L-band machines are so conclusive that construction contracts in excess of $3,000,000 have been awarded for ARCO L-band accelerators.

A major advantage of the new machine is that it is not subject to the limitations (such as pulse shortening) in peak and average beam power levels that have plagued performance of earlier machines. Pulse shortening above the 4 kw level has been eliminated, despite output many times that of previous linacs. Performance of the new L-band machine shows that high power can be obtained even at energies up to 80 Mev.

Purchasers and engineers who have inspected the new ARCO machine believe it will usher in a completely new era in research and processing.

In research, the ARCO L-band machine makes possible exotic physics experiments such as neutron time-of-flight studies using flight paths up to ¼ mile in length. It greatly extends the range of experiments possible in single pulse radiation effects studies. It also permits measurement of transient effects in neutron multiplying assemblies.

In industrial processing, the higher performance and corresponding reduction in cost per kw-hr. are expected to make practical many applications which have looked promising in the laboratory but have been ruled out by high operating costs. Examples are polymerization processes, reforming of petroleum fractions, modification of polymers as in cross-linking, grafting and vulcanizing and commercial production of isotopes.

Data on the new ARCO L-band accelerator awaits your letter. Specific proposals appropriate to your application can be provided quickly and comprehensively. Your inquiry is invited.

ARCO APPLIED RADIATION CORPORATION

World's largest manufacturer of linear electron accelerators

Walnut Creek, California • YEllowstone 5-2250 • Cable "ARCO"

6051

INTERNATIONAL

advertise

YOUR NUCLEAR PRODUCTS IN

sell

YOUR NUCLEAR PRODUCTS

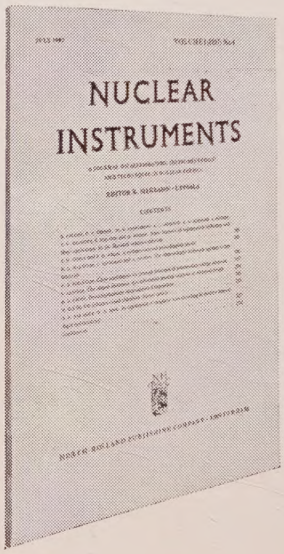

reap

YOUR NUCLEAR SALES
REWARDS

world wide

KEY NUCLEAR MANAGEMENT
NUCLEAR SCIENTISTS
NUCLEAR ENGINEERS
NUCLEAR PRODUCTION
PERSONNEL

SUBSCRIBE TO

you reach

THE WHOLE
NUCLEAR SALES WORLD IN

Entirely international in scope Nuclear Instruments and Methods is the one nuclear scientific journal that has an established subscription clientele throughout the whole world-where-ever nuclear men are at work—they want your nuclear products—they need your nuclear products—advertise in Nuclear Instruments and tell them WHAT – HOW – WHERE they can get your nuclear products

GO INTERNATIONAL WITH YOUR SALES PROGRAM TODAY WRITE

WILLIAM F. BAARS - ADVERTISING MANAGER NORTH-HOLLAND PUBLISHING COMPANY

P.O. BOX 103 – AMSTERDAM, HOLLAND

INTERNATIONAL

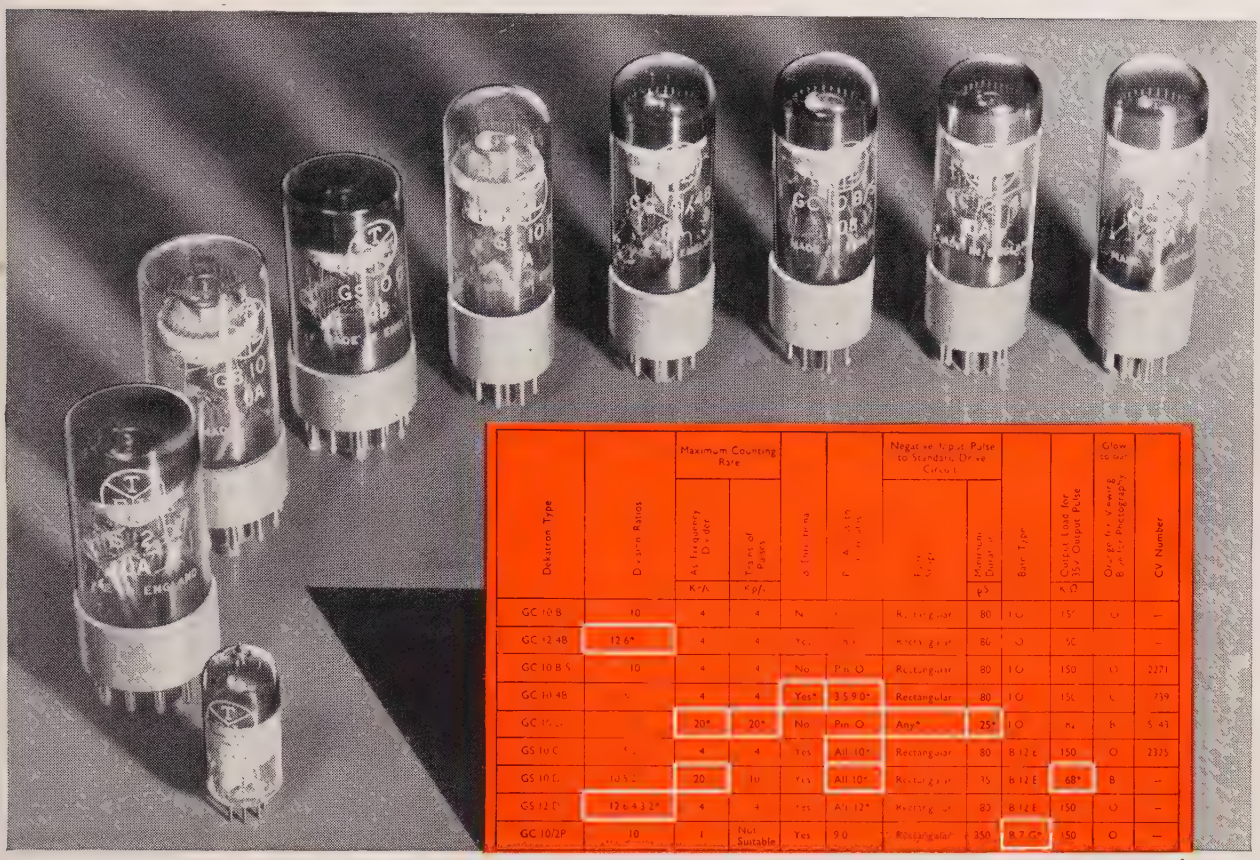

Dekatron Type	Division Ratios	Maximum Counting Rate: As Frequency Divider (K/s)	Maximum Counting Rate: Trains of Pulses (kp/s)	Guard Anode	Pin Connection	Negative Input Pulse to Standard Drive Circuit: Form	Negative Input Pulse to Standard Drive Circuit: Minimum Duration (μs)	Base Type	Output Load for 35V Output Pulse (kΩ)	Glow to base	CV Number
GC 10/8	10	4	4	No		Rectangular	80	10	15*	O	–
GC 12/4B	12.6*	4	4	Yes		Rectangular	80	O	50		–
GC 10/8S	10	4	4	No	Pin O	Rectangular	80	10	150	O	2271
GC 10/4B		4	4	Yes*	3.5 9.0*	Rectangular	80	10	150	C	739
GC 1[illegible]		20*	20*	No	Pin O	Any*	25*	10	[illegible]	B	5.43
GS 10/C		4	4	Yes	All 10*	Rectangular	80	B12E	150	O	2325
GS 10/E	1.3.5.7	20	10	Yes	All 10*	Rectangular	75	B12E	68*	B	–
GS 12/D	12.6.4.3.2*	4	4	Yes	All 12*	Rectangular	80	B12E	150	O	–
GC 10/2P	10	1	Not Suitable	Yes	9.0	Rectangular	350	B7G*	150	O	–

Table showing comparative characteristics and special features.*

DEKATRONS

The most comprehensive range of glow-transfer scaling tubes in the world

FEATURES INCLUDED IN THIS RANGE

- BI-DIRECTIONAL COUNTING
- SPEEDS UP TO 20,000 COUNTS PER SEC.
- ONLY RANGE TO INCLUDE 10 OR 12 CATHODE TUBES
- ACCESS TO ONE, FOUR OR ALL CATHODES
- NO SHAPING OF INPUT WAVEFORM NECESSARY

Described as the most significant advance in the technique of slow and medium speed counting during the last decade, Dekatron scaling tubes have logged hundreds of thousands of unfailing working hours. Leading manufacturers of counting, timing and measuring instruments prefer these reliable tubes because they allow simplified circuitry, replace a number of thermionic tubes, operate at low current, dissipate negligible heat and are moderately priced.
Available in decade and duo-decade types, the Dekatron is the original and the leading counting tube for superior performance.
Are *you* taking full advantage of the economy, long life and versatility of these cold-cathode scaling tubes?

If you would like more information please write to:—

THE TECHNICAL SERVICES DEPT.,
TUBE DIVISION
BEESTON · NOTTINGHAM · ENGLAND

ETELCO

DEKATRON IS AN ETELCO TRADE MARK

ETELCO LIMITED, HEAD OFFICE: 22 LINCOLNS INN FIELDS LONDON, W.C.2. Telephone: HOLborn 6936

E115AR/93A

ORIGINATORS AND SOLE MANUFACTURERS OF DEKATRON SCALING TUBES

NORTH-HOLLAND BOOKS

ELECTROMAGNETIC ISOTOPE SEPARATORS AND APPLICATIONS OF ELECTROMAGNETICALLY ENRICHED ISOTOPES

By J. KOCH *(Editor)*,

R. H. V. M. DAWTON, M. L. SMITH and W. WALCHER

6 x 9″ xii + 314 pp. 156 illus. 53 s.

"This is a very welcome book on a subject which had its beginnings 24 years back, which has grown to undreamt of proportions during and after the war, and of which this is the first comprehensive monograph. It is written by a team of experts with first-hand experience in electromagnetic separators... it tells in a masterly way the fascinating "success story" of a physical instrument which has grown into a giant". (D. GABOR in *British Journal of Applied Physics*)

Sole Agency for U.S.A.:

Interscience Publishers Inc. New York

NORTH-HOLLAND PUBLISHING COMPANY

AMSTERDAM

FOR SCINTILLATION & PROPORTIONAL COUNTING

Non-overloading Linear Amplifiers

MODELS 108 and 108 p

* GAIN–40,000, continuously variable
* RISE TIME–0.2 microsecond
* ACCEPTS + AND — PULSES

Tremendous Dynamic Range

EXCEEDS 1,000,000 (0.1 mV to 100 V)

Excellent linearity for small pulses in the presence of tremendous overloads that paralyze other amplifiers.
Model 108 P includes precision trigger type Pulse-Height Selector.

Model 413 Mercury relay precision sliding Pulser

The **one** pulser that fills **every need** of the Nuclear Physics Laboratory
0 to 100 Volts

10 full scale ranges from 1 mV to 100 volts
Fast rise and exponential decay of 1, 3, 10. 30, and 100 microsec simulate pulses from scintillation, proportional and Geiger counters.
Incorporates both manual control and precision motor drive.
The ideal instrument for precise calibration and test of pulse-height analyzers and other nuclear instrumentation.

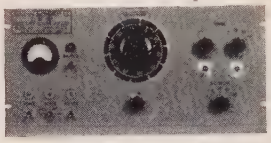

Window widths are determined AUTOMATICALLY, 10 × more ACCURATELY, 40 × FASTER than with conventional pulsers.

Model 108 Amplifier . . . . . $ 545.00
Model 108 P Amplifier (includes pulse-height selector) $ 595.00
Model 413 Precision Sliding Pulser . . . . . $ 630.00
Prices f.o.b. Silver Spring. Md.

RADIATION INSTRUMENT CO.

P.O. BOX 733 SILVERSPRING, MARYLAND, U.S.A.

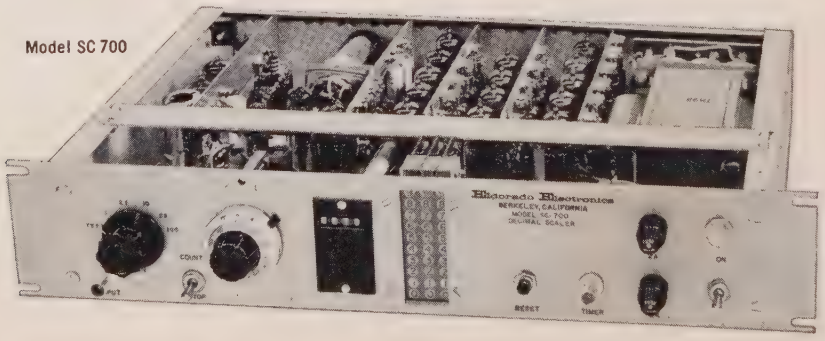

New Eldorado SC 700 Decimal Scaler with

better than 1 microsecond resolution

Designed for general radiation counting, Eldorado's compact new SC700 Decimal Scaler provides high performance at a budget price, $595.

FEATURES

- Small Size – 3½″ panel height, weighs only 16 pounds.
- 25 Millivolt Sensitivity
- Seven Decades of Count Storage
- Calibrated Input Amplifier
- Precision Integral Discriminator
- Building Block Construction
- Built-in Test Circuit
- Provision for External Timer

For complete technical information, please address Dept. 9

Eldorado Electronics

2821 TENTH ST. • BERKELEY 10, CALIF.
Phone THornwall 1-4613

RIDL presents a complete multi-channel analyzer family

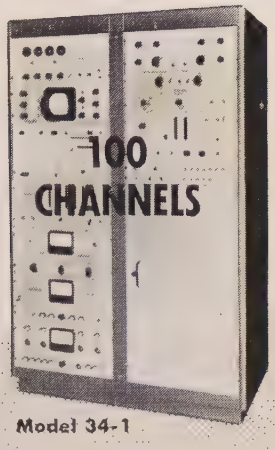

Model 34-1

RIDL is proud to present the most complete line of Multi-Channel Analyzers ever offered by any manufacturer. From 100 channels to 400 channels - from vacuum tube units to transistorized models, these are all STANDARD items. Whatever your analyzer requirement may be, we feel sure that we have a unit well suited to fulfill your requirements.

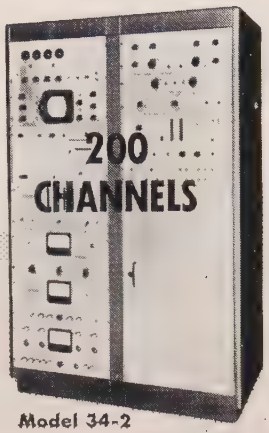

Model 34-2

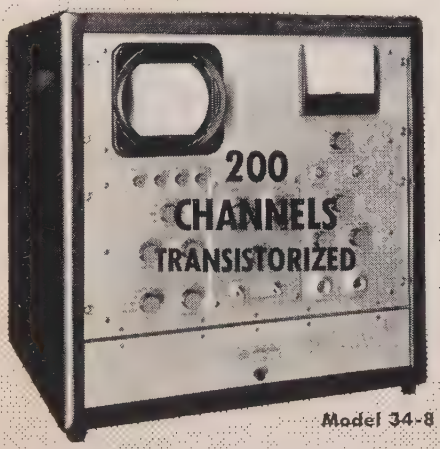

Model 34-8

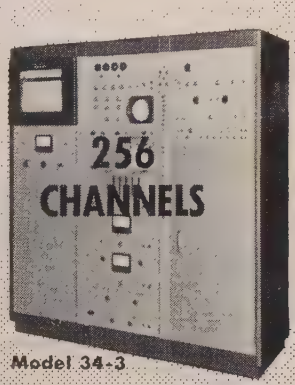

Model 34-3

Aside from the standard features present in these units, RIDL is always ready to incorporate special modifications tailored to fit a particular requirement. The following are some of the specialized features that have been incorporated into various RIDL analyzers.

- Print While Store
- Multi-Channel Scaler Operation
- 10 Megacycle Input Rate
- Stepping Subgroups
- Punched Tape Readout
- External Programming Packages
- Time Analyzers

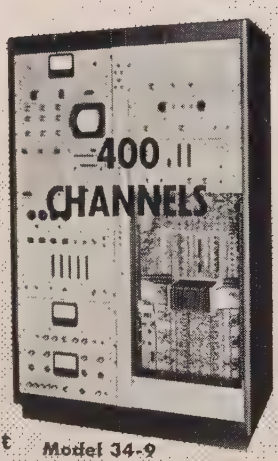

Model 34-9

In addition to the Model 34 Series Multi-Channel Analyzers, RIDL manufactures a complete line of nuclear instrumentation. REMEMBER, whatever your instrumentation problem may be, RIDL has the solution. Our staff is always available to answer your inquiries. Write today to Department 34 for complete information.

RIDL INC.

Radiation Instrument Development Laboratory, Inc.

5737 South Halsted Street, Chicago 21, Illinois USA TRiangle 3-2345

Representatives in major cities

The place of the Particle Accelerator in Basic Research...

Particle Accelerators for Nuclear Physics Teaching - IV

Laboratory demonstrations of nuclear phenomena are invaluable in illustrating the problems that will be encountered by the student in nuclear physics research. They are a vital adjunct to classroom instruction in theoretical and experimental nuclear physics. The experiments themselves should illustrate the techniques commonly used for particle detection, as well as problems that will be encountered in vacuum systems, high-voltage breakdown, and general electronic and nucleonic instrumentation.

A most fruitful method for nuclear investigation involves high-energy bombardment of the target nuclei. A number of charged-particle accelerators are available for this type of work, one of the most useful and versatile of these being the Van de Graaff. High Voltage Engineering Van de Graaff equipment can produce homogenous beams of protons and deuterons with continuously variable energy. Accelerators are available with maximum energies of 0.25, 1.0, 2.0, and 3.0 Mev. These allow many heavy-particle reactions to be demonstrated, as well as several photonuclear reactions above 1.66 Mev.

Scattering Experiments

Proton-proton scattering experiments are readily carried out with hydrogenous targets, and can be used to demonstrate isotropic scattering in the center-of-mass system characteristic of

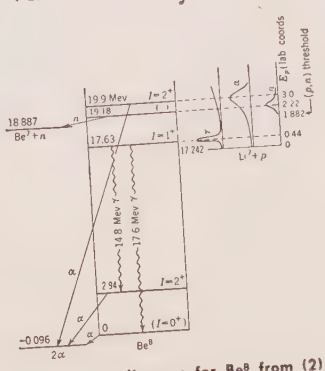

Energy-level diagram for Be^8 from (2).

s-wave interactions. The heavier nuclei in the target material will produce a different energy-angular relationship and thus demonstrate the effects of high-Z materials. Analysis of the data can illustrate the difference between the high- and low-Z materials, and show the departure from pure Rutherford scattering with low-Z targets.[1]

Nuclear Reactions

Some typical reactions can be shown using a Li^7 target. The first two excited levels of the compound nucleus in the reaction Li^7 (p,γ) Be^8 can be determined by measuring the gamma rays emitted at the 0.441 kev resonance. Measurement of the energies of the alpha rays resulting from the disintegration of the Be^8 nucleus can be used to determine the angular momentum and parity of the excited nuclear levels. The energy-level diagram shows these levels[2]; the cross-section for the various reactions is sketched at the right hand side. Inelastic proton scattering of the incident protons can also be demonstrated and shows resonances at 0.8 and 1.04 Mev[3].

Neutron Production

Neutron production is also possible with suitable particle target combinations. The D-D reaction will produce neutrons with energies of the order of 2 Mev. The D-T reaction will produce neutrons with energies of the order of 14 Mev[4]. These fast neutrons can be used to demonstrate neutron-nuclear phenomena such as moderation, inelastic scattering, and capture with resultant radioactive decay.

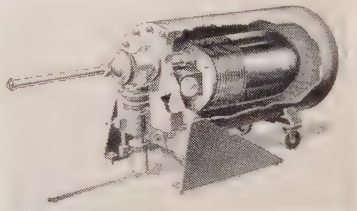

Small 0.25-Mev pulsed-neutron source for reactor research and teaching, Model PN-250 Van de Graaff.

Typical experiments such as those described can be applied to show the student how to analyze experimental data, and how to use different types of particle and electromagnetic radiation detectors. They also bring to the attention of the student some of the problems which are still unsolved in the theory of the nucleus.

The advanced nature of the Van de Graaff accelerator design, suitable for teaching at the student level, also permits original research programs to increase man's understanding of nuclear phenomena.

Write to HVEC for a set of typical experiments which can be performed with pulsed or continuous neutron sources.

References:
1. The Atomic Nucleus, R. D. Evans, p. 338, McGraw-Hill Book Company, New York, 1955.
2. F. Ajzenberg, T. Lauritsen, Revs. Mod. Phys. 27, 77, 195
3. Brown, Snyder, Fowler, T. Lauritsen, Phys. Rev. 82, 159, 1951
4. A. O. Hansen, R. F. Taschek, J. H. Williams, Revs. Mod. Phys. 21, 635, 1949

High Voltage Servicing Company, Ltd.
London, England

High Voltage Engineering Europa N.V.
Amersfoort, The Netherlands

HIGH VOLTAGE ENGINEERING CORPORATION

BURLINGTON MASSACHUSETTS

NUCLEAR INSTRUMENTS AND METHODS 5 (1959) 133–141; NORTH-HOLLAND PUBLISHING CO.

MAGNETIC LOSSES IN CORES OF VARIOUS SHAPES

DAVID S. ROBERTSON
Australian National University
and
DAVID ELLIOTT
University of Adelaide

Received 18 June 1959

The shape of magnetic cores determines the distribution of flux within them, so that it is reasonable to expect magnetic losses to be a function of core shape. In this paper, hysteresis and eddy current losses are calculated for the following cases: (1) Rectangular cores; (2) Rectangular cores with air gaps; (3) Ring cores.

The results show that a square core is only slightly inferior to an equivalent ring core. Although an air gap is shown to be of value in relieving the high concentrations of loss near the inside corners of the core, it is found to have little effect on the total loss. Similarly, the "rounding off" of inside corners is shown to be of limited value.

The results of the analysis are checked experimentally.

1. Introduction

A 10 GeV Proton Synchrotron is being built at the Australian National University. The radio frequency accelerating cavity will contain about a ton of ferrite. Nearly all the R.F. power fed to the cavity will be absorbed in the ferrite, so that it is important to know the magnitude and distribution of the losses.

When ferrite is operated at moderately high flux densities, most of the power loss is due to magnetic hysteresis. Eddy current and residual losses are negligible. This paper deals with the problem in general terms. The results apply to magnetic cores of any size and not only to the very large structures commonly used in particle accelerators. Eddy current losses are computed, but the results must be applied with caution because they are only valid under certain conditions.

Hysteresis loss may be defined in terms of magnetic field, $\boldsymbol{H}$, or of magnetic flux, $\boldsymbol{B}$. Because of the shape of the hysteresis loop, the magnetic permeability, μ, is not constant, but is a function of $\boldsymbol{H}$[1]). It is therefore convenient to think in terms of $\boldsymbol{H}$, and, for this reason, we have departed from usual practice and have defined our "flux function", ψ, in terms of $\boldsymbol{H}$ rather than $\boldsymbol{B}$.

2. Symbols

ψ	Flux function (oersteds × centimetres)
$\boldsymbol{H}$	Magnetic field strength (oersteds)
H_θ, H_r, H_x, H_y	Magnetic field components
P_e	Eddy current loss (watts)
P_h	Hysteresis loss (watts)
a, b	Dimensions of block of magnetic material (centimetres)
h	Mesh size (centimetres)
d	Gap width (centimetres)
μ	Magnetic permeability (C.G.S.)
I	Total current (amps)
L	Single turn inductance (henries)
α, γ, K_e, K_h, K	Constants.

3. The Square Core

Power is dissipated in cores through eddy currents and magnetic hysteresis. Cores made from conducting material are usually laminated for the purpose of limiting eddy current losses. The use of powdered material is also common at high frequencies. In either case, eddy currents are restricted to small circuits. The eddy currents

[1]) Victor E. Legg, Magnetic Measurements at Low Flux Densities Using the Alternating Current Bridge, Bell System Technical Journal 15 (1936) 39.

at any point within the core are then proportional to the value of the magnetic field at that point and do not depend on its value elsewhere.

Under these conditions, the total eddy current loss is proportional to $\int H^2 \mathrm{d}V$ and, assuming a Rayleigh hysteresis loop, the total hysteresis loss is proportional to $\int H^3 \mathrm{d}V$ [1]). H is the magnitude of the magnetic field $\boldsymbol{H}$ and $\mathrm{d}V$ is an element of volume. In terms of the magnetic flux function ψ we have

$$\boldsymbol{H} = \frac{\partial \psi}{\partial y}\hat{\boldsymbol{i}} - \frac{\partial \psi}{\partial x}\hat{\boldsymbol{j}}$$

where, at all points within the core,

$$\nabla^2 \psi = 0 .$$

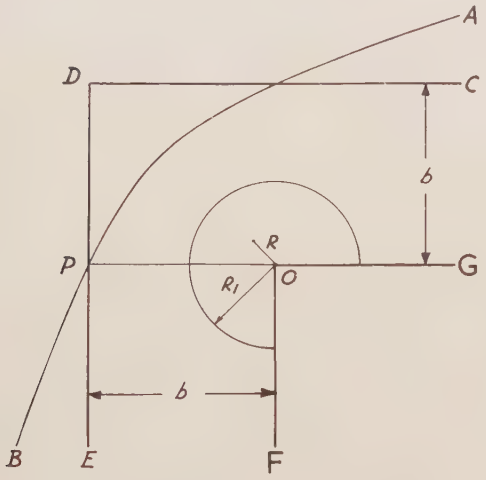

Fig. 1. Corner region of a rectangular core.

For the case for a square within a square, Bowman[2]) has calculated the capacitance by a conformal mapping technique involving elliptic integrals. It was apparent that to use this method to evaluate ψ, and the loss integrals, would be very difficult analytically. Furthermore, the analysis could not be readily extended to the case with an air gap.

The numerical approach to the case of a square core has been given by Woods[3]), and Butler and Fagg[4]). They solved the boundary value problem for ψ using relaxation methods. No estimate was made of the losses, and no account was taken of any air gap.

In this paper, we have used numerical methods to solve the general square core problem both with and without an air gap. A complete description of the numerical methods used will be given in section 4 and appendix 1. Before proceeding with this, let us consider the idealized case of the field near a square corner when all other boundaries are removed to infinity (fig. 1). By means of a Schwarz-Christoffel transformation it can be shown that the flux function ψ is given by

$$w = \phi + i\psi = \alpha\,(Re^{i\theta})^{2/3} \tag{1}$$

where α is a constant.

The lines of force are given by $\psi = \text{const.}$ and the two field components are given by

$$H_\theta = \frac{\partial \psi}{\partial R} \quad \text{and} \quad H_r = -\frac{1}{R}\frac{\partial \psi}{\partial \theta} .$$

From equation (1),

$$\begin{aligned} \psi &= \alpha R^{2/3} \sin \tfrac{2}{3}\theta \\ H_\theta &= \tfrac{2}{3}\alpha R^{-1/3} \sin \tfrac{2}{3}\theta \\ H_r &= -\tfrac{2}{3}\alpha R^{-1/3} \cos \tfrac{2}{3}\theta \end{aligned} \tag{2}$$

and

$$H = \sqrt{H_\theta^2 + H_r^2} = \tfrac{2}{3}\alpha R^{-1/3} .$$

In a region inside a sector of radius R_1 (fig. 1), the eddy current loss P_e, is given by

$$P_\mathrm{e} = K_\mathrm{e} \int_0^{R_1}\int_0^{\frac{3}{2}\pi} H^2 R \,\mathrm{d}\theta \,\mathrm{d}R = \tfrac{1}{2} K_\mathrm{e}\, \alpha^2 \pi\, R_1^{4/3} \tag{3}$$

where K_e is a constant depending on the resistivity of the material. The average eddy current loss per unit volume, $(P_\mathrm{e})_\mathrm{ave}$, is then

$$(P_\mathrm{e})_\mathrm{ave} = \frac{P_\mathrm{e}}{\frac{3}{4}\pi R_1^2} = \tfrac{8}{9} K_\mathrm{e}\, \alpha^2\, R_1^{-2/3} . \tag{4}$$

By a similar analysis it can be shown that the hysteresis loss P_h, and average hysteresis loss $(P_\mathrm{h})_\mathrm{ave}$, are given by

$$P_\mathrm{h} = K_\mathrm{h} \int_0^{R_1}\int_0^{\frac{3}{2}\pi} H^3 R \,\mathrm{d}\theta \,\mathrm{d}R = \tfrac{4}{9} K_\mathrm{h}\, \alpha^3 \pi\, R_1 \tag{5}$$

$$(P_\mathrm{h})_\mathrm{ave} = \tfrac{16}{27} K_\mathrm{h}\, \alpha^3\, R_1^{-1} . \tag{6}$$

Eqs. (3) and (5) show that the losses are finite for finite values of R_1. However, the average loss

[2]) F. Bowman, Introduction to Elliptic Functions with Applications (English Universities Press Ltd., London, 1953).

[3]) L. C. Woods, The Relaxation Treatment of Singular Points in Poisson's Equation, Quarterly Journal of Mechanics and Applied Mathematics 6 (1953) 163.

[4]) R. Butler and S. V. Fagg, Error at a Rectangular Corner in Relaxation Methods, Nature 182 (1958) 600.

per unit volume, given by eqs. (4) and (6), increases without bound as R_1 tends to zero. There is clearly a very large loss concentration at the inside corners of a square core.

The solution is exact when the outside boundary of the core coincides with a line of force such as AB in fig. 1. We can obtain an approximation to the losses for a square core by integrating the flux function ψ given by eq. (2) over a region bounded by CDE as the outer boundary. This will not be exact, since the line CDE is not a line of force. Then

$$P_h = K_h \iint_{CDEFOG} H^3 \, dx \, dy \approx 1.567 \, K_h \alpha^3 b$$

where b is the width of the core. Choosing $\psi = 0$ on boundary GOF and $\psi = 1$ on CDE, α can be evaluated by using the condition $\psi = 1$ when $R = b$ and $\theta = \frac{1}{2}\pi$. This choice of a point on the outer boundary is quite arbitrary but it does give an approximate value of α. Substituting in eq. (2) we find that

$$\alpha \approx \frac{2}{\sqrt{3}\, b^{2/3}},$$

and hence, from eq. (5)

$$P_h \approx 2.41 \frac{K_h}{b}$$

for the quarter square.

4. Square Core with Air Gap

From symmetry we need consider only one quarter of the square core, ABCD (fig. 2). Along AB and DE there are air gaps, separating ABCD from the adjacent blocks of the core, shown by broken lines. The gap size can vary from zero up to some small value.

Within the block ABCD, ψ satisfies Laplace's equation, and in Cartesian co-ordinates we have

$$\frac{\partial^2 \psi}{\partial x^2} + \frac{\partial^2 \psi}{\partial y^2} = 0 . \qquad (7)$$

Around the outer boundary of the core we have chosen $\psi = 1$, and around the inner boundary, $\psi = 0$. For the rectangle ABCD

$$\begin{aligned} &\psi = 1 \text{ along BC and CD} \\ &\psi = 0 \text{ along AE} . \end{aligned} \qquad (8)$$

It is necessary to find the boundary condition along AB and DE. This is found from the condition that the line integral of $\boldsymbol{H}$ around any

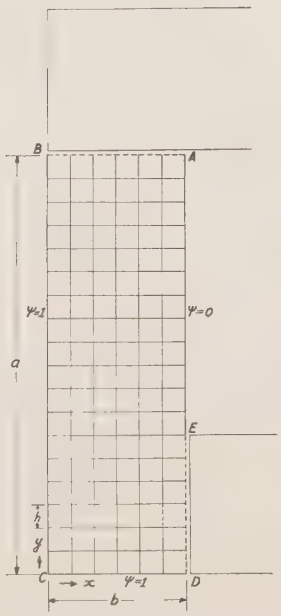

Fig. 2. One quarter of a square core with an air gap.

closed circuit, within the outer and inner boundaries of the square core, is zero. Consider fig. 3 where a square path has been taken about

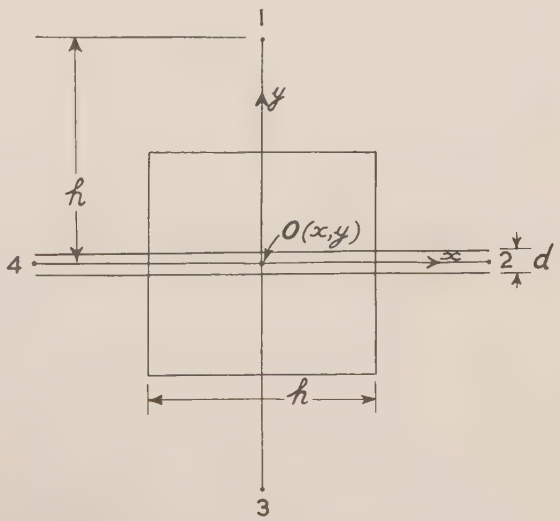

Fig. 3. The air gap region of a rectangular core.

a region including an air gap. Within the gap, the field is assumed to be uniform. The elementary square is of side h. If $(H_x)_a$ and $(H_y)_a$ are

the magnetic field components at the point O (x,y) within the air gap, then

$$H_x = \frac{\partial \psi}{\partial y} = (H_x)_a$$
$$H_y = -\frac{\partial \psi}{\partial x} = \frac{1}{\mu}(H_y)_a \qquad (9)$$

where H_x, H_y are field components at points in the core adjacent to the boundary, and μ is the permeability of the core. Summing each part of the line integral, and neglecting higher order terms, we find

$$hH_x(x,y-\tfrac{1}{2}h) - hH_x(x,y+\tfrac{1}{2}h) + hH_y(x+\tfrac{1}{2}h,y) + \mu\, dH_y(x+\tfrac{1}{2}h,y) - hH_y(x-\tfrac{1}{2}h,y) - \mu\, dH_y(x-\tfrac{1}{2}h,y) = 0\,.$$

Using the following first order approximations,

$$H_x(x,y-\tfrac{1}{2}h) \approx \frac{1}{h}(\psi_0 - \psi_3)$$
$$H_x(x,y+\tfrac{1}{2}h) \approx \frac{1}{h}(\psi_1 - \psi_0)$$
$$H_y(x-\tfrac{1}{2}h,y) \approx -\frac{1}{h}(\psi_0 - \psi_4)$$
$$H_y(x+\tfrac{1}{2}h,y) \approx -\frac{1}{h}(\psi_2 - \psi_0)$$

where ψ_0 is the value of ψ in the core in the neighbourhood of 0, we find that

$$\psi_1 + \psi_3 + \left(1 + \frac{\mu d}{h}\right)(\psi_2 + \psi_4) - \left(4 + \frac{2\mu d}{h}\right)\psi_0 \approx 0\,. \qquad (10)$$

This finite difference equation is the approximate boundary condition along AB and DE (fig. 2). In common with all finite difference equations, the approximation improves as the "mesh size" h is decreased. Eqs. (7), (8) and (10) define the boundary value problem for ψ. The losses in block ABCD (fig. 2), are given by

$$P_e \propto \iint_{ABCD} \left[\left(\frac{\partial \psi}{\partial x}\right)^2 + \left(\frac{\partial \psi}{\partial y}\right)^2\right] dx\, dy$$

and

$$P_h \propto \iint_{ABCD} \left[\left(\frac{\partial \psi}{\partial x}\right)^2 + \left(\frac{\partial \psi}{\partial y}\right)^2\right]^{3/2} dx\, dy\,.$$

The single turn current I, necessary to produce the internal field in a complete square is given by

$$\frac{4\pi I}{10} = 4 \int_{AE} (\nabla^2 \psi)_{\text{boundary}}\, ds$$

where $(\nabla^2\psi)_{\text{boundary}}$ denotes the value of $\nabla^2\psi$ on the boundary AE (fig. 2).

These equations have been solved numerically on the electronic computing machine at the University of New South Wales (an English Electric DEUCE). Full details of the method of solution are given in appendix 1. The output of the computer consisted of:

1. values of ψ at internal pivotal points
2. $\iint H^2\, dx\, dy$
3. $b \iint H^3\, dx\, dy$
4. $4\pi I/10$.

Results derived from these calculations for different values of the gap size are given in table 1, and field patterns are shown in fig. 4.

Table 1

$\mu d/b$	Mesh size (h)	$\iint H^2 dy dx$ [a]	$b\iint H^3 dy dx$ [a]	$L \times 10^9$ [b]	α
0	$b/30$	2.5614	2.6465	1.226 μ 1.228 μ [c]	1.111
0.2	$b/30$	2.5722	2.6097	1.130 μ	0.942
0.4	$b/30$	2.5811	2.6034	1.050 μ	0.921
1.0	$b/30$	2.5977	2.6055	0.8710 μ	0.900
2.0	$b/10$	2.6219	2.6322	0.6799 μ	0.890

a) For a quarter of complete square.
b) For a square, 1 cm thick.
c) Theoretical value Bowman[2]).

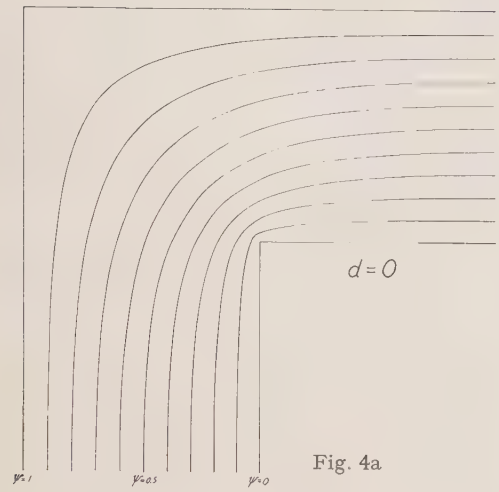

Fig. 4a

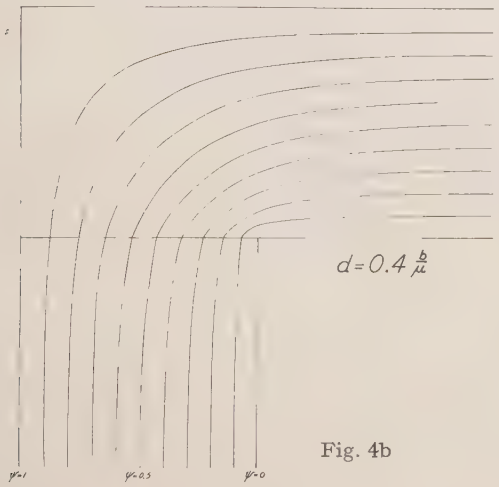

Fig. 4b

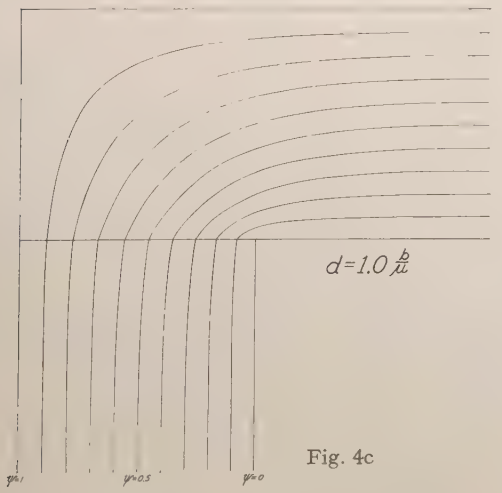

Fig. 4c

Fig. 4. Field patterns in one quarter of a square core with various air gaps.

From the field patterns it is evident that the field becomes more uniform as the gap is widened. A uniform field is desirable if one is concerned with making the loss concentration uniform over the whole core, but the conditions of uniform field and minimum total core loss are not the same. As the gap is increased, the field strength decreases at the inside of the core, but increases towards the outside, when the total flux is held constant. The increasing hysteresis loss on the outside compensates for the decreasing loss on the inside, and the result is that a minimum total hysteresis loss occurs when $d \approx 0.5\, b/\mu$.

This minimum is of no practical importance, because, as shown in table 1, the optimum gap only gives a 2% reduction in loss over the gap free case. There is no minimum for total eddy current loss which increases steadily with gap width.

5. Rounded Corners

Apart from saturation and flux leakage, the only way of removing the infinite loss at the inside corner is to "round it off". This process will not reduce the total core loss by more than a few percent, as the corner region only contributes a small amount to it.

For example, from eq. (5), the contribution of the hysteresis loss by a sector of radius $0.1\, b$ around the inside corner is given by $P_h \approx 0.215\, K_h/b$. The total hysteresis loss is $2.65\, K_h/b$ for one quarter of the square, (table 1). This sector therefore only accounts for 8.2% of the total loss, and rounding off the corner would not reduce the total loss by more than this amount.

6. The Ring Core

A ring core can be regarded as the end result of rounding off all corners, and it is instructive to compare the losses in such a ring with those in a square core.

A ring core having the same inductance as a square with no gap, and containing the same quantity of material has the following dimensions:

$$\text{inner radius} = r_1 = 1.260\,b$$

$$\text{outer radius} = r_2 = 2.326\,b$$

$$H = \frac{K}{2\pi r}, \qquad \psi = 0 \quad \text{when} \quad r = r_1,$$

$$\psi = 1 \quad \text{when} \quad r = r_2.$$

Then

$$\frac{K}{2\pi}\int_{r_1}^{r_2}\frac{1}{r}\,\mathrm{d}r = 1 \qquad \text{and} \qquad K = \frac{2}{\ln 1.847}.$$

The total hysteresis loss for the whole core is

$$K_\mathrm{h}\int_{r_1}^{r_2}\int_0^{2\pi}\frac{1}{r^3}\left(\frac{1}{\ln 1.847}\right)^3 r\,\mathrm{d}\theta\,\mathrm{d}r = 9.904\,\frac{K_\mathrm{h}}{b}.$$

Comparing this with a loss of $10.586\,K_\mathrm{h}/b$ for the square, (table 1), shows that the ring core only offers a 7% reduction in hysteresis loss. A similar calculation shows that the reduction in eddy current loss is only 0.1%.

The Q value of the core is proportional to the ratio of total loss to inductance, so that the Q values of square cores operating at high flux densities will be only slightly inferior to those of equivalent ring cores.

7. Extension to a Rectangle

In regions remote from the corners and air gap, the stream lines of fig. 4 are approximately equispaced and parallel to the boundaries. Little error is introduced by simply extending the straight sections and the stream lines together to form larger squares or rectangles. The field strength in these regions is approximately $1/b$. The eddy current loss is therefore increased by K_e/b for each centimetre added to the perimeter of the core.

Similarly, the hysteresis loss is increased by K_h/b^2 and $4\pi I/10$ is increased by $1/b$ for each centimetre added to the perimeter of the core. The reverse process of reducing the length of the straight sections is also permissible, but this will obviously produce excessive errors if carried too far.

8. Experimental Results

Values of Q and μ were measured at a frequency of 1 Mc/s, using various flux densities and air gaps, in a square ferrite core with $a = 36$ cm and $b = 10$ cm. The core was enclosed in a single turn can, and the single turn inductance so formed was resonated with a variable capacitance. The voltage across the tuned circuit compared with the voltage across a standard series

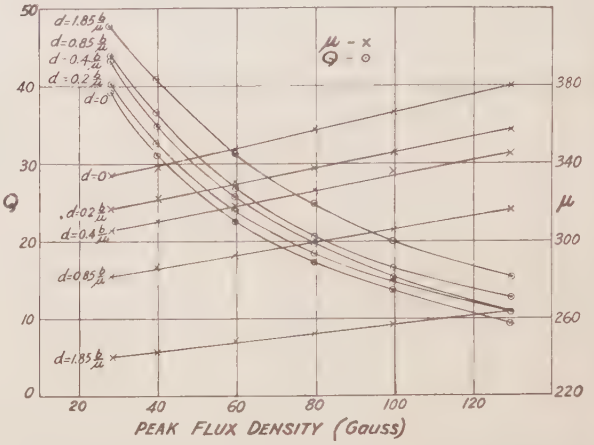

Fig. 5. Experimental curves showing μ and Q as a function of the R.F. flux density, with the air gap width as the parameter. The coil is a single turn on a square core of Steatit-Magnesia A.G. Keraperm 03186, (46 cm o.d., 26 cm i.d., 2 cm thick). The operating frequency is 1 Mc/s.

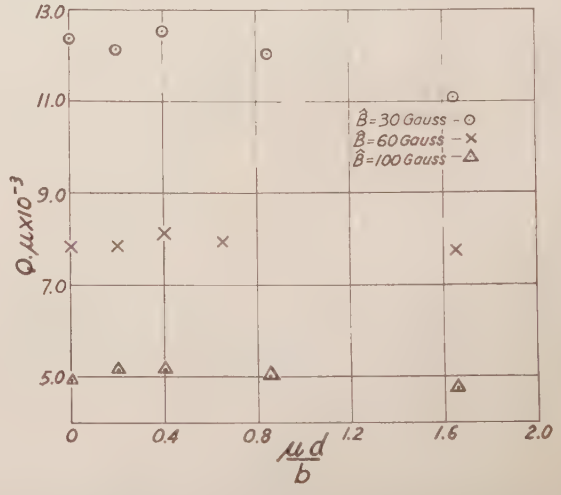

Fig. 6. Curves derived from fig. 5, showing $Q\mu$ as a function of air gap width, with the R.F. flux density as the parameter.

resistance gave the value of Q. The values of μ were given by the values of capacitance. The method was essentially that of Plotkin[5]).

Fig. 5 shows the experimental results, and fig. 6 shows the variation of the product $Q\mu$

[5]) M. Plotkin, High Level R.F. Ferrite Tests, Brookhaven National Laboratory report MP/JDK (1 August 1954).

with air gap for various average flux densities. This product is proportional to the equivalent shunt resistance of the tuned circuit ($Q\omega L$) when ω is held constant. The power loss, which is almost entirely hysteresis loss, is therefore inversely proportional to $Q\mu$. The core loss remains substantially constant as the gap is varied. The shallow maxima confirm the results of table 1, but their significance is questionable owing to the unavoidable experimental errors associated with such measurements.

9. Conclusions

Eddy current and hysteresis losses are surprisingly independent of the shape of the core and the dimensions of the air gaps. The shape of the core and the width of the air gaps determine the flux distribution, but have little effect on the total power loss. Changes of flux distribution, due to modifications of core shape or to the introduction of air gaps, result in a redistribution of power loss within the core, but the total loss tends to remain constant.

It is only in applications where local heating is a problem, or where a high value of Q is necessary, that the shape of the core and the dimensions or air gaps are of importance. The total power loss is a function of the properties of the material and the total flux carried by the core, rather than the distribution of flux within it.

Appendix 1

NUMERICAL SOLUTION

Eqs. (7), (8) and (10) have been solved by approximating them with a set of finite difference equations. These were solved by the Richardson-Liebmann process[6]).

Sub-divide the rectangle ABCD (fig. 2) by a square mesh of side h. Taking C as the origin of a Cartesian co-ordinate system, with Ox parallel to CD, and Oy parallel to CB, we can write

$$x = mh \quad \text{for} \quad 0 \leqslant m \leqslant M$$

$$y = nh \quad \text{for} \quad 0 \leqslant n \leqslant N\,,$$

where $b = Mh$ and $a = Nh$.

Writing

$$\psi(x,y) \equiv \psi_{m,n}$$

then, to a first approximation, eq. (7) gives

$$\psi_{m,n} = \tfrac{1}{4}\left[\psi_{m-1,\,n} + \psi_{m,\,n-1} + \psi_{m+1,\,n} + \psi_{m,\,n+1}\right] \tag{11}$$

$$\text{for} \quad 1 \leqslant m \leqslant M - 1$$

$$\text{and} \quad 1 \leqslant n \leqslant N - 1\,.$$

The boundary conditions, to the same order of approximation, are given by

$$\psi_{o,n} = 1 \quad \text{for} \quad 0 \leqslant n \leqslant N$$

$$\psi_{m,o} = 1 \quad \text{for} \quad 0 \leqslant m \leqslant M$$

$$\psi_{M,n} = 0 \quad \text{for} \quad M \leqslant n \leqslant N$$

$$\psi_{m,N} = \frac{1}{\left(4 + \frac{2\mu d}{h}\right)}\left[\psi_{m,N-1} + \left(1 + \frac{\mu d}{h}\right)\psi_{m+1,N} + \psi_{M-1,m} + \left(1 + \frac{\mu d}{h}\right)\psi_{m-1,N}\right] \quad \text{for} \quad 1 \leqslant m \leqslant N-1$$

and (12)

$$\psi_{M,n} = \frac{1}{\left(4 + \frac{2\mu d}{h}\right)}\left[\psi_{M-1,n} + \left(1 + \frac{\mu d}{h}\right)\psi_{M,n-1} + \psi_{n,N-1} + \left(1 + \frac{\mu d}{h}\right)\psi_{M,n+1}\right] \quad \text{for} \quad 1 \leqslant n \leqslant M-1$$

where use has been made of the symmetry of the complete configuration. In the boundary conditions at the air gap, we have chosen the h in eq. (10) to be the mesh size.

Eq. (11), with boundary conditions (12), can be solved by a simple iterative technique. Initial values, usually zero, are assigned to each interior point and the values are modified in turn using (11) and (12). Following Fraenkel[6]), a modification of this technique has been used which increases the convergence rate. If $\psi^{(i)}_{m,n}$ is the value of $\psi_{m,n}$ after i iterations, we have taken for each internal point,

$$\psi^{(i+1)}_{m,n} = \psi^{(i)}_{m,n} + \gamma\left[\tfrac{1}{4}\left(\psi^{(i+1)}_{m,n-1} + \psi^{(i)}_{m,n+1} + \psi^{(i+1)}_{m-1,n} + \psi^{(i)}_{m+1,n}\right) - \psi^{(i)}_{m,n}\right]$$

where

$$\gamma = 2 - \sqrt{2}\pi\left(\frac{1}{M^2} + \frac{1}{N^2}\right)^{\frac{1}{2}}\,.$$

[6]) S. P. Fraenkel, Convergence Rates of Iterative Treatments of Partial Differential Equations, Mathematical Tables and Other Aids to Computation 4, No. 30 (April 1950).

A similar modification has been made for points along the boundaries AB and DE.

In this problem, we have taken $N = 3M$, i.e. $a = 3b$. Most of the values given in table 1 and fig. 4 correspond to $M = 30$. The gap makes no difference to the scheme of computation, and the value of $\mu d/b$ has been taken to vary from 0 (no gap) up to 2.0.

With

$$H^2 = \left(\frac{\partial \psi}{\partial x}\right)^2 + \left(\frac{\partial \psi}{\partial y}\right)^2$$

the double integrals

$$\iint_{ABCD} H^2 \, dx \, dy \qquad \text{and} \qquad b \iint_{ABCD} H^3 \, dx \, dy$$

were computed by writing

$$\left(\frac{\partial \psi}{\partial x}\right)_{m,n} = \frac{\psi_{m+1,n} - \psi_{m-1,n}}{2h},$$

$$\left(\frac{\partial \psi}{\partial y}\right)_{m,n} = \frac{\psi_{m,n+1} - \psi_{m,n-1}}{2h}$$

evaluating H^2 and H^3 from these, and integrating by Simpson's rule first in the x-direction and then in the y-direction.

There is a singularity in ψ at the point A where its derivatives become infinite. It has been shown in section 3 that the double integrals remain bounded in spite of this singularity. In the numerical analysis, we have attempted to overcome the singularity by using a fine mesh. The values of ψ have been found to agree well with the form indicated by eq. (2).

An estimate of the error in the double integrals is given in appendix 2. It is found to be within 0.5% for both the eddy current and hysteresis losses.

Appendix 2

The flux function is of the form

$$\psi = \eta\,(r,\theta) + \alpha\,(r)^{2/3} \sin \tfrac{2}{3}\theta \qquad (13)$$

where η is well behaved everywhere and zero on the inside boundary. α is a constant whose value can be calculated from the values of ψ in the neighbourhood of the corner (eq. (2)).

The second term in eq. (13) is responsible for the singularity in ψ at the corner, and its magnitude is proportional to α. As the width of the air gap increases, α decreases, so that consideration of the gap free case alone can be expected to give an upper bound to the errors produced by neglecting the singularity. Values of α for various air gaps are given in table 1.

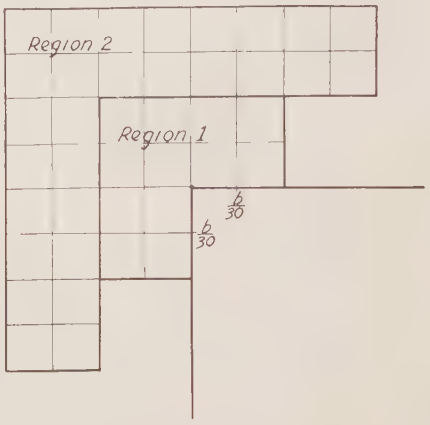

Fig. 7. Inside corner of rectangular core.

To estimate the effect of the singularity, the values of ψ near the corner were corrected by Wood's method[3]). Using a mesh of side $b/30$, the necessary corrections to ψ were found to be + 7% for the mesh points adjacent to the inside corner, falling to + 1% at a distance of 0.1 b from it.

The hysteresis loss was calculated in the two regions of fig. 7, using the corrected and original ψ values, and the results are given in table 2.

Table 2

	Region 1	Region 2
Original ψ values	0.1514 K_h/b	0.1140 K_h/b
Corrected ψ values	0.1430 K_h/b	0.1108 K_h/b

In region 1, the loss with corrected ψ values was found by using eq. (13) with $\eta = 0$ and $\alpha = 1.111/b^{2/3}$. The equation then fits the corrected ψ values to within 1%, so that it is better to use it than to attempt numerical differentiation and integration so close to the singularity.

The error in region 1 is + 0.0084 K_h/b and in region 2 it is + 0.0032 K_h/b. There should be little contribution to the total error from the

rest of the core, since the corrections to the ψ values are less than 0.5% on the boundary of region 2 and fall rapidly beyond it.

The sum of the errors in regions 1 and 2 is $0.0116\, K_h/b$, and the total hysteresis loss is $2.647\, K_h/b$. This suggests that, with a mesh of side $h = b/30$, neglect of the singularity causes an error of about + 0.5% in the computed value of the hysteresis loss.

The error in the eddy current loss has not been estimated, but it will be considerably smaller, since in this case the loss depends on H^2 and not H^3.

Acknowledgements

We wish to thank Professor K. J. Le Couteur for his generous assistance, and Professor L. C. Woods for helpful discussions. We are also grateful to J. W. Blamey and R. G. Smart for their help and to Steatit-Magnesia. A. G. for supplying exceptionally large blocks of ferrite.

NUCLEAR INSTRUMENTS AND METHODS 5 (1959) 142–147; NORTH-HOLLAND PUBLISHING CO.

AN APPARATUS FOR THE VACUUM DEPOSITION OF RADIO ACTIVE MATERIALS

W. PARKER

Institute of Physics, University of Uppsala

Received 5 August 1959

An apparatus is described for the preparation of radio-active sources by means of vacuum deposition for use in nuclear spectroscopy. The collimated crucibles described allow for smaller amounts of active material to be used in the preparation because of the higher yield obtained. Also the risk of contamination to the vacuum system is greatly reduced. Special attention is paid to the preparation of sources of the point of the strip variety. Total yields obtained from the evaporations, and curves showing the distribution of active deposits, together with a list of sources so far prepared in this manner are given.

1. Introduction

It is often necessary that the radio-active sources for use in nuclear spectroscopy have the following requirements.

1. That the active area is thin and uniformly distributed.

2. That the backing material supporting the source is also thin and of low atomic number.

3. Where the backing material is organic, a conducting metal substrate must be employed to prevent charging of the source.

For the purpose of comparison the three most commonly used methods[1]) of source preparation will be described. The first and simplest is known as the drop method, whereby the activity in solution is dropped onto the receiving backing and the solution allowed to evaporate. With this technique most backing materials can be used and only as much activity as is required for the final experiment is necessary. Unfortunately, sources so produced are rather poor with respect to homogenity. The second method, electroplation, has many applications and thin homogeneous deposits can be obtained. Here the backing material forms one electrode in the active solution and a material inert to the solution forms the second electrode. Although the deposits obtained conform with the requirements, the choice of backing materials is a limited one. Metals and rather thick organic films together with a metal substrate, may be used, but considerable care in the suspension of such materials must be exercised. Another difficulty encountered is the adhesion of activity to the wall of the container and also in the case of organic material, of the metal substrate coming away from the backing. Finally, where thermal evaporation in vacuum is employed, thin backings of any material may be used, and thin, homogenious deposits produced. The most common arrangement is for the backing to be masked to suitable dimensions, and the activity placed in some type of receptable for heating. In other work with arrangements of this type, large amounts of activity are necessary, even if the source required is a weak one. Another serious hazard, is that of contamination of the apparatus which in turn may lead to contamination of other different preparations. Methods of preventing such contamination have been described[2,3]) which although effective do not reduce the handling of strong activities. Where the preparation of radio-active sources are frequent, this last point is worth considerable consideration. Frauenfelder[4]) described an appa-

[1]) H. Slätis, Source and window technique, Beta and Gamma Ray Spectroscopy, Ed. K. Siegbahn (North Holland Publishing Company, Amsterdam, 1955).

[2]) M. C. Inman and D. Quigley, J. Sci. Inst. 35 (1958) 226.

[3]) L. W. Barr and D. A. Blackburn, J. Sci. Inst. 36 (1959) 197.

[4]) H. Frauenfelder, Helv. Phys. Acta 23 (1950) 347.

ratus used for the investigation of surface processes on solids by means of radio-activity. The evaporation crucibles in this apparatus were made in such a way as to afford collimation of the vapour stream. However, because the crucibles are directly heated and the top and bottom have considerably larger dimensions than the centre, this latter portion of the crucible reaches the evaporation temperature first. This may result in the vapourised material condensing at the top of the crucible only to vapourise a second time as a normal 2π evaporation. The use of mica as a backing material in this apparatus, allowed the backing to be placed near the crucible without danger of burning. A crucible with good collimating properties will allow for much smaller amounts of active material to be used, but in order to take advantage of such properties, the backing must be placed extremely close to the crucible. If organic backings are to be used, water cooling must be introduced to protect them from burning. Also, collimated crucibles must be heated at the top so as to prevent the process of evaporation condensation taking place. More recently, a device has been described[5]) suitable for the preparation of sources as described here, for use in an intermediate lens spectrometer[6]) and double focussing spectrometer[7]). In this device, the two crucibles are made of platinum sheet and hard soldered. The point source crucible, resembling an inverted cone with a shallow dish bottom from which two arms extend for electrical connection. The active material is loaded through the vapour exit situated at the cones apex. Since the crucible is loaded already in position, the undesirable necessity of handling radioactive material in the apparatus itself arises. The alternative choice of removing the crucible after each evaporation for loading leads to mechanical failure, as with most directly heated crucibles. The crucible for making strip sources is provided with a slit 0.6 mm wide and 12 mm long which makes loading difficult. The backings employed with this device (mostly Al) are placed extremely close to the crucible which has a tendency to change its position when heated. In spite of these drawbacks and the limited temperature range (1500° C), it is possible to obtain yields of 90% with good distribution of active material. Other work has been described dealing with source preparation in connection with thesis work[8,9]) and other major programs[10]). In conclusion it should be pointed out that vacuum deposition has many advantages not found in other methods, one example, is that of selective evaporation whereby unwanted impurities may be vapourised prior to the final deposition[11]). Also, when the activity has been mass separated onto a metal backing, it is possible, by placing the backing in a crucible, to evaporate the activity onto a more suitable backing material, while leaving the original in the crucible. However, if source preparations are frequent, it is necessary that the handling of active materials be kept to a minimum, and in the case of vacuum deposition, such handling be carried out under safe conditions away from the apparatus. In the design of the present apparatus, every effort has been made to restrict the use of high activities as far as possible, while increasing the efficiency of source preparation.

2. Description of Apparatus

2.1. VACUUM CHAMBER

The base plate A, shown in fig. 1, measures 300 mm in diameter and supports the chamber wall B which is 150 mm high. Three pairs of water cooled pillars, placed symmetrically 30° apart at C, are supplied with 200 amps at 20 volts from a variac controlled transformer.

The six glass metal seals D are provided for temperature measurement by means of thermo-

[5]) R. Stockendal and K. E. Bergkvist, Nuclear Instruments **1** (1957) 53.

[6]) H. Slätis and K. Siegbahn, Arkiv f. Fysik **1** (1949) 339.

[7]) A. Hedgran, N. Svartholm and K. Siegbahn, Proc. Phys. Soc. A **63** (1950) 960.

[8]) J. H. Hamilton, Thesis, University of Indiana, U.S.A. (1958).

[9]) B. I. Deutch, Thesis. University of Pennsylvania, U.S.A. (1959).

[10]) Miscellaneous Phys. and Chem. Techn. of the Los Alamos Project (Mc Graw-Hill, 1952) 22.

[11]) J. H. Hamilton, As above.

couples. An "○" ring E, directly above the pumping port F, is for additional apparatus such as that used for sputtering. Two ports G and a rotating vacuum seal H are fitted in the out of contact. The height of the crucible is 25 mm. While suitable for application, where the material is in solid form, these crucibles are both fragile and difficult to load. Only the minor

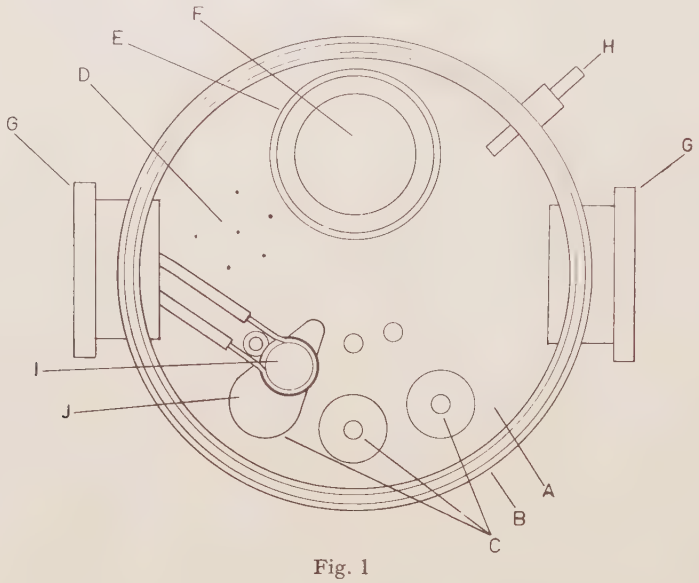

Fig. 1

chamber wall. As can be seen one of the ports is used for the introduction of water cooling to the backing support I and radiation shield J. The tubes used for this purpose are plastic and stand the pressure without difficulty. A lucite plate 20 mm thick covers the chamber top and a second plate (not shown) provides for the attachment of liquid air trap for use when highly volatile materials are to be evaporated.

2.2. CRUCIBLE CONSTRUCTION

The following requirements were thought to be necessary in the design of suitable crucibles to hold the activity: ease and speed in the loading of active material, sufficient collimator length to ensure efficient collimation and finally, strong construction. A crucible, which for some time had been in use in this institute†, can be seen in fig. 2b. These crucibles made from graphite rod 7 mm in diameter, have a 2 mm diameter collimator which extends to within 1 mm of the crucible bottom. D supports the crucible in the oven and E keeps the main body modifications shown in fig. 2a, were necessary to improve the efficiency. The collimator A has been reduced to 1 mm, and the body B shortened by 6 mm to make provision for a removable

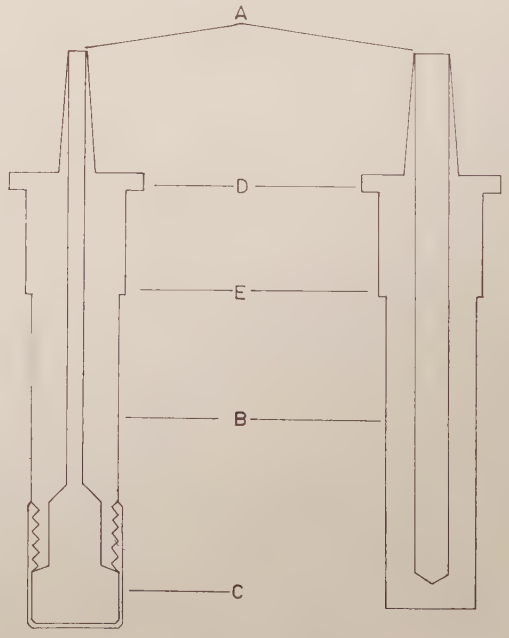

Fig. 2

† U. Wetzenstein, AB Atomenergi, Studsvik, Sweden.

screw cup C. Crucibles of this new design have been made from four materials Ta, Mo, Fe and Al, and used according to application. Since radiation heating is employed, it is only necessary to place the crucible in the oven and position the radiation shield. Because of the construction, this type of crucible is virtually indestructable and may be used indefinitely.

2.3. OVEN ARRANGEMENT

Shown in fig. 3 is the crucible heating arrangement, the ovens are of split graphite tube construction and made in such a way, that when in

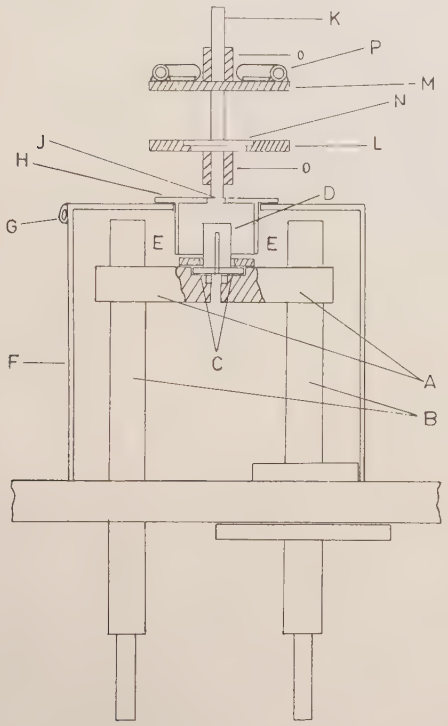

Fig. 3

position, the bottom of the crucible hangs clear of the oven. In this way, the main body receives uniform heating which reaches the activity by conduction last. Two massive copper supports A are clamped to the water cooled pillars B. These supports are recessed at C to take the oven D, which in turn is held in position by the two plates E. The oven and supporting assembly is covered by a heat radiation shield F and water cooled through a single loop of copper tube G. A smaller radiation shield H passes through F and comes to within 2 mm of the oven supports. In the top of this shield, there is a hole J, 4 mm in diameter, for the crucible chimney to pass through this is the only exposed heat radiation area.

2.4. POINT SOURCES

Also shown in fig. 3, is the arrangement for the production of point sources. A rod graduated in millimeters K and screwed into the base plate beside the radiation shield, supports two copper plates L and M. The former plate is recessed at N, and accomodates the source ring and backing. The plate L is brought down into close contact and fastend with a thumb screw O. Both plates can be adjusted for distance by means of fixing screws behind the supporting rod. Another loop of copper tube P is provided for cooling the backing on plate L.

2.5. STRIP SOURCES

For the preparation of strip sources the method is more complicated although simple enough in principle. The backing is attached to a cylinder which is rotated at a speed of 100–200 r.p.m. above a point source arrangement. Fig. 4, shows the construction. The required width of backing material is wrapped around the main

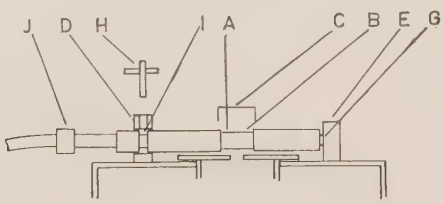

Fig. 4

body A (the length is defined by the circumference) and the ends inserted in the slot at B. A spring clip C holds the ends in position. Two bearings D and E support the cylinder on top of a radiation shield. After passing through D, the cylinder comes to rest on the steel ball G. To ensure smooth running, a square cut pin H drops through D and locates in the groove 1. Connection to the rotating seal in the chamber wall, is by a flexible steel coupling fixed at J.

With the described method extra care is necessary when removing and subsequently mounting the backings. The additional effort, however, is well worth while when one considers the uniform deposits obtained in this way.

2.6. VACUUM SYSTEM

A vacuum of the order 5×10^{-6} mm Hg is obtained in four to five minutes from atmospheric pressure by using a three stage oil diffusion pump, backed by a two stage rotary oil pump. Connection between the vacuum chamber and diffusion pump is made via a water cooled baffle valve, which together with a second valve of two way construction allows the chamber to be let down to air and re-evacuated without switching off the pumps. Pressure measurement is by means of a Pirani/Penning combination with the gauge heads situated beneath the base plate.

3. Performance

Initially a list of ten radio-active elements with a wide range (200–2 900° C) of evaporation temperatures was decided upon, however, it has since grown to twice this number. Uusally the active material was derived from chemical separation and loaded in its chloride form into the crucible. This procedure allows for good thermal contact between material and crucible and has the further advantage that chlorides often have a lower evaporation temperature. The activity is loaded into the crucible cup which is kept warm by use of a heat lamp. (The chloride

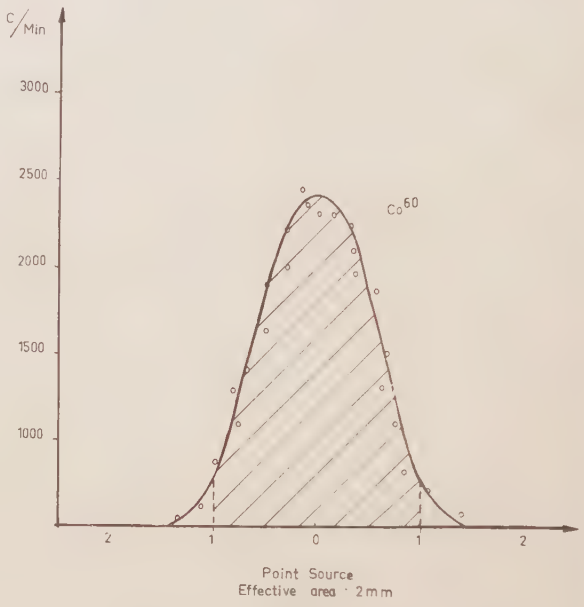

Fig. 5a

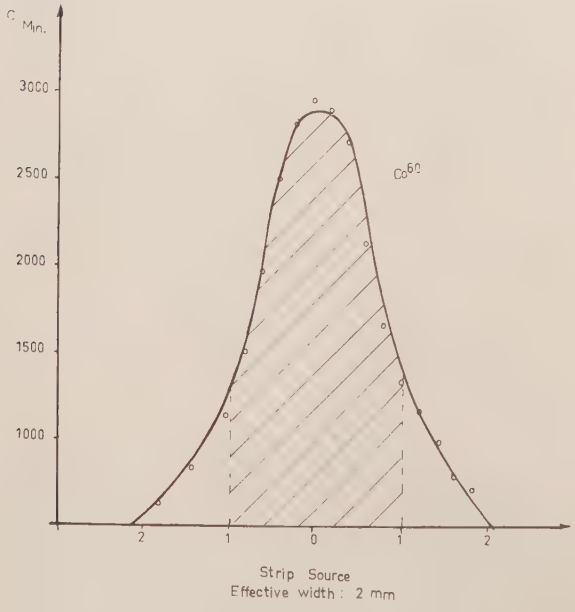

Fig. 5b

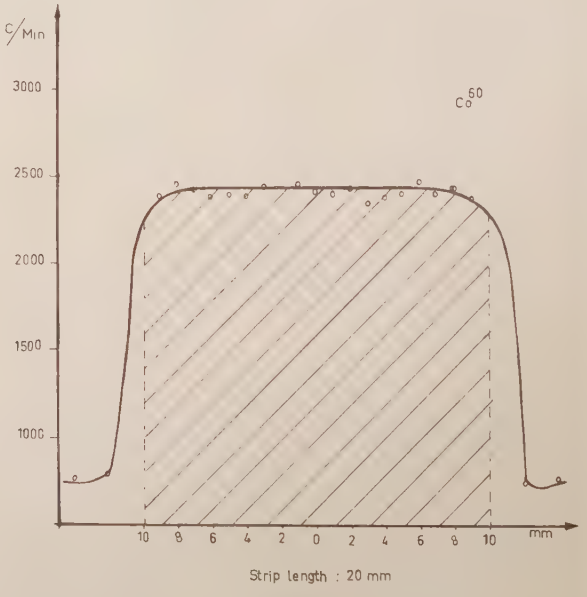

Fig. 5c

in HCl is evaporated and taken up in ether.) The backing material used through out for the point source preparations was zapon films. These films were prepared by spreading a drop of the zapon on water, and subsequently mounting the film on a ring with an internal diameter of 18 mm. Finally, a thin metal substrate was evaported onto the backing, and if necessary, a drop of aqua dag† to establish electrical contact between substrate and ring. The thicknesses, of both the backing and substrate were determined by a comparison method of alpha absorption[12]) in dry air. The average thickness of backing and substrate was 10 μg/cm^2 and 40 μg/cm^2 respectively. In some cases where the source could be expected to volatize over a long period in vacuum, a thin zapon film 10 μg/cm^2 was placed over the deposit. Materials used for strip sources were commercially produced plastic†† with an evaporated substrate, or aluminium foils with a tickness down to 200 μg/cm^2. On completion of the evaporation the distribution of the active deposits were determined by use of a scintillation counter in front of a collimator 0.1 mm wide formed with two polished lead blocks. The source in question was moved past the slit with a micrometer screw. Fig. 5 shows the results obtanied from this measurement. The effective source areas are shaded. The total yields obtained in the evaporations of the following materials were: Se, Ca, Pb, Rh, Ce, Au, Cu, Co, Pt and Ni (90% and over); Ho, Sm, Eu, La, Nd and Pr (40–70%); As, Rb, Hg, P and Ga (15–50%). The above yields were arrived at in the following manner. The relative gamma radiation of the active material in the crucible was first measured. After the evaporation the crucible was again measured together with the active deposit. From these measurements an accurate estimate of both the active deposit and the material lost in the system could be arrived at the source. The apparatus described has been in continual use for five months and has proved itself satisfactorily. The only difficulties have arisen when elements, or there compounds, changed composition because of heating. A major problem with an apparatus of the type described, is the limited choice of the materials available for the construction of crucibles. Carbon, even though it has a melting point about 500° C above tantalum, absorbs many materials and reacts with others. An alternative method of heating, that of bombarding the material itself with electrons[13]), would appear to be the answer, providing some form of collimation, of the vapour stream, can be applied.

† Collodial graphite.
†† Mylar, DuPont, U.S.A.

Acknowledgements

The author would like to thank Professor K. Siegbahn for his interest and encouragement in this work. Also my thanks are due to the beta spectroscopy group for valuable discussions. Finally, I would like to thank Dr. J. H. Hamilton for helpful suggestions and for his comments on the manuscript.

[12]) W. H. T. Davidson, J. Sci. Inst. **34** (1957) 418.
[13]) H. Smith, J. Sci. Inst. **26** (1949) 378.

NUCLEAR INSTRUMENTS AND METHODS 5 (1959) 148–151; NORTH-HOLLAND PUBLISHING CO.

CIRCUIT DE COÏNCIDENCE RAPIDE A TROIS DIODES

R. MEUNIER † et J. TEIGER ††

Service de Physique Corpusculaire à Haute Energie, C.E.N., Saclay, Gif-sur-Yvette (S & O), France

Reçu le 25 juin 1959

A differential coincidence circuit is described which has an effective resolving time of les than one mμs. The principle consists of having two pulses travelling in opposite directions through the same coaxial cable, and they meet at a given point. The circuit is very simple. It has been built for use on experiments with high energy accelerators.

1. Introduction

Dans les circuits de coïncidence classiques, la coïncidence est définie par la superposition de deux impulsions; cette définition de la coïncidence est de nature qualitative. Nous avons cherché, dans le présent circuit, à utiliser toute l'information donnée par l'impulsion du photomultiplicateur et de définir la coincidence par l'égalité à zéro du retard relatif entre les centres de gravité des impulsions. Gatti[1]) a montré que la fluctuation du centre de gravité d'une impulsion peut être de l'ordre du 0.01 de la largeur de l'impulsion.

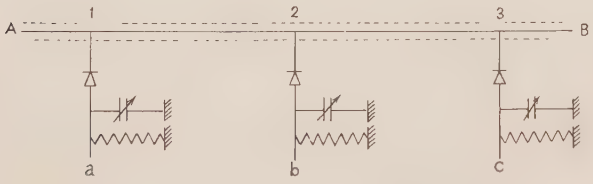

Fig. 1. Principe du circuit de coïncidence.

Le principe[2]) du circuit de coïncidence est le suivant (fig. 1): on envoie, à l'extrémité A d'un câble coaxial, une impulsion négative et courte de l'ordre de 2 à 3 mμs; cette impulsion, à travers trois diodes, charge trois capacités à la même tension de crête $a = b = c$. Les trois capacités constituent un circuit de mémoire et donnent une impulsion de l'ordre de 2 à 3×10^{-7} s, ce qui permet d'adopter, pour l'observation, des circuits classiques.

Si on envoie maintenant une impulsion positive en B, simultanée de l'impulsion négative en A, ces deux impulsions se propagent en sens inverse, se rencontrent sur la deuxième diode et s'y annulent; par suite, sur les diodes 1, 2 et 3 on observe une combinaison d'amplitude $a = c$ inférieure à b. On mesure les différences $a - b$ et $c - b$ pour détecter une coïncidence.

Un tel circuit possède l'avantage d'avoir une réponse qui est indépendante de la hauteur des impulsions entre certaines limites. En effet, une coïncidence est accepté seulement lorsque $a - b$ et $c - b$ sont simultanément supérieurs à une certaine valeur qui est le seuil de déclenchement du circuit[3]). D'autre part, si l'on ne tient pas compte des fluctuations dans les photomultiplicateurs, la largeur théorique totale de résolution est égale à la distance entre les point *ac* mesurée en temps. Ce circuit a un temps de résolution indépendant de la largeur de l'impulsion.

2. Description du Circuit

Le schéma du circuit est donné sur la figure 2. Il consiste en un câble coaxial 100 MD d'impédance caractéristique 100 Ω et dont la vitesse de propagation est de 0.66 fois celle de la lumière.

† Actuellement en mission: Division du Synchro-Cyclotron, Organisation Européenne pour la Recherche Nucléaire, CERN, Genève.

†† Attaché de recherche au C.N.R.S. Laboratoire de Physique Corpusculaire de Caen, actuellement en stage à Saclay.

[1]) Cottini et Gatti, Nuovo Cimento **4** (1956) 1550.

[2]) G. Davidson et R. Meunier, Rev. Sci. Instr. **28** (1957) 1010.

[3]) R. Meunier, Industries Atomiques **2** (1955) 6.

La distance entre deux diodes est de 12 cm. Nous avons choisi comme diodes détectrices des DPO et des OA85, mais les meilleurs résultats sont donnés avec des S 570 G qui ont un faible temps de recouvrement. La sortie des diodes est reliée à la grille d'une triode montée en inverseuse de phase. La comparaison des amplitudes a — b et c — b est faite ensuite dans un circuit d'addition composé de trois résistances R_1, R_2, R_3. Après amplification du signal par deux penthodes 6AK5, on attaque les deux grilles d'une 6BN6 montée en circuit de coïncidence lent. Une triode permet de sortir une impulsion positive ou négative qui peut déclencher une échelle de comptage. On observe à l'aide d'une ligne à retard Hackethall HH4000 la répartition des impulsions à la sortie des trois diodes, ce qui permet un réglage rapide de la coïncidence.

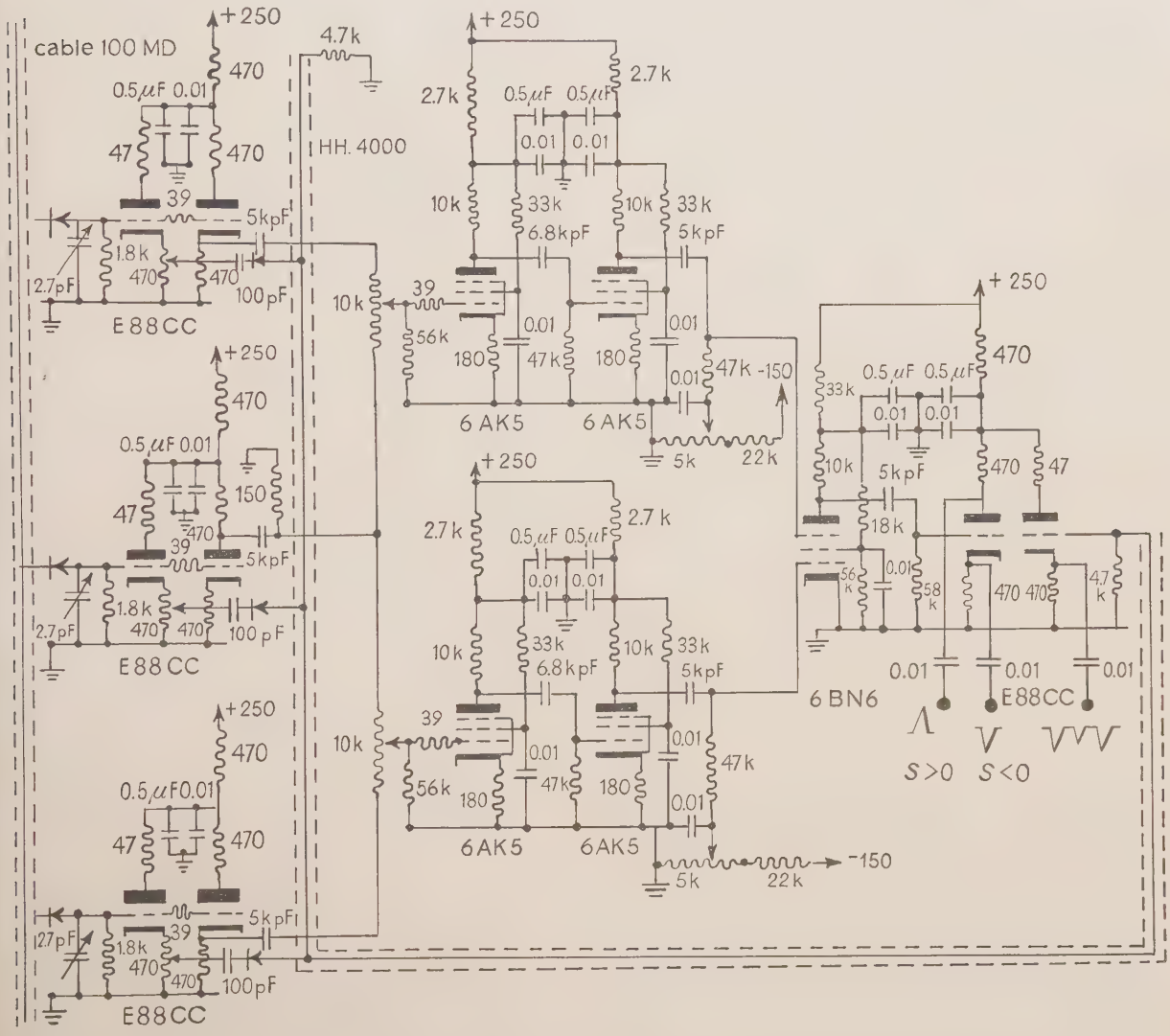

Fig. 2. Schéma du circuit.

3. Résultats et Essais du Circuit de Coïncidence

Nous avons fait des essais avec un relais à mercure donnant des impulsions de 1×10^{-9} à 5×10^{-9} s, sans constater d'augmentation du temps de résolution du circuit, qui est de

1.2×10^{-9} s, nous obtenons simplement une diminution de la sensibilité du circuit.

Avec des impulsions de 2.5×10^{-9} s, la sensibilité du circuit est de 0.6 V. Le "rapport de rejet", c'est-à-dire le quotient entre la plus grande amplitude de l'impulsion simple qui ne produit pas une fausse coïncidence et la sensibilité définie ci-dessus, est de 80.

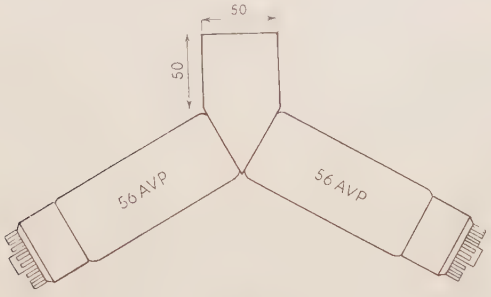

Fig. 3.

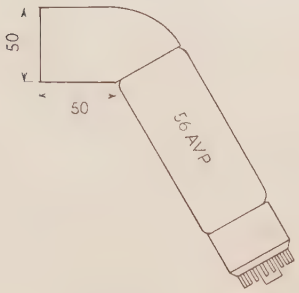

Fig. 4.

Compteurs de Čerenkov pour les essais du circuit de coïncidence.

Des essais ont ensuite été faits avec des impulsions de photomultiplicateur. En raison de la faible distance entre les diodes, il nous fallait des photomultiplicateurs capables de donner une impulsion courte et possédant une très faible fluctuation du temps de transit; nous avons adopté des 56AVP (Radiotechnique). Les deux photomultiplicateurs collectent la lumière Čerenkov produite dans un même bloc de plexiglass par les particules du rayonnement cosmique (fig. 3).

Le temps de résolution obtenu de cette façon avec une efficacité de 95%, a été de 0.65×10^{-9} s (fig. 5). Avec ces mêmes photomultiplicateurs, mais montés sur deux compteurs de Čerenkov indépendants (fig. 4), nous avons refait les mesures dans un faisceau de π^+ de 1 GeV/c obtenu au synchrocyclotron de Saclay. Le temps de résolution est de 0.8×10^{-9} s avec une efficacité supérieure à 85% (figs. 6–7).

Quant au taux de comptage que l'on peut accepter dans le circuit sans le surcharger, il est

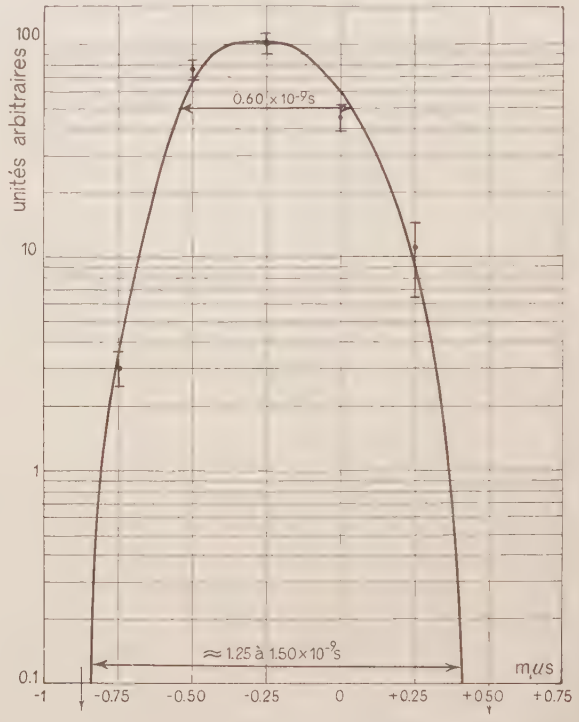

Fig. 5. Courbe de résolution avec un bloc de plexiglass et le rayonnement cosmique.

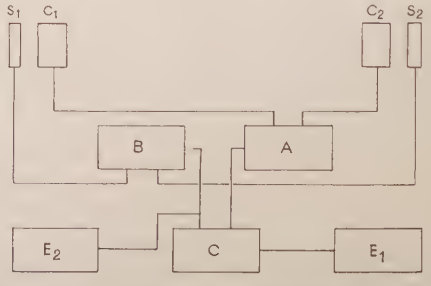

Fig. 6. Schéma de principe des essais d'efficacité du circuit de coïncidence à 3 diodes. S_1–S_2: scintillateurs de définition. C_1–C_2: compteurs de Čérenkov. A: circuit de coïncidence à essayer. B: circuit de coïncidence ($2\tau = 6$ mμs). C: circuit de coïncidence lent (0.1 μs). E_1–E_2: échelles de comptage.

de 10^5 à 10^6 coups/s. Cet essai a été fait avec des sources α, d'intensité variable, enrobées dans

une feuille de plastique scintillant et placées entre deux photomultiplicateurs.

Remerciements

Les auteurs remercient le groupe des compteurs du S.P.C.H.E. de leur avoir donné la possibilité de faire ce travail.

J. Teiger remercie Monsieur Scherer, Professeur de l'Université de Caen, de lui avoir permis de faire un stage à Saclay.

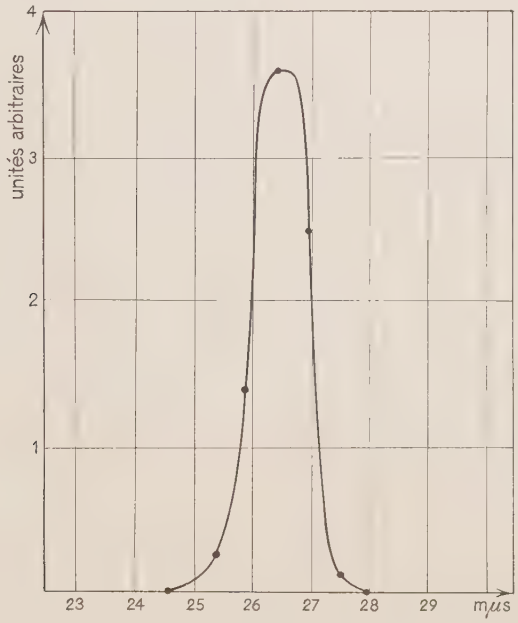

Fig. 7. Courbe de résolution avec des π^+ de 1 GeV/c.

NUCLEAR INSTRUMENTS AND METHODS 5 (1959) 152–155; NORTH-HOLLAND PUBLISHING CO.

DESIGN OF ALTERNATING GRADIENT QUADRUPOLE LENSES

JORGE ROSENBLATT

Comisión Nacional de Energía Atómica, Buenos Aires

Received 5 June 1959

A graphical method is described by means of which it is possible to design quadrupole lenses once locations of object and image are given. It is shown that similar procedures would be valid in the para-axial (Gauss) approximation, when applied to electron optical devices of any kind.

1. Introduction

Strong focusing[1]) of ion and electron beams has become widely used in many laboratories. A common assembly is that composed of two quadrupoles. Although this system is intrinsically astigmatic, so are generally the "objects" and the over-all result is a real, well defined image.

Different authors[2–4]) have treated the problem of designing strong focusing magnets, i.e. the problem of asigning currents and dimensions to both quadrupoles once the object position and the required location of the image are known. It seems worth while, however, to work out a method with a minimum of simplifying assumptions on the geometrical and electrical parameters. These parameters are: k_1 and k_2, field gradients in each quadrupole; d_1 and d_2, thickness of each quadrupole, and L, distance between both quadrupoles. In this paper we are going to assume that $d_1 = d_2 = d$. As a matter of fact, this only reflects t he way in which quadrupole lenses are generally constructed.

2. Optical Analogy of Quadrupole Lenses

Magnetic and electric quadrupoles behave as lenses convergent in one plane and divergent in another perpendicular to the first one. This effect can be best described by the well known matrix relations:

$$\begin{pmatrix} x_a \\ \dot{x}_a \end{pmatrix} = \begin{pmatrix} \cos \omega d & \frac{1}{\omega} \sin \omega d \\ -\omega \sin \omega d & \cos \omega d \end{pmatrix} \begin{pmatrix} x_b \\ \dot{x}_b \end{pmatrix} \qquad (1)$$

for the convergent plane, and

$$\begin{pmatrix} x_a \\ \dot{x}_a \end{pmatrix} = \begin{pmatrix} \cosh \omega d & \frac{1}{\omega} \sinh \omega d \\ \omega \sinh \omega d & \cosh \omega d \end{pmatrix} \begin{pmatrix} x_b \\ \dot{x}_b \end{pmatrix} \qquad (2)$$

for the divergent plane.

In eqs. (1) and (2) x_b and x_a refer to the distance of the particle from the z axis (optical axis of the quadrupole) before entrance to and after exit from the quadrupole field, $\dot{x}_b = (\mathrm{d}x/\mathrm{d}z)_b$, $\omega^2 = k/\mathrm{BR}$ in the magnetic case and $\omega^2 = k/2T$ in the electric case; here BR stands for the magnetic rigidity of the particle and T for its kinetic energy. Similarly, for a field-free region of length L:

$$\begin{pmatrix} x_a \\ \dot{x}_a \end{pmatrix} = \begin{pmatrix} 1 & L \\ 0 & 1 \end{pmatrix} \begin{pmatrix} x_b \\ \dot{x}_b \end{pmatrix}. \qquad (3)$$

The preceding equations apply in the para-axial approximation to square shaped fields, which obviously do not represent the real case. However, it has been pointed out[5]) that calculations with the more realistic "bell" shaped fields give results that differ from those obtained with the previous equations in quantities of the order of 1%.

Let us consider now the usual two quadrupole lens. We have a CD plane (first convergent and

[1]) E. D. Courant, M. St. Livingston and H. S. Snyder, Phys. Rev. 88 (1952) 1190.

[2]) A. V. Crewe *et al.*, Use of strong focus magnet, internal report (The Enrico Fermi Institute for Advanced Studies).

[3]) D. A. Bromley and J. A. Bruner, AEC/NYO-3823 (1954).

[4]) H. Schneider, Nuclear Instruments 1 (1957) 268.

[5]) P. Grivet, A. Septier and J. Hue, CERN Symposium 1 (1956) 192.

then divergent) and a DC plane (first divergent and then convergent). The corresponding matrices are obtained by multiplication of those appearing in eqs. (1), (2) and (3) in the same order as the particle actually "sees" the respective fields. We call ω_1 and ω_2 the "strengths" of the first and second quadrupoles, respectively. The mean strength is defined as

$$\omega = (\omega_1\omega_2)^{\frac{1}{2}} \tag{4}$$

and the asymmetry parameter as

$$\gamma = \frac{\omega_1}{\omega} = \frac{\omega}{\omega_2}. \tag{5}$$

If we further take the quadrupole thickness d as unit of length, we have for the matrix elements

$$M_{11} = \cosh\frac{\omega}{\gamma}\cos\omega\gamma - L\omega\gamma\cosh\frac{\omega}{\gamma}\sin\omega\gamma - \gamma^2\sinh\frac{\omega}{\gamma}\sin\omega\gamma \tag{6a}$$

$$M_{12} = \frac{1}{\omega\gamma}\cosh\frac{\omega}{\gamma}\sin\omega\gamma + L\cosh\frac{\omega}{\gamma}\cos\omega\gamma + \frac{\gamma}{\omega}\sinh\frac{\omega}{\gamma}\cos\omega\gamma \tag{6b}$$

$$M_{21} = \frac{\omega}{\gamma}\sinh\frac{\omega}{\gamma}\cos\omega\gamma - L\omega^2\sinh\frac{\omega}{\gamma}\sin\omega\gamma - \omega\gamma\cosh\frac{\omega}{\gamma}\sin\omega\gamma \tag{6c}$$

$$M_{22} = \frac{1}{\gamma^2}\sinh\frac{\omega}{\gamma}\sin\omega\gamma - L\frac{\omega}{\gamma}\sinh\frac{\omega}{\gamma}\cos\omega\gamma + \cosh\frac{\omega}{\gamma}\cos\omega\gamma \tag{6d}$$

(CD plane) and

$$N_{11} = \cosh\omega\gamma\cos\frac{\omega}{\gamma} + L\omega\gamma\cos\frac{\omega}{\gamma}\sinh\omega\gamma + \gamma^2\sin\frac{\omega}{\gamma}\sinh\omega\gamma \tag{7a}$$

$$N_{12} = \frac{1}{\omega\gamma}\cos\frac{\omega}{\gamma}\cosh\omega\gamma + L\cos\frac{\omega}{\gamma}\cosh\omega\gamma + \frac{\gamma}{\omega}\sin\frac{\omega}{\gamma}\cosh\omega\gamma \tag{7b}$$

$$N_{21} = \omega\gamma\cos\frac{\omega}{\gamma}\sinh\omega\gamma - L\omega^2\sin\frac{\omega}{\gamma}\sinh\omega\gamma - \frac{\omega}{\gamma}\sin\frac{\omega}{\gamma}\cosh\omega\gamma \tag{7c}$$

$$N_{22} = \cos\frac{\omega}{\gamma}\cosh\omega\gamma - L\frac{\omega}{\gamma}\sin\frac{\omega}{\gamma}\cosh\omega\gamma - \frac{1}{\gamma^2}\sin\frac{\omega}{\gamma}\sinh\omega\gamma \tag{7d}$$

(DC plane). Inspection shows immediately the following relations to hold

$$M_{11}\left(\omega, \frac{1}{\gamma}\right) = N_{22}(\omega, \gamma) \tag{8a}$$

$$M_{12}\left(\omega, \frac{1}{\gamma}\right) = M_{12}(\omega, \gamma) \tag{8b}$$

$$M_{21}\left(\omega, \frac{1}{\gamma}\right) = N_{21}(\omega, \gamma) \tag{8c}$$

$$M_{22}\left(\omega, \frac{1}{\gamma}\right) = N_{11}(\omega, \gamma) \tag{8d}$$

$$M_{11}M_{22} - M_{12}M_{21} = N_{11}N_{22} - N_{12}N_{21} = 1. \tag{9}$$

We are thus left with three independent relations, from where in principle the three important parameters ω, γ and L could be solved. This appears as an impossible task from the analytical point of view. We are then going to look for a graphical method, based on the following well known optical relations:

$$f = -\frac{1}{M_{21}} \tag{10a}$$

$$z_{\pi_0} - z_1 = -\frac{M_{22} - 1}{M_{21}} \tag{10b}$$

$$z_{\pi_1} - z_2 = -\frac{M_{11} - 1}{M_{21}} \tag{10c}$$

$$\frac{1}{p_0} - \frac{1}{p_1} = \frac{1}{f}. \tag{10d}$$

Eqs. (10a) to (10d) are valid for the CD plane; the corresponding equations for the DC plane are obtained just replacing the M's by the N's. The meaning of the distances p_0, p_1 and f, and ordinates z_1, z_2, $z_{\pi 0}$ and $z_{\pi 1}$ is shown in the optical construction of fig. 1; π_0 and π_1 refer to the object and image principal planes. It is easy to see from fig. 1 and eqs. (10) that

$$s_0 = p_0 - \frac{M_{22} - 1}{M_{21}} \tag{11a}$$

$$s_1 = p_1 - \frac{M_{11} - 1}{M_{21}} \tag{11b}$$

for the CD plane and

$$s'_0 = p'_0 - \frac{N_{22} - 1}{N_{21}} \tag{12a}$$

$$s'_1 = p'_1 - \frac{N_{11} - 1}{N_{21}} \tag{12b}$$

for the DC plane.

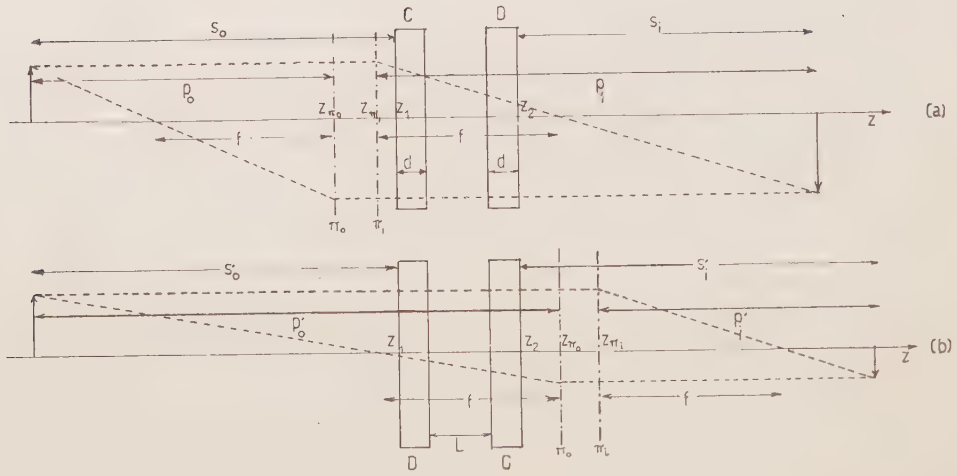

Fig. 1. Optical construction that relates object and image; (a) CD plane, (b) DC plane.

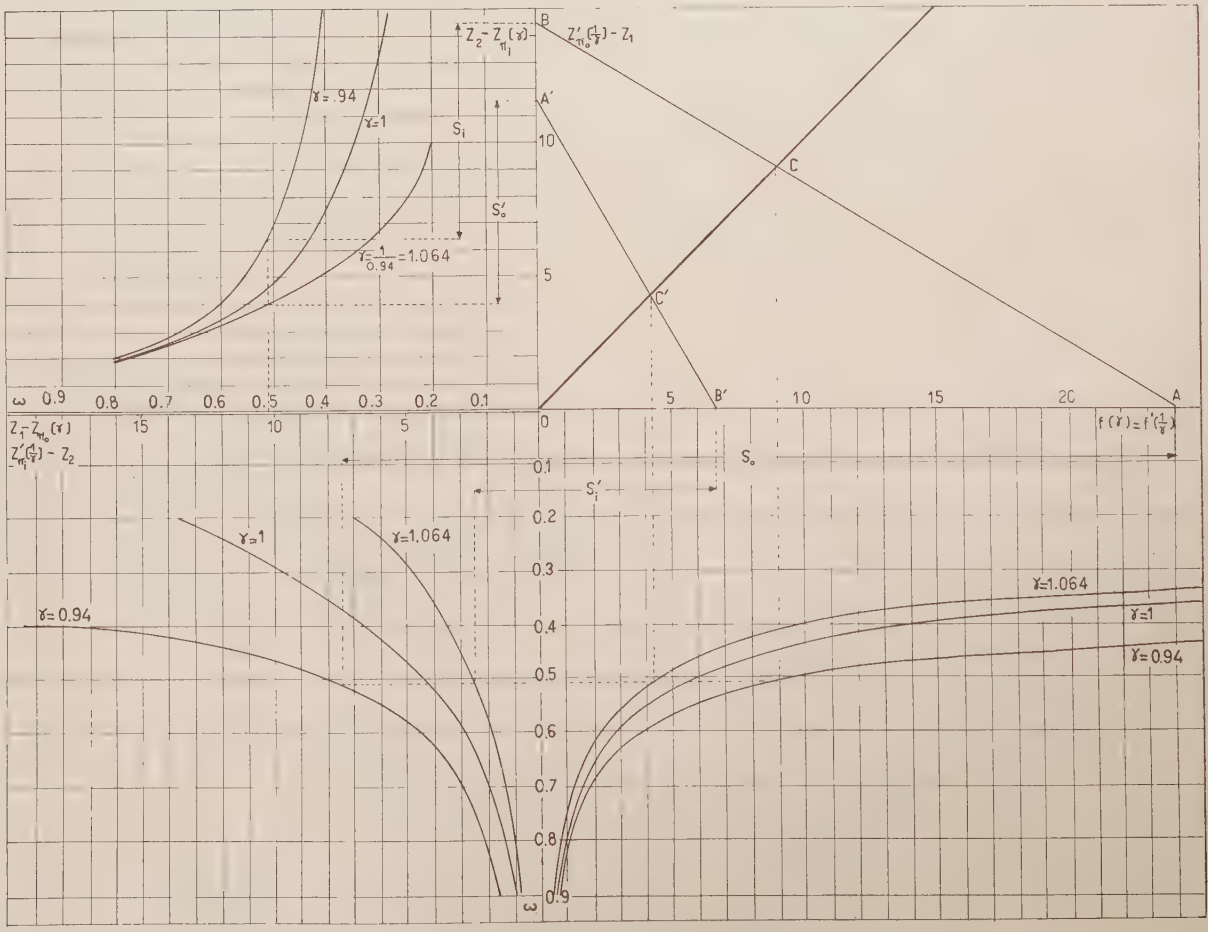

Fig. 2. Example of graphical method for $\gamma = 0.94$, $L = 2$.

3. Trial-and-Error Graphical Method

The whole preceding discussion is condensed in fig. 2, drawn for the particular value $L = 2$. In the first quadrant we have the geometrical construction resulting from (10d): if OA and OB stand for p_0 and p_1, (10d) implies that A, B and C must be aligned. The second quadrant contains the curves corresponding to

$$\frac{M_{11}(\gamma) - 1}{M_{21}(\gamma)} = \frac{N_{22}\left(\frac{1}{\gamma}\right) - 1}{N_{21}\left(\frac{1}{\gamma}\right)}$$

as functions of ω, for three different values of the parameter γ: $\gamma = 0.94$, $\gamma = 1.0$ and $\gamma = 1/0.94 = 1.0638$. As (10b) and (10c) show, the ordinates are the distances (in units of d) $z_2 - z_{\pi 1}(\gamma)$ for the CD plane and $z'_{\pi 0}(1/\gamma) - z_1$ for the DC plane.

In the third and fourth quadrants the downward vertical axis is used for abscissae, ω. In the third quadrant the functions

$$-\frac{M_{22}(\gamma) - 1}{M_{21}(\gamma)} = -\frac{N_{11}\left(\frac{1}{\gamma}\right) - 1}{N_{21}\left(\frac{1}{\gamma}\right)}$$

[$z_1 - z_{\pi 0}(\gamma)$ in the CD plane, $z'_{\pi 1}(1/\gamma) - z_2$ in the DC plane] are plotted. We finally have the focal distance

$$f = -\frac{1}{M_{21}(\gamma)} = -\frac{1}{N_{21}\left(\frac{1}{\gamma}\right)}$$

plotted against ω for the same aforementioned values of γ in the fourth quadrant.

Suppose now we are given the values of s_0, s_1, s'_0, s'_1 (in units of d; generally $s_1 = s'_1$, because anastigmatic images are sought). We then choose an arbitrary value of ω (a good rule of thumb is that the horizontal distance through ω between corresponding curves in the third and fourth quadrants be less than s_0) and $\gamma = 1$. Fig. 2 shows how to determine points A, B and C and correspondingly s_1, which of course will not generally coincide with that previously given; but information is obtained from the graph about where to look for a more accurate value of ω, which after two or three more trials is finally found. Repeating the same process for the DC plane (in this case s'_1 [s'_0] is read in the same axis as previously s_0 [s_1]). Attainment of a different value of ω shows the need of $\gamma \neq 1$. The same trial-and-error process must be accomplished with $\gamma \neq 1$, taking now into account that because of eqs. (8), when γ curves are used for the CD plane, $1/\gamma$ curves are required for the DC plane. Of course, curves for other values of γ and graphs for other values of L could be drawn, thus covering all possibilities.

4. Discussion and Final Remarks

The method just outlined allows the determination of the required parameters with far greater accuracy than that either implied by the approximations used or needed for the mechanical and electrical design of quadrupole lenses. Final adjustments are to be done experimentally[6]). The trial and error process is not very long (after some practice an hour is enough), but it requires long and tedious calculations for the plotting of curves. Fortunately, as a rough guide one graph as the one shown here suffices.

The whole discussion in this paper applies equally well to magnetic and electric quadrupoles. Moreover, it can be shown[7]) that the matrix formulation is generally valid for electron or ion optical instruments in the paraaxial approximation. Eqs. (10), (11) and (12) are then also valid, and so is the whole procedure described on the basis of these equations; naturally, different curves would appear in each case as a result of the different dependence of the matrix elements on the fundamental parameters.

Acknowledgement

The author wants to express his gratitude to Dr. S. Mayo, for his encouragement during completion of this work.

[6]) F. B. Schull, C. E. McFarland and M. M. Bretscher, Rev. Sci. Instr. **25** (1954) 365.

[7]) P. A. Sturrock, Static and dynamic electron optics (Cambridge University Press, 1955).

NUCLEAR INSTRUMENTS AND METHODS 5 (1959) 156–160; NORTH-HOLLAND PUBLISHING CO.

A SYNCHRO-CYCLOTRON PULSE SIMULATOR FOR TESTING ELECTRONIC CIRCUITS

T. FAZZINI, G. FIDECARO and H. PAUL†

CERN, *Geneva*

Received 15 June 1959

An electronic pulse generator is described that can be used to test electronic circuits under conditions of alternating high and zero counting rate similar to those existing at a synchro-cyclotron. It consists of a gated oscillator and a pulse sharpener.

1. Introduction

In an electronic pulse circuit the operating point of a vacuum tube or a crystal diode may shift to an unfavourable position if any one of the applied potentials changes due to the charging of a condenser or the building up of a current in an inductance. In the case of a condenser two basic circuits (fig. 1) are responsible for such voltage changes; both are characterised by a time constant $\tau = RC$.

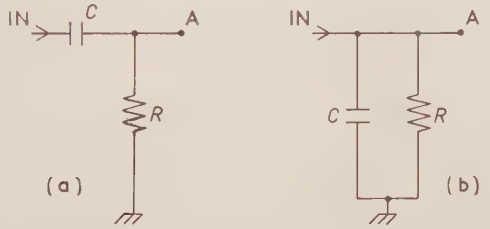

Fig. 1. Bias change at point A during pulsed operation.

Assume, for example, that one of these circuits is continuously fed with rectangular pulses of length Δt seconds, at an average rate of f pulses per second, randomly distributed in time. Then the average d.c. level at point A, as compared to quiescent conditions, changes by

$$\Delta V_\infty = V_0 f \Delta t \qquad (1)$$

where

V_0 = — voltage pulse amplitude (circuit a)

or

V_0 = + R × current pulse amplitude (circuit b).

† On leave from Institut für Radiumforschung, Wien, Austria.

The r.m.s. fluctuation of the d.c. level for $\Delta t \ll \tau$ is given by Campbell's theorem as

$$\sigma = | V_0 | \Delta t \sqrt{f/(2\tau)} . \qquad (2)$$

It is clear from (1) and (2) that the average d.c. level is independent of τ, while the fluctuations are inversely proportional to the square root of τ.

In the case of a pulse particle accelerator, the pulses come grouped in bunches with the repetition rate and the time distribution within the bunch characteristic of the accelerator. The d.c. level does not necessarily reach the value given by (1) (where f is the average rate within the bunch), but approaches it exponentially with the time constant τ:

$$\Delta V = \Delta V_\infty (1 - e^{-t/\tau}) \qquad (3)$$

and decays between bunches with the same time constant.

In the design of electronic circuits for use with particle accelerators, eqs. (1) to (3) are important for the choice of the most convenient time constant from the point of view of minimum change of bias voltages. However, it may be necessary to test a circuit under conditions similar to those of normal use, especially if this circuit, designed to work at high counting rate, is rather complicated or contains non-linear components, like e.g. the grid-cathode part of a vacuum tube if grid current flows part of the time.

2. Description of the Simulator

We have built a fast pulse generator which produces groups of pulses at regular intervals and may be used to test coincidence circuits, discriminators, and scalers under pulsed conditions. In particular, we were interested in simulating pulses due to mesons produced at an internal target of the CERN Synchro-cyclotron, which come in bunches of 200–300 μs duration, the spacing between bunches being 18 ms. Actually, our simulator produces groups of pulses 170 μs long, at 7 ms intervals, the difference being of no practical importance. The pulse frequency within a bunch can be 1 Mc/s or 10 Mc/s, according to the position of a switch.

The output pulses are negative and shaped by a suitably terminated delay line to simulate shaped photomultiplier output pulses. Their amplitude is 4–8 V, which is sufficient to operate our coincidence circuit[1]) directly (minimum pulse height required about 2 V).

The simulator is used to test a circuit by verifying with an oscilloscope that the pulses in a bunch are all properly transmitted through the circuit and appear at all points of the circuit with the expected height and shape independently of the position of the pulse in the bunch. Simple inspection of the envelope of the bunch will show the change in the bias voltage. Because the simulator pulses are uniformly distributed in time within a bunch, this is the *average* bias change. In the practical use with a particle accelator, there will be fluctuations superimposed. As a first approximation, one can assume that neglecting the fine structure within a bunch due to the radio-frequency cycle, the particles get to the counters with a random time

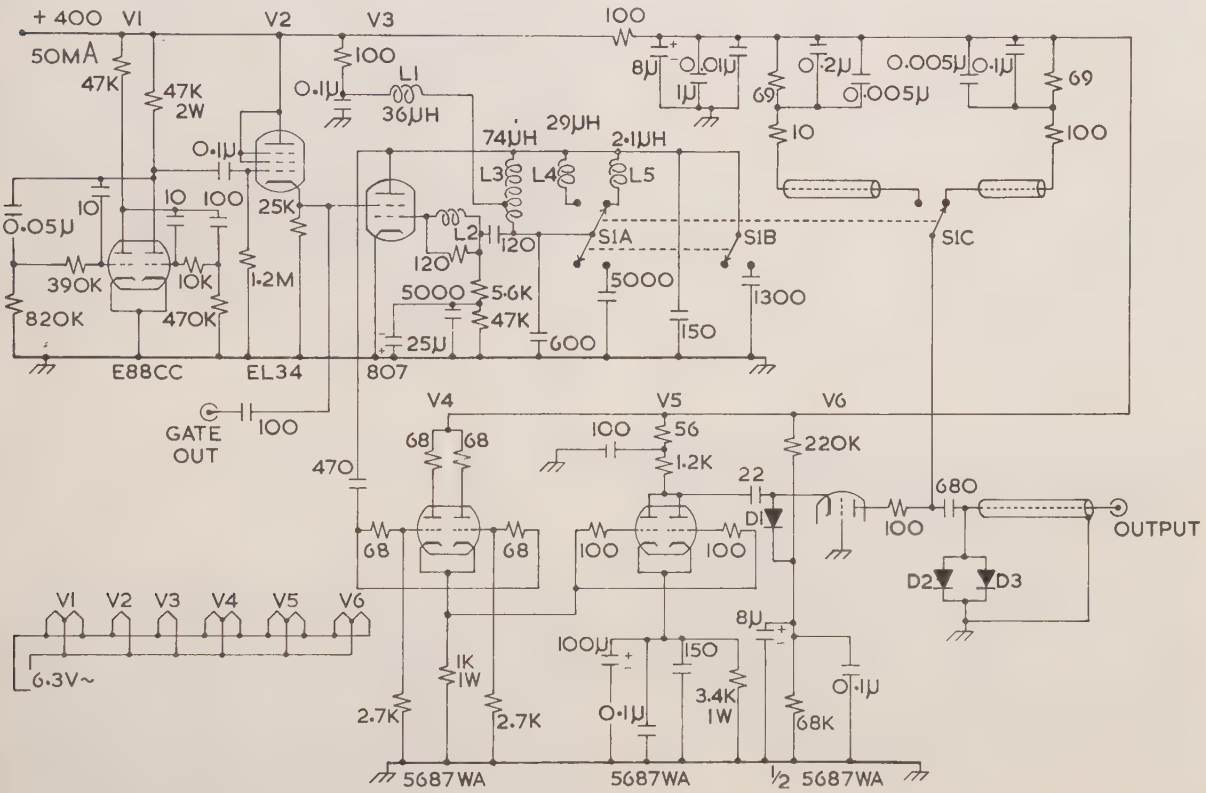

Fig. 2. Circuit diagram. Cables are 125 ohms. Capacities in the resonant circuits are mica, all others up to 0.2 μF are ceramic. Those marked + — are electrolytic. All resistances are carbon, rated $\frac{1}{2}$ W or less unless otherwise marked. Resistances given in ohms, capacities in pF unless otherwise marked. Diodes: D_1, CG1E (BTH). D_2 and D_3, HD 2130 (Hughes).

[1]) T. Fazzini and G. Fidecaro, to be published.

distribution though the average frequency is not necessarily constant within the bunch. In this case the random fluctuations can be estimated by eq. (2). For example, with $\Delta t = 10^{-8}$ s, $f = 10$ Mc/s and τ equals ten times the length of a bunch, i.e. with $\tau \approx 10^{-3}$ s for the CERN Synchro-cyclotron, the r.m.s. fluctuation is smaller than 0.1% of the pulse height.

It should be noted that a circuit which has been found to work at a simulator frequency of 10 Mc/s, will not be overloaded by bias changes when used with the CERN Synchro-cyclotron at an average counting rate as high as 100 000–150 000 particles/s (depending on the duty cycle). Even though there are at present no scalers that would count such high rates of random pulses without considerable losses, such a severe test will give confidence in actual work at lower pulse rates.

The simulator essentially consists of three parts: multivibrator, gated oscillator and pulse sharpener (see the circuit diagram, fig. 2, and also table 1). The repetition rate and duration of the output pulse train are determined by the gate multivibrator (V1) which delivers—via the cathode follower (V2)—a positive gate pulse to the second grid of the oscillator tube (V3).

Table 1

Gate pulse:	duration 0.19 ms repetition rate 140 c/s amplitude (after V2) + 220 V		
Oscillator	frequency	10 Mc/s	1 Mc/s
	grid bias output (peak to peak)	— 6 V 320 V	— 4 V 270 V
Pulse shaper:	cathode bias of V5	+ 42 V	+ 41 V
	voltage swing (anode of V5)	200 V	320 V

During the gate pulse, the oscillator produces a sine-wave of 1 or 10 Mc/s (depending on the position of switch S_1). In between gate pulses, oscillations are prevented by the negative grid bias which is originally produced by grid current and is maintained by the 25 μF condenser. Since the oscillator is not continuously running, there is a time correlation between the gate pulse and the single output pulses. If one uses the Gate

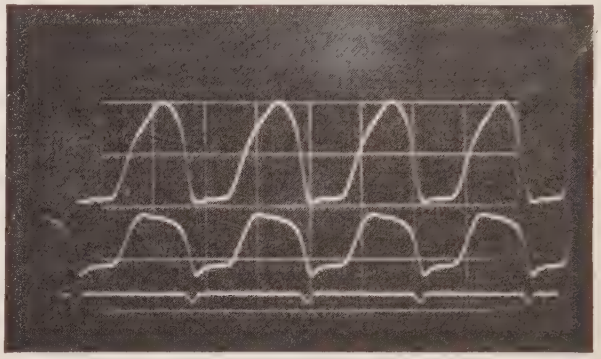

Fig. 3. Function of pulse shaper at 10 Mc/s, 50 mμs/division. Upper trace: anode of V5, 100 V/div. Middle trace: cathode of V6, 100 V/div. Lower trace: anode of V6, 50 V/div.

Output to trigger a delayed sweep oscilloscope like the Tektronix 545, then it is possible to look at single pulses or groups of pulses at any point of the whole output pulse train.

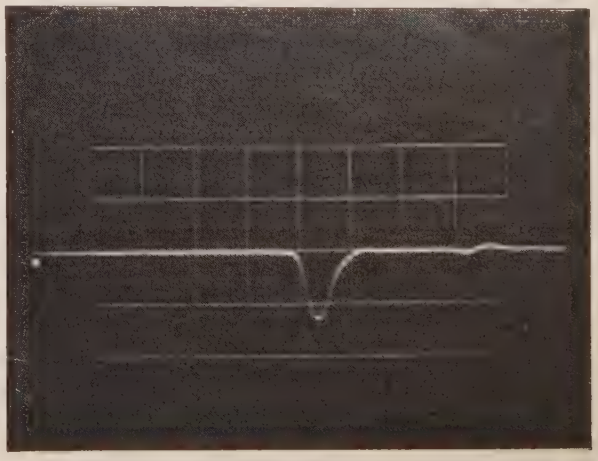

Fig. 4. Output pulse at 10 Mc/s. Horizontal: 10 mμs/div. Vertical: 8 V/div.

A cathode follower (V4) presents the sine-wave at low impedance to the pulse shaper[2]). The latter consists of two triode amplifiers, one with grounded cathode (V5) and the other with

[2]) Similar to the ones described by P. R. Orman and F. H. Wells, Nuclear Instruments **1** (1957) 183; and by H. I. Pizer and H. Verweij (private communication). We would like to thank Dr. Pizer and Mr. Verweij for useful discussions on the subject.

TABLE 2

Specifications of coils

	Diameter of coil (mm)	Number of turns	Wire diameter (mm)	Core
L_1	16	50	0.4	Air
L_2	6	14	0.9	$\frac{1}{2}$W resistor
L_3	29	96 (19:77)	0.85	Bakelite
L_4	29	57	1.3	Bakelite
L_5	29	8	1.3	Bakelite

grounded grid (V6). Both are normally biased off. During the pulse period, the grid of V5 is driven far into the positive region by the sine-wave (a d.c.-level shift being avoided by the direct coupling from V4 to V5), and the anode of V5 comes down by a few hundred volts (fig. 3, upper trace). The anode is coupled to the cathode of V6 via a 22 pF condenser (see fig. 3, middle trace). The pulse opens V6 and produces a fast negative-going pulse at the output (fig. 3, lower trace, and fig. 4).

In somewhat greater detail, the action of V5 and V6 can be described as follows: V6 starts to conduct only when its cathode comes close to ground potential. While it is still cut off, the coupling condenser simply transmits the anode pulse of V5 to the cathode of V6 (proportionally reduced to 60% of the original amplitude due to the finite cathode-to-ground capacity). When V6 conducts, however, the tube current charges the coupling condenser positively, so that the cathode potential cannot follow the anode pulse as freely as before. In other words, coupling condenser and cathode impedance now form an *RC*-combination which differentiates the anode pulse. The maximum output voltage is therefore proportional to the rate at which the anode voltage of V5 charges when V6 starts to conduct. Afterwards, the rate of voltage change decreases and hence also the current through V6; the falling edge of the output pulse (figs. 4 and 5) is, of course, also governed by the clipping line.

Between pulses, the cathode voltage of V6 is restored via diode D1. To avoid a condenser between the anode of V6 and the clipping cable, the anode voltage is supplied through the clipping cable itself. Switch S_1 selects the proper cable length and terminating resistance. The

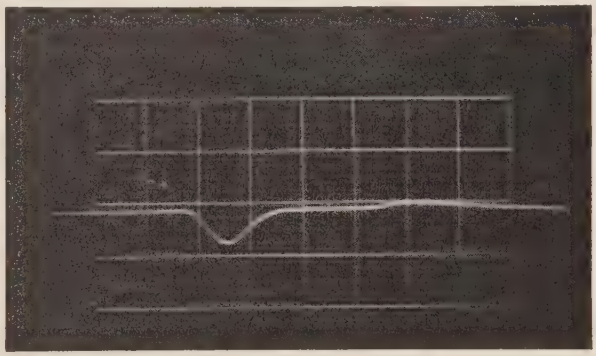

Fig. 5. Output pulse at 1 Mc/s. Sensitivities as for fig. 4.

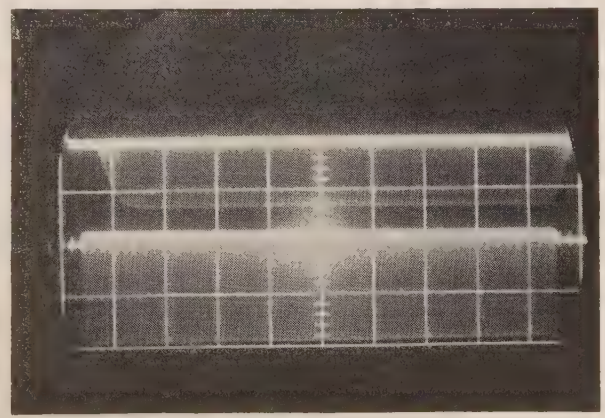

Fig. 6. Entire output pulse trains (unclipped). 20 μs/div. Upper trace: 1 Mc/s. Lower trace: 10 Mc/s. In the lower trace a residual bias change is still visible.

resistances are chosen so as to give minimum positive overshoot. Diodes D_2 and D_3 reduce the remaining overshoot, especially at 1 Mc/s.

The full pulse train can be seen in fig. 6 for 1 Mc/s (upper trace) and 10 Mc/s (lower trace).

3. Conclusion

We have used this simple apparatus to test all our circuitry built for work with the CERN Synchro-cyclotron. It is worth remarking that almost in every case the tests suggested changes and modifications. In some cases the simulator even enabled us to detect the existence of overloading effects due to high counting rate in non-linear parts of the circuit where the overloading had been considered negligible with elementary considerations. We therefore feel that a test with an electronic simulator can be recommended whenever a circuit has to be used at high counting rate, in the particular conditions determined by the pulsed accelerator.

NUCLEAR INSTRUMENTS AND METHODS 5 (1959) 161–164; NORTH-HOLLAND PUBLISHING CO.

A NEW USE OF COUNTER CONTROL IN CLOUD CHAMBER OPERATION†

ROBERT W. BIRGE, ROBERT E. LANOU Jr. and MARIAN N. WHITEHEAD

University of California, Radiation Laboratory, Berkeley, Cal.

and

HANS COURANT

UCRL and *Yale University, New Haven, Conn.*

Received 5 August 1959

A method of cloud-chamber operation is described which in certain types of experiments can overcome the disadvantages usually inherent in the use of this instrument. The technique consists of counter-control of both the cloud chamber and the accelerator beam. By utilizing this method, it is possible to operate at beam levels considerably higher than otherwise permissible.

1. Introduction

In experiments utilizing expansion cloud chambers in conjunction with pulsed accelerators, the maximum rate at which data can be accumulated is often determined by two factors:

(a) the recycling time of the cloud chamber, and

(b) the number of background tracks which can be tolerated in a photograph.

Of these, the recycling time determines the rate at which the chamber may be expanded, and the background limit frequently sets the allowable beam intensity of the accelerator. This paper reports on a technique by means of which it is often possible to increase considerably the rate of accumulation of data.

The method described here consists of using countercontrol both to trigger the expansion of the chamber and to cut off abruptly the beam from the accelerator.

2. Accelerator Beam

The accelerator is operated in such a fashion as to eject a beam on each pulse with constant intensity for as long a time as possible. It is also necessary to have the possibility of aborting, upon receipt of a trigger-signal, that portion of the beam-pulse which has not yet been ejected.

In an experiment in which the hereindescribed technique was tried, the Bevatron at Berkeley was operated to give a beam "spillout" of 200 milliseconds, and a 500-millisecond spill was attained on occasion. (The latter setting was not used, however, since it rendered the Bevatron useless for other experiments which were being conducted simultaneously.) During beam-ejection, the target was located in the vacuum tank just outside of the equilibrium beam orbit. The beam was gradually steered outward onto the target by appropriate variation of the radio frequency accelerating voltage. Since this occurs while the magnetic field of the accelerator is still increasing, the beam-orbit which is expanding onto the target will cease expanding and start to contract away from the target when the accelerating radio-frequency voltage is turned off. The trigger-signal from the counters was used to turn off the accelerating R.F. and thus to arrest the beam of particles emerging from the target.

3. The Cloud Chamber

The cloud chamber is operated in normal counter-controlled manner. That is to say, the chamber is expanded only when a trigger-

† Supported in part by the U.S. Atomic Energy Commission.

signal from the counter-system is received. A strong clearing field which is cut off at the time of the triggerpulse provides that almost all ions in the chamber previously created by the traversal of charged particles have been swept out.

In the Berkeley experiment mentioned earlier, a field of about 600 V/cm was used. The experiment utilized a multiplate chamber with plate separation of about 2.5 cm. The resulting sweep-time turned out to be about 2 milliseconds. In order to avoid poisoning of the chamber by discharges between plates and by electrolysis of liquid on wet surfaces, the field was turned on only during the periods of beam-ejection.

As an integrating instrument, the cloud chamber renders photographable the trajectories of those ionizing particles which have traversed the sensitive volume during a period of 20 to 100 milliseconds starting at the time the clearing field is removed and the expansion initiated. Tracks corresponding to particles which have traversed the region just prior to the expansion will be seen as incompletely swept out, older ones being almost completely removed.

4. Operation

The operation of counters, accelerator, and cloud chamber is as follows:

The secondary beam emerging from the target traverses the cloud chamber with uniform intensity during a period of time T on every accelerator pulse. A system of counters capable of identifying the event to be studied monitors the beam. The counter system then sends the trigger-signal when an event of interest has taken place. The trigger-signal simultaneously turns off the cloud-chamber clearing field, starts the cloud-chamber expansion, and halts the secondary beam by the method described earlier.

Fig. 1 shows in a schematic manner the effect of the occurrences during an accelerator pulse in which an "event" has been identified. It is seen that the clearing field which would have been left on for the duration of accelerator pulse is cut off abruptly at the time t of the trigger. At the same time, the accelerator beam is shut off so that no more particles will traverse the chamber during its sensitive time. The effective beam, then, corresponds to those tracks which are not completely cleared, the tracks of particle-traversals which correspond in time to the trigger-signal, and tracks from those particles which traverse the chamber during the time that the beam is being turned off. The time duration of the "effective beam" is about 5 milliseconds.

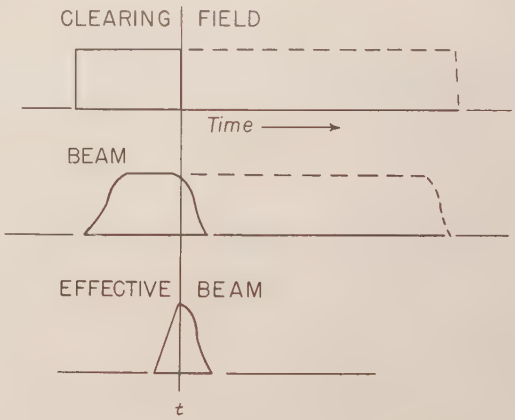

Fig. 1

5. Examples of Experiments in which this Technique may be Exploited to Advantage

The experiment at Berkeley mentioned earlier was designed to study interactions of K^+ particles. The chamber was located in a beam of π^+ mesons and K^+, with a K-to-π ratio of about one to 150. An intensity-level of thirty to fifty π-mesons per accelerator-pulse was used. Figs. 2 and 3 demonstrate the ability of the technique to permit selection of an individual track. The photographs were taken from the Berkeley K^+ experiment. Fig. 2 shows the track of a K^+ meson coming to rest near the center of the chamber and subsequently undergoing decay. The track of the charged decay-product is seen in the lower left-hand corner of the picture. Fig. 3 is a picture taken under similar beam-level conditions, showing the beam-background resulting from the omission of selective triggering.

It might be of interest to study high-energy interactions of antiprotons in heavy materials. A multiplate cloud chamber might then be used in a beam of π^--mesons and antiprotons. If ten tracks can be tolerated in one picture, it should be possible to operate the accelerator to give a beam of 1000 π^- per pulse, so that an antiproton track might be photographed at the rate of about one per hour.

considerably higher intensity-levels in the secondary beam than would be possible if other track-detection techniques were used.

The technique described also has certain drawbacks which must be considered:

First, the method requires sufficient control of the accelerator to make it difficult in many cases to operate other experiments simultaneously in a mutually compatible manner.

Fig. 2

Fig. 3

6. Limitations and Drawbacks

The usefulness of the above technique is limited to experiments where the following factors apply:

(a) the event to be studied is accompanied by otherwise unavoidable background;

(b) the event to be studied does not occur so often as to make the recovery time (dead time) of the chamber an important factor.;

(c) the occurrence of an "event" can be electronically established.

Where applicable, this technique permits

Second, electronic identification of events must be efficient enough to avoid expanding the chamber frequently on false counts. Since every expansion is followed by a recycle period T during which the chamber is inoperative, false triggerpulses must not occur with a frequency comparable to $1/T$. Thus, in an experiment on antiprotons in an antiproton beam in which the π^--meson-to-antiproton ratio is 500 000/1, it would be necessary to reject π^- related counts with an efficiency of $1\text{–}10^{-5}$.

7. Power Supply for Clearing

The clearing-field power supply must be able to provide voltages in the kilovolt region. The supply must deliver this voltage to the electrodes in a pulsed manner, i.e., the voltage should be turned off between accelerator-beam pulses. It is also necessary to be able to cut the clearing-field voltage to zero (or a small value) in times comparable to 10 microseconds whenever a trigger-signal is received. Such a power supply has been designed and constructed by G. F. Schrader†.

† G. F. Schrader, A Gated High Voltage Supply for Cloud Chamber Clearing Fields, UCRL 3408 (1957).

NUCLEAR INSTRUMENTS AND METHODS 5 (1959) 165–169; NORTH-HOLLAND PUBLISHING CO.

AIMANTS DE FOCALISATION ET D'ANALYSE DU CYCLOTRON DE SACLAY

J. THIRION et J. SAUDINOS

Section des Réactions Nucléaires à Moyenne Energie, C.E.N., *Saclay*

Reçu le 5 août 1959

Two strong gradient magnets deflect and refocus the beam of the cyclotron in both directions. The beam is then analysed by a double focusing magnet which gives a definition in energy of 1.5/1000 for 2 mm slits. This analyser can also be used for analysing secondary particles.

L'ensemble d'aimants qui est présenté est en fonctionnement depuis environ un an.

1. Disposition Générale

Les données de l'implantation des aimants successifs† ont été choisies en fonction des salles existantes et pour les buts suivants:

1. Obtenir un faisceau analysé en énergie dans la salle d'expériences; si possible, obtenir des énergies différentes par absorbants placés avant l'analyse du faisceau.

2. Disposer d'un analyseur de particules émises par les cibles, tout au moins pour des angles d'observation de 0 à 60°.

Pour réaliser la première condition, le faisceau sorti est focalisé de façon à disposer des fentes-objet situées dans la salle du cyclotron. L'aimant d'analyse, situé dans la salle d'expériences, permet de définir l'énergie avec précision. Des absorbants peuvent être introduits au voisinage des fentes-objet; la diffusion multiple correspondante n'est pas prohibitive, les dimensions de l'aimant d'analyse étant grandes.

Pour réaliser la seconde condition, il a été envisagé de monter les cibles dans la salle du cyclotron et d'utiliser l'aimant d'analyse pour les particules émises. La possibilité de faire varier assez facilement l'angle d'analyse de 0 à 60° existe grâce à un aimant d'orientation situé dans la salle du cyclotron. Toutefois, aucune expérience de ce type n'a encore été effectuée.

2. Focalisation du Faisceau

Le faisceau sorti est très divergent dans le plan horizontal et relativement plat dans le sens vertical. Un système de deux aimants à gradient alterné†† permet de focaliser le faisceau dans les deux sens sur des fentes situées dans la salle du cyclotron. Ce système permet également, dans certaines limites, une orientation horizontale. La déflexion totale de 22° est indispensable dans notre cas pour des raisons géométriques; elle est insuffisante pour obtenir une analyse en énergie.

Les caractéristiques des deux aimants sont: $R = 250$ cm, $n = \pm 16$, $\theta = 10°$. Les pièces polaires ont un profil hyperbolique. L'entrefer au centre est de 5 cm; la largeur des pièces polaires est de 20 cm. Le gradient a été mesuré par la méthode de la bobine vibrante et est satisfaisant. La variation est inférieure à 3% pour une zone de 10 cm. Le premier aimant opère un resserrement dans le plan vertical. Environ 10 μA sur une zone de 1 cm^2 sont obtenus dans la région de focalisation. Une focalisation meilleure par variation de la distance entre les deux aimants ou par compen-

† Autres ensembles décrits dans les références suivantes: D. R. Bach, W. J. Childs, R. W. Hockney, P. V. C. Hough et W. C. Parkinson, Rev. Sci. Instr. 27, No. 7 (1956) 516; O.N.R. 32.505 Rapport No. 2 (mai 1952) Université de Pittsburgh.

†† H. J. Martin et A. A. Kraus, Rev. Sci. Instr. 28, No. 3 (1957), 175. Ces auteurs ont développé un spectromètre de même principe.

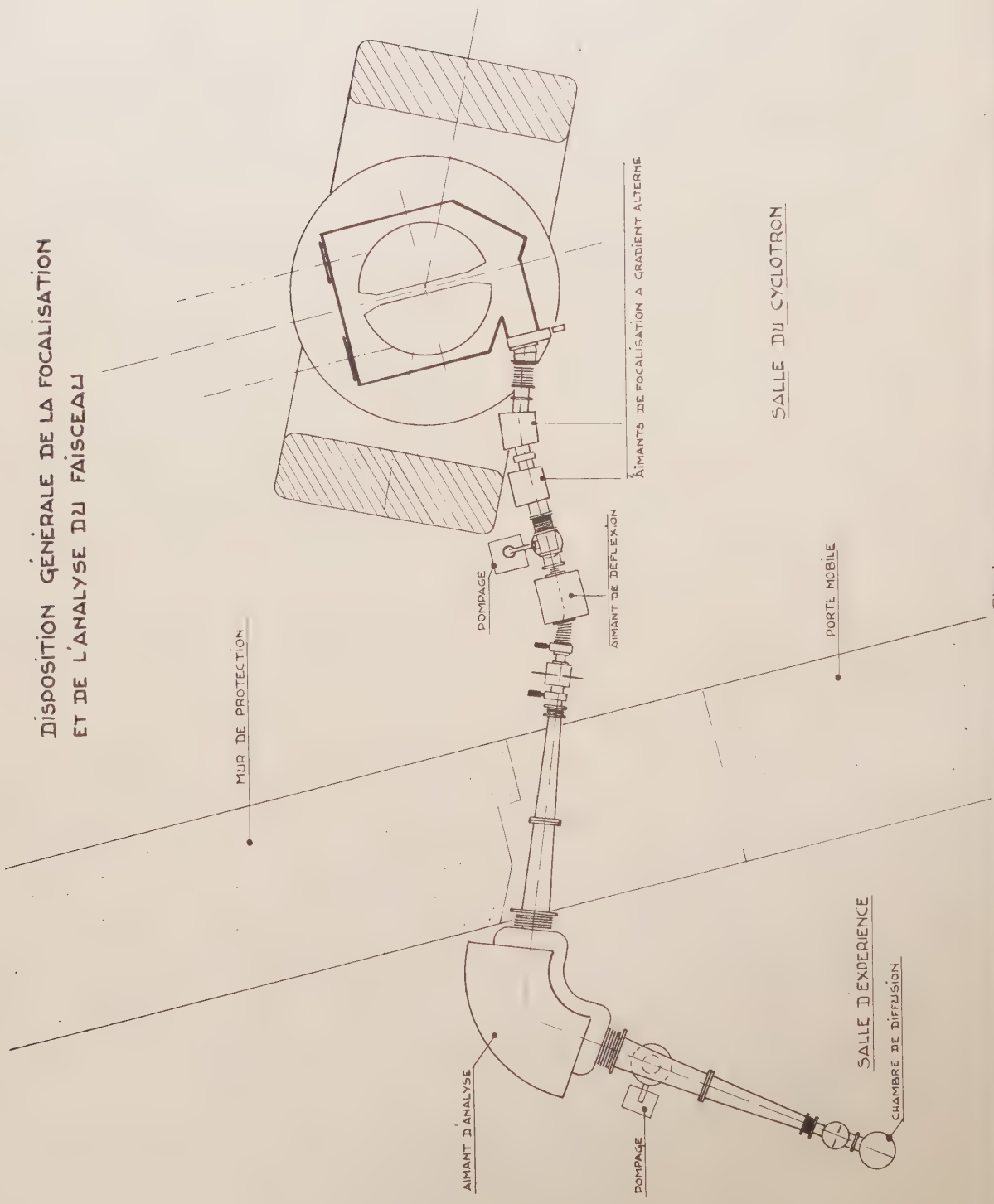
DISPOSITION GÉNÉRALE DE LA FOCALISATION
ET DE L'ANALYSE DU FAISCEAU
SALLE DU CYCLOTRON
AIMANTS DE FOCALISATION A GRADIENT ALTERNÉ
POMPAGE
AIMANT DE DÉFLEXION
MUR DE PROTECTION
PORTE MOBILE
AIMANT D'ANALYSE
POMPAGE
SALLE D'EXPÉRIENCE
CHAMBRE DE DIFFUSION

Fig. 1

sation des champs de fuite n'a pas été essayée, les résultats actuels étant suffisants.

Un troisième aimant à champ homogène sert à l'orientation supplémentaire du faisceau. Il permet des déviations de $\pm 30°$. Il est utilisé pour obtenir un faisceau analysé dans la salle d'expériences à un endroit commode. Il est envisagé de s'en servir pour obtenir facilement des distributions angulaires de 0 à 60° avec l'aimant d'analyse.

3. Aimant Analyseur

L'aimant analyseur est un aimant en C à double focalisation, l'angle de déflexion étant de 70°. Le rayon de courbure moyen est de 90 cm. Les pièces polaires sont coniques. Des barrettes en fer placées aux rayons maximums et minimums compensent les effets de bord. La hauteur de l'entrefer est de 10 cm, la largeur utile de 30 cm. Des diaphragmes, réglables sous vide à l'entrée et à la sortie de l'entrefer,

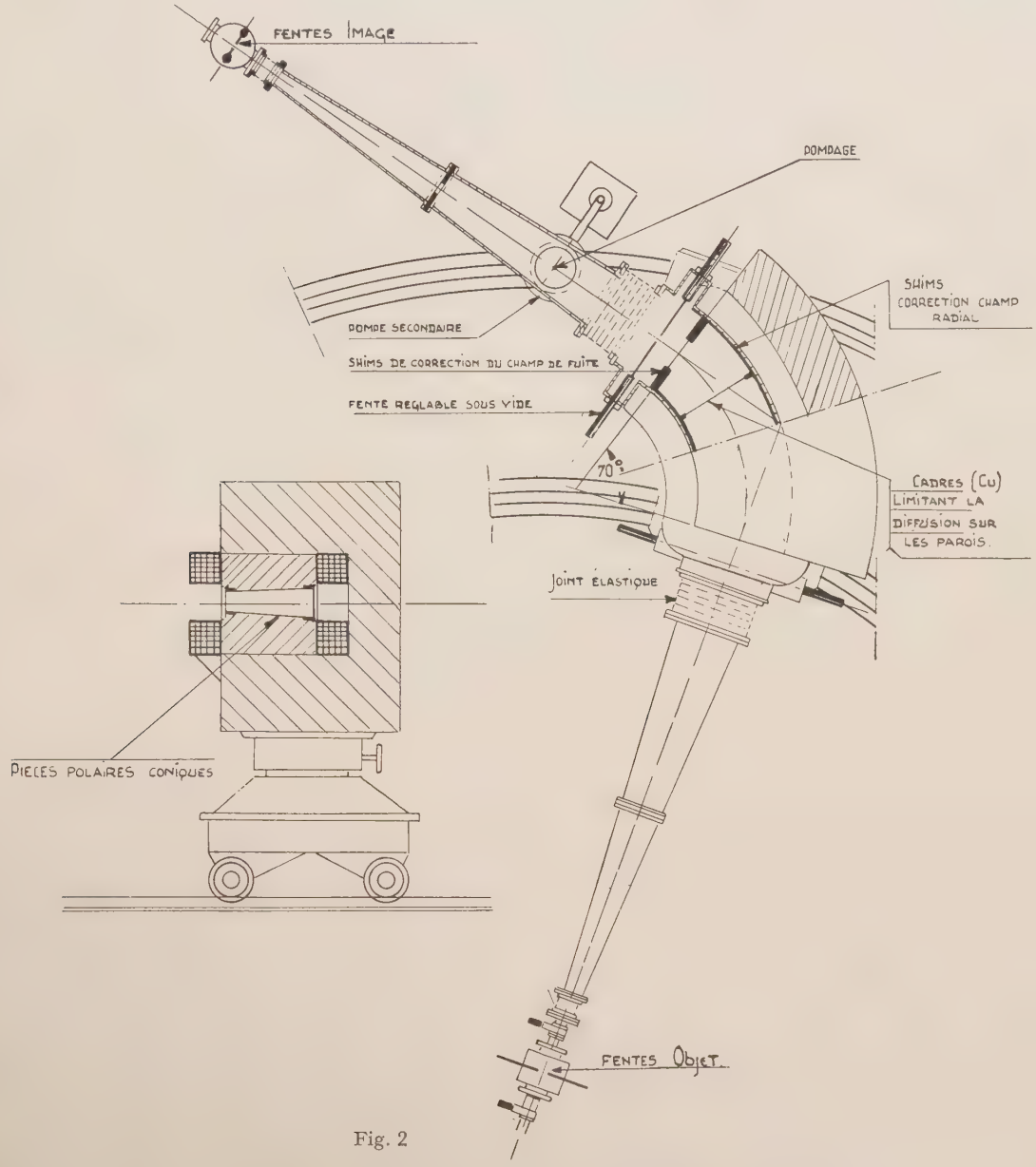

Fig. 2

permettent de faire varier l'ouverture utile (fig. 2).

Le courant de l'aimant est constant à 5×10^{-4} près. Le paramètre $n = (-r_0/Hz_0) \cdot (dH_r/dr)$ est égal à 0.5 pour le rayon moyen $r_0 = 90$ cm et varie linéairement en fonction de r, la pente étant de l'ordre de 0.25.

Pour des largeurs objet et image de 2 mm, on obtient une résolution $\Delta E/E$ de 1.6×10^{-3} pour une largeur utile de l'entrefer de 10 cm, et une résolution de 2.5×10^{-3} pour une largeur utile de 30 cm (fig. 3).

Ces résultats sont en bon accord avec le

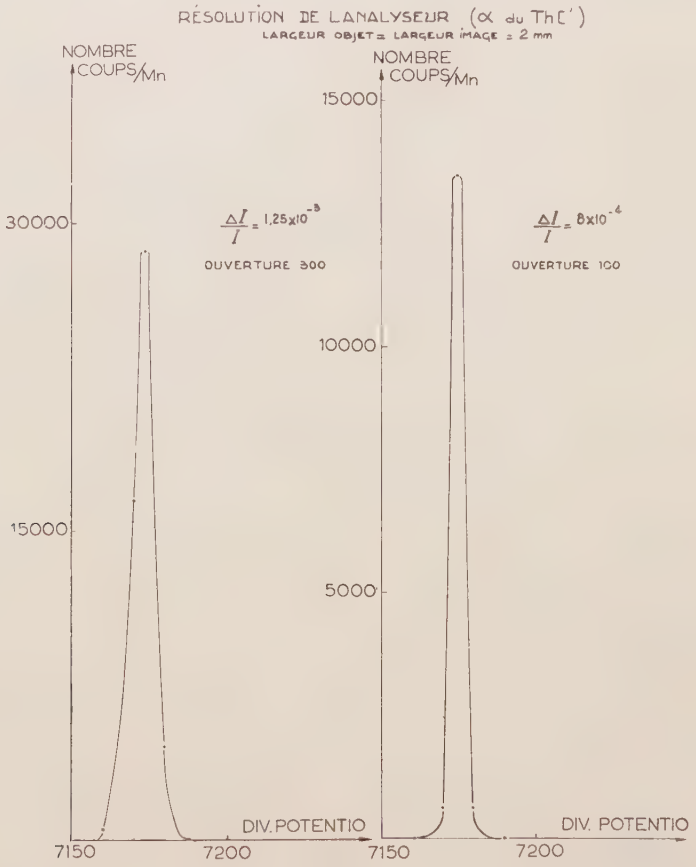

Fig. 3

La distance image mesurée grâce à une instabilité de la focalisation verticale qui apparaît dans la méthode du fil est de 2.84 ± 0.05 m en accord avec le calcul théorique qui prévoit 2.80 m pour une distance objet de 2.80 m. On a utilisé pour l'étude de la résolution de l'analyseur le rayonnement de 8.776 MeV du thorium C'. On a mesuré d'abord la résolution à faible ouverture et l'angle de déviation totale 77° s'est avéré le plus favorable. Ensuite, la zone utile a été augmentée en plaçant des shims aux bords des pièces polaires, la compensation étant plus forte pour les faibles rayons.

calcul théorique : à faible ouverture, la théorie du premier ordre donne, pour la résolution, 1.2×10^{-3}.

Des variations de la distance objet de 5 cm n'affectent pratiquement pas la résolution.

CARACTÉRISTIQUES DE L'AIMANT ANALYSEUR

Rayon de courbure moyen : 90 cm
Angle du secteur magnétique : 70°
Paramètre $n = 0.5 \pm 4\%$
Distance objet : 280 cm
Distance image calculée : 280 cm
Distance image mesurée : 284 ± 5 cm
Résolution pour une largeur objet = largeur image = 2 mm

ouverture 10 cm $\Delta E/E = 1.6 \times 10^{-3}$
ouverture 30 cm $\Delta E/E = 2.5 \times 10^{-3}$
Entrefer moyen: 10 cm
Angle solide maximum: 2.7×10^{-3} stéradian.

4. Définition et Energie du Faisceau

Lors des expériences de diffusions élastique et inélastique, l'aimant analyseur a servi à définir le faisceau. On a travaillé à faible ouverture (5 cm de largeur utile de l'entrefer) et l'énergie du faisceau est constante à $\pm$ 20 keV. Pour mesurer l'énergie du faisceau, on a placé sur son trajet une feuille d'aluminium d'une épaisseur de l'ordre de 250 μg. Elle ne change pratiquement pas l'énergie du faisceau mais transforme l'hydrogène moléculaire une fois ionisé H_2^+ en protons H^+. Le champ magnétique étant alors voisin de celui utilisé pour ThC', on évite les erreurs dues à la saturation magnétique.

La largeur totale du faisceau avant analyse est de 2%; on obtient ainsi 11.1 $\pm$ 0.05 MeV pour l'énergie correspondant au point de fonctionnement.

On a effectué la même mesure pour des protons ralentis par une feuille de 0.1 mm de béryllium. On obtient 10.45 $\pm$ 0.02 MeV.

L'aimant a été réalisé avec précision par la Société Batignolles Chatillon. Nous remercions particulièrement M. Rougier de cette Société pour ses contributions précieuses. Nous remercions également l'équipe du cyclotron de Saclay qui a participé à la mise au point des aimants.

NUCLEAR INSTRUMENTS AND METHODS 5 (1959) 170–176; NORTH-HOLLAND PUBLISHING CO.

EFFICACITE ET DISPERSION DU TEMPS DE COLLECTION DE LA LUMIERE D'UN DETECTEUR DE ČERENKOV A PAROIS REFLECHISSANTES

J. SÉGUINOT, M. SCHÉRER et J. TEIGER

Laboratoire de Physique Corpusculaire, Université de Caen

Received 25 April, 1959

The distribution of rise time of Čerenkov pulses has been measured for a Čerenkov detector of 23 × 10 × 10 cm³ with reflecting outer surfaces, and constant output level. A method of study of linings is proposed.

An efficiency of détection nearly 100% was measured. This detector is associated with cloud chambers for scattering measurements of Mu mesons.

1. Introduction

Nous avons construit un détecteur de Čérenkov destiné à être associé à une installation de chambres de Wilson et devant permettre la séparation des mésons mu des protons, pour des moments compris entre 0.15 et 1 GeV/c, du rayonnement cosmique au niveau de la mer.

On sait que l'amplitude de l'émission Čérenkov est donnée par la relation[1])

$$N = F(\beta,n)\cdot\frac{2\pi z\Delta\lambda}{137\lambda^2}\,l$$

où

N, est le nombre de photons émis dans la bande comprise entre λ et $\lambda + \Delta\lambda$

l, le parcours de la particule dans le milieu et,

$$F(\beta,n) = 1 - \frac{1}{\beta^2 n^2}$$

n, étant l'indice de réfraction du diélectrique. Soit encore,

$$F(\beta,n) = 1 - \frac{1}{n^2}\left[1 + \left(\frac{m_0c^2}{pc}\right)^2\right]$$

où pc est le moment de la particule.

On trouvera sur la fig. 1, $F(\beta,n)$ tracée pour les mésons μ et les protons lorsque le milieu diélectrique est de l'eau pure.

On peut voir ainsi, que l'information donnée par le détecteur de Čérenkov permet, connaissant le moment de la particule incidente d'écarter ou de sélectionner les protons pour l'intervalle d'énergie déjà défini. Pour l'eau, et une sensibilité spectrale du type S.11 des photomultiplicateurs, l'émission Čérenkov correspond pour $\beta = 1$ à environ 210 photons utilisables par cm de trajectoire.

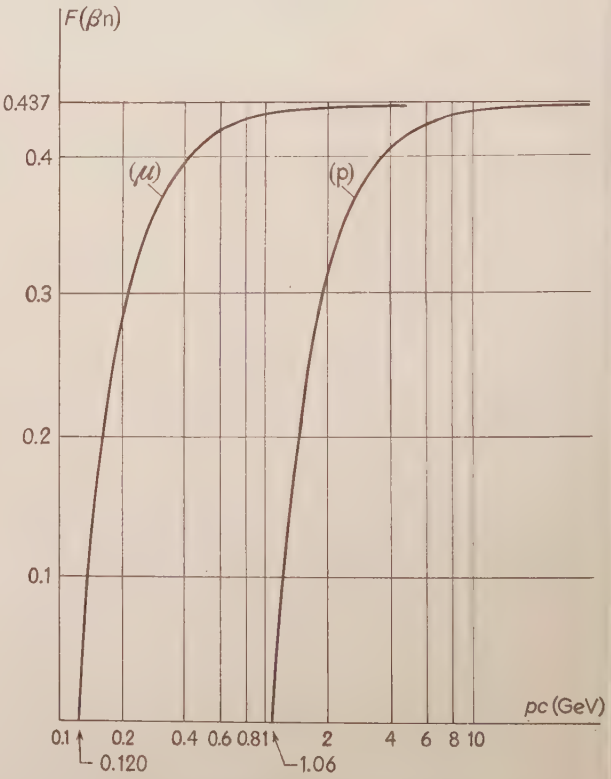

Fig. 1. Taux relatif classique d'émission de quanta pour l'eau.

[1]) J. V. Jelley, Čerenkov Radiation, and its applications (Pergamon Press).

Il était demandé à ce compteur une efficacité de détection aussi grande que possible, tant pour le seuil de façon à éviter une coupure inférieure trop haute de l'énergie, que pour sa géométrie, l'efficacité de détection devant rester constante quelque soit le point d'impact de la particule.

Cette disposition imposée par la nécessité de blinder magnétiquement les P.M., pour un champ de fuite de 200 oersteds, avec un encombrement limité, n'est pas favorable au voisinage du seuil de l'émission Čérenkov. En effet, la surface d'onde conique est alors très ouverte de sorte que, pour des particules arri-

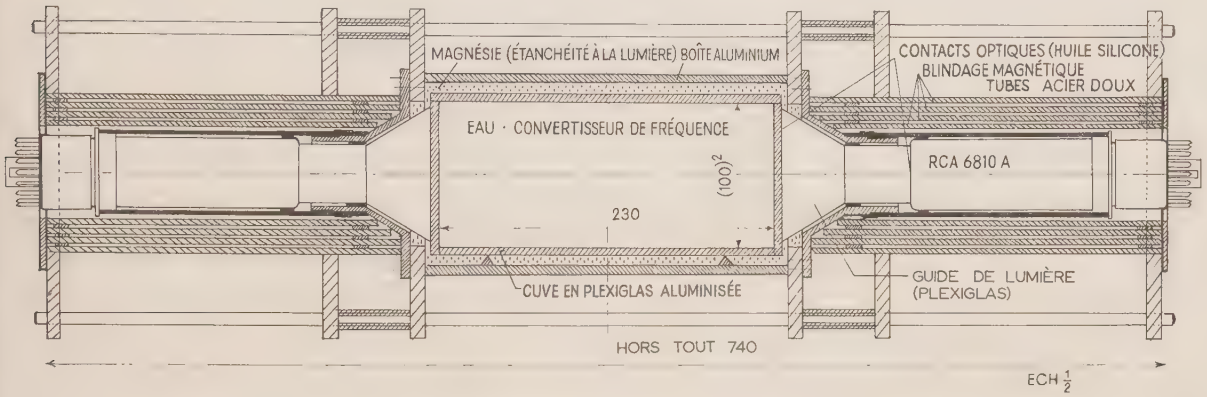

Fig. 2. Section longitudinale du détecteur.

Nous décrirons dans cette note la réalisation du détecteur, et quelques uns des tests qui ont été utilisés pour son étude. Une méthode générale d'investigation des radiateurs de grandes dimensions peut être déduite des résultats obtenus.

2. Description du Détecteur-Chaine Électronique

Cuve Čérenkov: sa forme et ses dimensions sont conditionnées par la géométrie du reste de l'installation (chambres de Wilson, champ magnétique). C'est un parallélipipède de plexiglas de dimensions intérieures $23 \times 10 \times 10$ cm³, rempli d'eau bi-distillée dans laquelle on a incorporé un convertisseur de fréquence, destiné à réémettre isotropiquement dans le bleu, l'émission U.V. A un revêtement diffusant des parois de la cuve, à priori meilleur mais difficile à obtenir de facon valable au point de vue optique, nous avons préféré un revêtement réfléchissant par aluminisation des parois extérieures, obtenu par évaporation thermique.

Ce radiateur est regardé (fig. 2) à chaque extrémité au moyen de guides de lumière en plexiglas, par 2 photomultiplicateurs 6810A RCA. vant verticalement, les photons sont émis presque normalement à l'axe des P.M. Nous verrons que les tests confirment ce point de vue, mais que l'utilisation d'un convertisseur de fréquence permet de rétablir une efficacité de détection optimum. Cette disposition par contre,

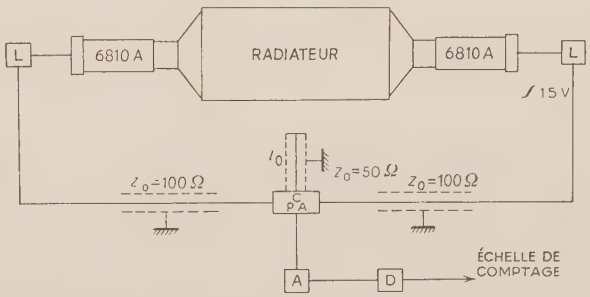

Fig. 3. Diagramme schématique de la chaîne électronique. L = limiteuse d'amplitude (niveau 1.5 V); C = circuit de coïncidence à diode; PA = préamplificateur; A = amplificateur 2 Mc/s; D = discriminateur.

assure une bonne symétrie de collection de la lumière pour des points d'impacts quelconques des particules incidentes.

Le convertisseur de fréquence utilisé, préconisé par Marshall[2]) est le sel de sodium de

[2]) Marshall, Rev. Scient. Inst. **27**, No. 8 (1956).

l'acide amino 2-disulfonique 6–8 naphtalène en concentration de 10 mg/l. Il accroît de 30% l'amplitude de l'émission lumineuse pour la sensibilité spectrale S.11 des P.M. Nous avons vérifié qu'aucune scintillation n'était introduite par ce corps ainsi que le signalait Marshall; par contre celle produite dans le plexiglas des guides de lumière était détectée.

La mise en coïncidence des P.M., en éliminant le bruit de fond permet de travailler à des niveaux de lumière faibles et par suite plus près du seuil de l'émission.

Le circuit électronique de coïncidence est du type classique de Bell Graham et Petch[3]) dont la chaîne est schématisée ci-dessous par la fig. 3.

3. Étude du Détecteur

Les propriétés de résolution et de durée de collection de la lumière du radiateur ont été étudiées en mettant en coincidence rapide un des 6810A du détecteur avec un 5819 équipé d'un scintillateur plastique Sc. Le dispositif

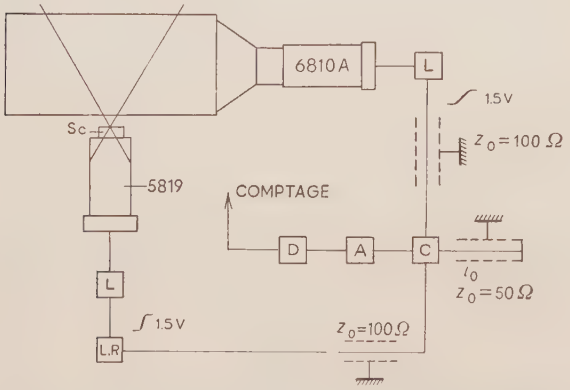

Fig. 4. Dispositif expérimental d'étude du radiateur. L.R. est une ligne à retard constituée par du câble 100 ohm qui est insérée sur la ligne du 5819 ou du 6810A.

expérimental est celuide la fig. 4.

L'électronique est la même que précédemment, le niveau de sortie des E180F étant réglé à 1.5 V sous 100 ohms. La longueur $2\,l_0$ du câble 50 ohms, définit le temps de clipping des impulsions (coupure des impulsions dans le temps par l'utilisation d'un câble court circuité) et l_0 de façon approximative le pouvoir de résolution du sélecteur (mi-largeur à mi-hauteur de la courbe de résolution).

La fig. 5 donne quelques unes des courbes de résolution obtenues de cette facon, où le nombre d'impulsions de coincidence est porté en fonction du retard en mètres de câble de 100 ohms introduit sur la ligne du scintillateur ou du Čérenkov.

Les courbes,

(a) et (b) correspondent à de l'eau pure + convertisseur de fréquence

(a) pour $l_0 = 1$ m

(b) pour $l_0 = 1.9$ m

(c) à de l'eau pure pour $l_0 = 1.9$ m.

On peut voir, bien que toutes les courbes de paramètre l_0 ne soient pas représentées, qu'elles sont sensiblement centrées sur un même retard Δt_0, retard qui a été corrigé pour tenir compte de la différence de temps de transit des élec-

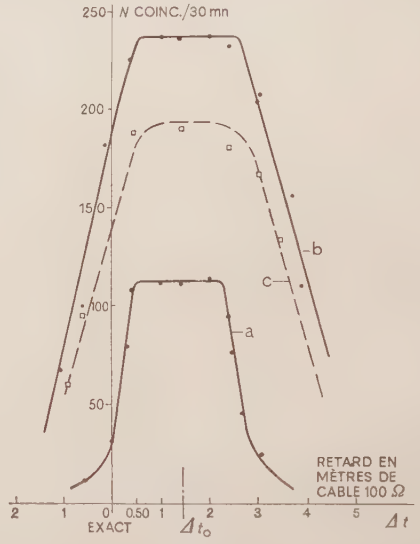

Fig. 5. Courbes de résolution relevées avec le dispositif de la fig. 4: (a) pour $l_0 = 1$ m; (b) pour $l_0 = 1.9$ m, lorsque l'eau + un convertisseur de fréquence sont utilisés; (c) pour $l_0 = 1.9$ m et de l'eau.

trons dans les deux types de photomultiplicateurs. Le réglage du seuil de discrimination de la diode du circuit de coincidence doit être soigneusement contrôlé si on veut obtenir des courbes qui soient répétables et cohérentes, le gain de l'amplificateur qui suit étant élevé.

La courbe de la fig. 6 correspond pour $\Delta t = cst = \Delta t_0$, au nombre d'impulsions de

[3]) I. A. D. Lewis et F. H. Wells, Millimicrosecond Pulse Technique (Pergamon Press).

coincidence en fonction de l_0. Normée sur un temps de comptage de 30 min, elle correspond en fait à des relevés, s'étendant pour chaque point sur un temps de l'ordre de 24 h.

L'analyse suivante du fonctionnement montre clairement l'intérêt de cette courbe dont la signification physique est liée directement aux caractéristiques de collection de la lumière.

On peut admettre que l'impulsion du scintillateur, qui définit avec une précision suffisante l'instant exact du passage de la particule, a un temps de montée rapide (de l'ordre de 2×10^{-9} s pour 1.5 V) indépendant du β de la particule incidente, et que pour l_0 donné, sa forme est standard et pratiquement rectangulaire (l_0 étant grand vis à vis du temps de montée, sauf pour le 1er point de la courbe).

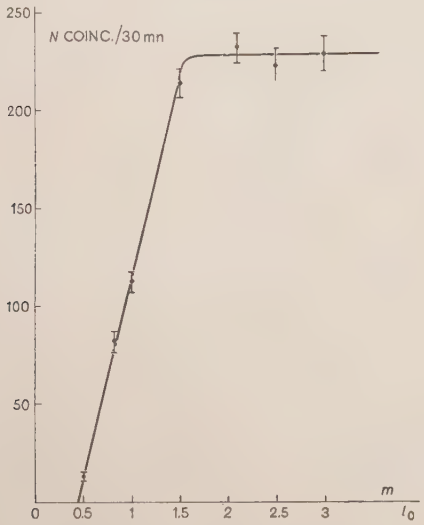

Fig. 6. Variation du taux de coincidence, pour le montage de la fig. 4, un fonction de la longueur l_0 du câble 50 ohm de coupure du circuit de coincidence.

Les impulsions Čérenkov ont, par contre, une certaine distribution de leur temps de montée indépendante des caractéristiques de temps de montée du photomultiplicateur utilisé; pour le scintillateur au contraire, le temps de montée est pratiquement celui du P.M.; Ces temps, longs on va le voir dépendent de la vitesse de collection des n premiers photons nécessaires pour donner une impulsion électrique à la sortie du P.M. de 1.5 V (constante d'intégration du P.M.: 0.1 μs). Cette vitesse dépend elle-même d'une part, du spectre des mésons qui traversent le dispositif (par l'amplitude de la radiation émise) et de leur distribution azimuthale autour de la verticale du scintillateur, et d'autre part, des caractéristiques du radiateur (forme, revêtement).

Toutefois, si pour chaque point de la courbe 6, les comptages sont faits sur des temps longs, les

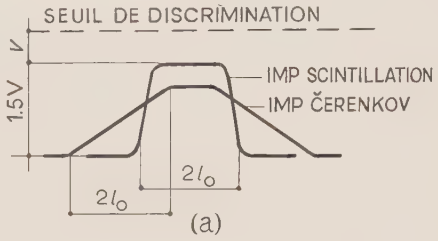

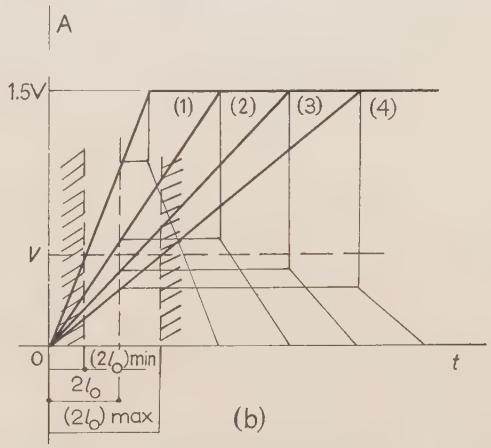

Fig. 7a et 7b. Représentation schématique du principe de fonctionnement du circuit de coincidence, qui fonctionne pour le montage utilisé, en discriminateur de temps de montée.

conditions de travail dûs aux premiers paramètres seront les mêmes, de sorte qu'en valeur relative on s'en sera affranchis. Les fluctuations inhérentes au P.M. n'interviennent pas.

A une distribution de temps de montée, correspondra après clipping (pour un choix convenable de l_0) une distribution en amplitude des impulsions Čérenkov. A un temps de montée long correspondra une amplitude faible.

La valeur Δt_0, correspond au retard optimum

pour lequel les impulsions Čérenkov et de scintillation sont en moyenne centrées. On peut schématiser la coincidence par la fig. 7a ci-contre, qui montre qu'après discrimination l'amplitude de l'impulsion résultante de coincidence ne dépend que de l'impulsion Čérenkov proportionnellement à $2\,l_0$ (approximativement car la somme des 2 impulsions n'est pas strictement linéaire) si pour $2\,l_0$ l'impulsion n'a pas atteint son maximum.

Sur la fig. 7b on a tracé une distribution de quelques impulsions, dont on a volontairement simplifié la forme, pour montrer le principe de la mesure. On peut voir que pour une longueur de clipping $2\,l_0$ quelconque, la largeur des impulsions mises en forme varie beaucoup, et que pour un seuil de discrimination déterminé on ne comptera que les impulsions dont le temps de montée est tel, que pour $2\,l_0$ leur amplitude soit supérieure au seuil choisi. Dans ce cas, les impulsions (1) et (2) seulement seraient comptées.

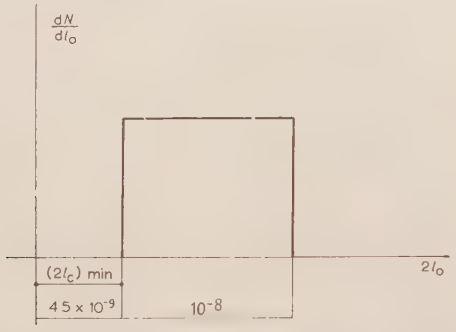

Fig. 8. Distribution différentielle des temps de montée des impulsions du radiateur de Čérenkov, pour un niveau de 1.5 V.

Lorsqu'on fait varier $2\,l_0$ entre $(2\,l_0)_{min}$ et $(2\,l_0)_{max}$ on relèvera donc le spectre intégral de la distribution des temps de montée des impulsions Čérenkov. La fig. 6 montre que ce spectre est parfaitement linéaire pour l_0 compris entre 0.50 et 1.60 m autrement dit, la distribution des temps de montée est rectangulaire (fig. 8) entre 1 et 3.2 m. Elle indique en outre très bien, la valeur $(l_0)_{min}$ prévue par la fig. 7b à la sensibilité près de l'appareillage. $(l_0)_{min}$ et $(l_0)_{max}$ correspondent à des temps longs puisque: $2\,(l_0)_{min} = 4.5 \times 10^{-9}$ s et $2\,(l_0)_{max} = 1.5 \times 10^{-8}$ s. Cette dernière valeur définit la valeur minimum qu'il faut utiliser pour le fonctionnement normal du sélecteur de coincidence avec les 2 P.M. du Čérenkov. Nous avons adopté:

$$2\tau = 2 \times 10^{-8}\ \text{s}\,.$$

La méthode qui vient d'être exposée peut être utilisée pour étudier, par comparaison, les propriétés de collection de la lumière des revêtements destinés à des radiateurs de Čérenkov de grandes dimensions. Un $(l_0)_{min}$ aussi faible que possible et une largeur minimum de la distribution des temps de montée correspondront à un meilleur rendement optique de l'ensemble et par suite à un meilleur facteur de mérite du revêtement.

Les renseignements qui sont obtenus de cette facon sont en fait plus complets que ceux que l'on déduit d'une analyse d'amplitude des impulsions, faite à l'aide du rayonnement cosmique.

Le retard $\Delta t_0 = 6.3 \times 10^{-9}$ s est la valeur moyenne du retard entre le passage de la particule et l'instant de la coincidence.

Par ailleurs, les courbes (b) et (c) de la fig. 5 montrent qu'une augmentation de 24% de l'efficacité de détection est obtenue par incorporation d'un convertisseur de fréquence. Cette efficacité sera déterminée plus loin.

La symétrie des résultats a été vérifiée lorsqu'on utilise l'un ou l'autre des deux P.M. du détecteur.

4. Efficacité Géométrique Relative

Elle est déterminée par la différence du taux de comptage lorsque l'on place le scintillateur successivement au deux extrémités de la cuve. Δt_0, dans ces conditions varie d'environ 10^{-9} s. Les comptages normés sur 30 min, pour Δt_0 et pour $l_0 = 1.90$ m sont résumés dans le tableau ci-dessous.

L'angle solide plus important lorsque le scintillateur est au milieu de la cuve, est responsable de l'augmentation du taux de comptage.

L'efficacité relative déduite de ces chiffres,

est de 91% pour l'eau pure, et de 97% pour l'eau additonnée d'un convertisseur de fréquence, ce qui constitue une augmentation très sensible.

	Sc près P.M. Čérenkov	Sc milieu cuve	Sc Côté opposé P.M Čérenkov
Eau pure	167	180	153
Eau pure + conv. de fréquence	194	233	187

5. Efficacité de Détection

L'efficacité de détection est celle du compteur lorsque les deux P.M. dont il est équipé sont montés en coïncidence. La courbe de résolution (taux de comptage en fonction du retard introduit sur l'un ou l'autre des P.M.) obtenue

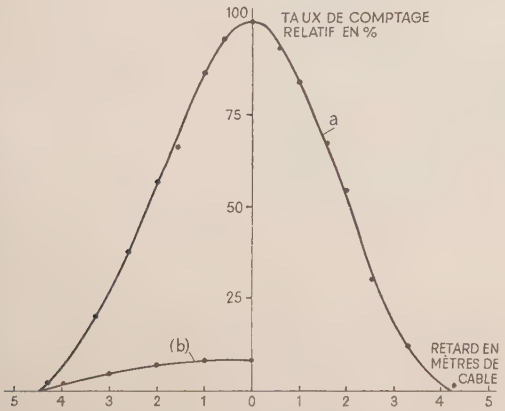

Fig. 9. Courbe de résolution relevée pour le montage normal de la fig. 3. l_0 est égal à 1.90 m. (a) = cuve remplie d'eau + convertisseur de fréquence (b) = cuve vidée.

dans ces conditions, pour $l_0 = 1.90$ m et lorsqu'un convertisseur de fréquence est utilisé, est donnée par la courbe (a) de la fig. 9. Elle correspond à un réglage du rapport signal/bruit de fond, à la sortie de l'amplificateur, de 5. La courbe (b) dans les mêmes conditions, a été relevée cuve vidée. Elle donne l'effet Čérenkov dans le plexiglas des guides et dans l'air de la cuve.

Le maximum de la courbe (a) correspond à un taux de comptage moyen de 260 cps/min. Après correction des comptages parasites, 240 cps/min résultent de particules qui ont effectivement traversé la cuve (estimation approximative). Le détecteur fonctionnant dans ces conditions en compteur 4π, on peut estimer le taux de comptage moyen théorique connaissant l'intensité de la radiation cosmique au niveau de la mer. Si I_0 est l'intensité verticale et si on admet une loi de distribution azimuthale de la forme $I_0 \cos^2 \varphi$, le flux de particule qui traverse le compteur est égal à,

$$\tfrac{1}{4}\pi I_0 \,(a^2 + 3ab) = \tfrac{7}{4}\,\pi\, a^2 I_0$$

où, a^2 est la section transversale de la cuve et,
$b = 2a$ sa longueur.

En adoptant I_0[4]) $= 0.83$ dm$^{-2}\cdot$sec$^{-1}\cdot$stérad^{-1} on trouve que l'efficacité en compteur 4π est de l'ordre de 90%. En fait, dans les conditions de l'expérience ou il est utilisé, l'angle solide du détecteur est considérablement réduit. La fig. 10

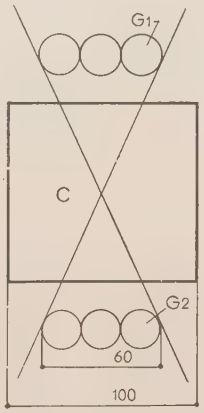

Fig. 10. Montage utilisé pour relever l'efficacité de détection du radiateur de Čérenkov. Le pouvoir de résolution du sélecteur auxiliaire est de 2.5 μs.

montre une partie du téléscope placé sous un filtre en Pb de 80 cm d'épaisseur. Le rapport,

$$\frac{\text{coïncidences } G_1 + G_2 + C}{\text{coïncidences } G_1 + G_2}$$

correspond à un comptage relatif de 96%, soit une efficacité de détection des particules relativistes qui peut être estimée de 100% à la connaissance près du spectre des particules du rayonnement cosmique dans les conditions du test.

[4]) B. Rossi, Revs. Mod. Phys. 20 (1948) 537.

6. Conclusion

La détermination de la distribution des temps de montée des impulsions, dans un radiateur allongé comme celui qui a été décrit ici, est intéressante pour l'étude du facteur de mérite des revêtements de parois (réfléchissants et diffusants) dont les résultats connus sont encore assez confus[5]). Cette étude comparative va être faite au laboratoire avec un nouveau détecteur équipé d'un photomultiplicateur Radiotechnique 54 AVP et les résultats comparés avec l'étude de Mando[6]).

L'augmentation de l'efficacité de détection, par incorporation d'un convertisseur de fréquence, indique un mauvais rendement de collection de la lumière inhérant à l'utilisation d'un réfléchissant, même d'excellent pouvoir réflecteur. Ce rendement est d'environ 20% après incorporation du convertisseur de fréquence (augmentation dûe surtout à l'isotropie de l'émission lumineuse) ce qui correspondrait au rendement que l'on aurait en appliquant les calculs de Mando pour de l'eau pure et une cuve à parois diffusantes.

La largeur de la distribution des temps de montée, trouvée égale à 10^{-8} s, indique par ailleurs un temps total de collection de la lumière qui peut atteindre 0.1 μs pour des particules de $\beta = 1$, ce qui correspond à un temps long pour un détecteur à parois réfléchissantes de cette dimension.

Nous adressons nos remerciements à Messieurs J. Launey et C. Vautier, qui ont bien voulu se charger de réaliser le revêtement d'aluminium du détecteur, et au C.N.R.S. pour les allocations et subventions qu'il nous a accordées.

[5]) Ref. [1]) p. 157. [6]) Mando, Nuovo Cimento **12**, No. 1 (1954).

NUCLEAR INSTRUMENTS AND METHODS 5 (1959) 177–183; NORTH-HOLLAND PUBLISHING CO.

SURFACE ANALYSIS BY CHARGED PARTICLE SPECTROSCOPY†

SYLVAN RUBIN

Stanford Research Institute, Menlo Park, California

Received 16 July 1959

The analysis of the momentum distribution of protons scattered from a solid surface can be used to determine the composition of the surface as a function of depth. Examples of such analyses obtained with a 2-MeV Van de Graaff accelerator and a high resolution magnetic spectrometer are given. The technique is applicable to the detection of all elements to a depth of several microns, with sensitivities in the range of 10^{-8} to 10^{-6} gram per square centimeter.

High resolution nuclear particle spectrometers have been extensively used in nuclear research for the measurement of Q-values of nuclear reactions, leading to precision nuclear mass determinations, and have also been found very useful in measurements of reaction cross sections as a function of incident particle energy. Their latter application results from the fact that it is possible to obtain so-called "thin-target" data, without the necessity of actually making thin targets, because the spectrometer is used to select a narrow momentum interval in the emitted particles, which corresponds to only those particles coming from a thin layer within a thick target.

The analysis of the resulting data is fairly simple if the target can be a pure isotope, but this is not always possible, so that one also wants to be able to use compounds or mixtures of isotopes, which include the particular isotope to be studied. To do this it is necessary, of course, to know the exact chemical composition of the target material, so that the effect of the stopping power of all the "inert" elements can be calculated.

The procedure can be inverted for the analysis of unknown substances. If we already know enough about the nuclear properties of all the elements, as in the case of elastic scattering of protons, we can then use the same techniques to study the chemical composition of unknown substances. Although there are many conventional methods of chemical analysis, most of them are not useful for examining surfaces of a micron or less in thickness. However, such fine depth discrimination is easily obtained with charged particles.

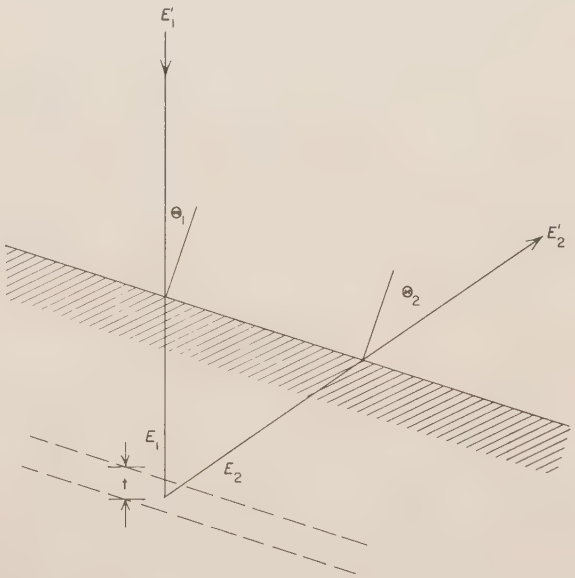

Fig. 1. Geometry of "thin target", t, defined within thick target by particle spectrometer.

Fig. 1 shows the geometry of the intersection of the energetic particles with the thick target. A monoenergetic collimated beam of incident particles is represented by E'_1, the incident energy, which enters the sample at an angle θ_1

† Previously published in Proceedings of the 1958 Accelerator Conference, Cambridge, Mass., sponsored by High Voltage Eng. Corp., Burlington, Mass.

with the normal. Somewhere in the interior a nuclear interaction occurs and a particle, which may be either one of the incident particles elastically scattered by a stationary nucleus, or a new particle emitted in a nuclear reaction, departs toward the surface at an angle θ_2 to the normal, and has an energy E'_2 after it leaves the sample. Of course, the emitted particles travel in various directions, but the spectrometer defines a small range of exit angles around θ_2 and a small range of energy around E'_2.

The effective target thickness is t, measured parallel to the direction of the incident beam. It is a function of the energy range accepted by the spectrometer and of the stopping power of the target material for both incoming and outgoing particles.

E_1 and E_2 are the energies of the incoming and outgoing particles at the position of the nuclear interaction. They differ from E'_1 and E'_2 in proportion to the depth of the effective target layer below the surface of the sample, which is in turn determined by the setting of the spectrometer for a given E'_2 relative to E'_1. As the spectrometer is set for smaller acceptance energy at a given beam energy, the effective target is made to move deeper into the sample.

The yield of particles from a specific interaction with any specific nucleus is given by the equation:

$$Y_j = \left(\frac{\mathrm{d}\sigma}{\mathrm{d}\Omega}\right)_j \Omega_s N n_j t$$

$(\mathrm{d}\sigma/\mathrm{d}\Omega)_j$ is the differential cross section of the interaction; Ω_s is the solid angle of the spectrometer, N is the number of incident particles; n_j is the concentration of the target nuclei of interest per unit of volume, and t is the effective target thickness, measured parallel to the incident beam.

Geometrical factors and the effects of stopping power enter into the magnitude of t [1]).

$$t = \frac{2\,E'_2}{R_c \sum_i n_i \left[\varepsilon_{i1}\left(\frac{\partial E_2}{\partial E_1}\right) + \varepsilon_{i2}\frac{\cos\theta_1}{\cos\theta_2}\right]}.$$

R_c is the momentum resolution factor of the spectrometer, n_i are the concentrations of each kind of nucleus or atom in the target, ε_{i1} are the stopping cross sections of each atom for the incident particles at the energy E_1, and ε_{i2} for the exiting particles at energy E_2; θ_1 and θ_2 are the angles between the normal to the target surface and the incident and scattered particle directions, respectively.

For elastic scattering:

$$\frac{\partial E_2}{\partial E_1} = \frac{E_2}{E_1}.$$

The equations above enable one to measure nuclear reaction cross sections in mixed targets, if the concentrations of the components and their stopping powers are known. Fig. 2 is a set of stopping cross section curves for all elements and for protons from 0.5 to 2.0 MeV, obtained from the compilation of Fuchs and Whaling [2]).

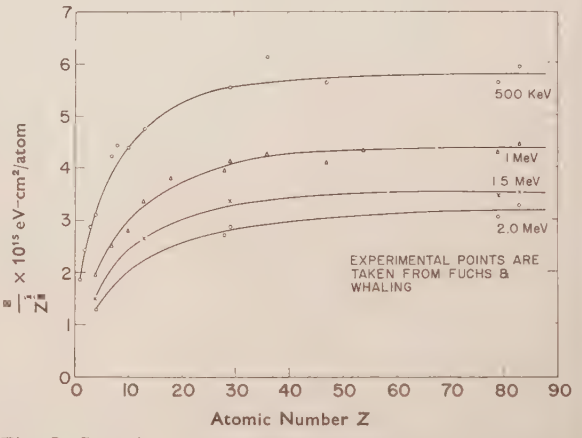

Fig. 2. Stopping cross sections, ε, for protons of various energies.

Most of the work in our laboratory has been concerned with the application of particle spectroscopy to surface analysis. Using elastically scattered protons, we can determine the elemental composition of the surfaces of solid samples, and quantitatively measure concentrations as a function of depth.

Different nuclear masses are identified by measuring the change in momentum of protons scattered from the nuclei in the surface of the

[1]) A. B. Brown, C. W. Snyder, W. A. Fowler and C. C. Lauritsen, Phys. Rev. 82 (1951) 159–181.

[2]) R. Fuchs and W. Whaling, Stopping Cross Sections, Kellogg Radiation Laboratory, California Institute of Technology (unpublished).

sample. The dynamics of elastic scattering gives a relation between the change of momentum at a given angle and the mass of the scattering nucleus.

An approximate equation for the fractional change in velocity on scattering is

$$\frac{\Delta V}{V} \cong -\frac{M_1}{M_0 + M_1}(1 - \cos\varphi)$$

where M_1 and M_0 are, respectively, the masses of the scattered particle and the scattering nucleus, and φ is the scattering angle.

have sufficient energy for adequate penetration into the surfaces of even heavy element materials. The accelerator is operated in the conventional way, with energy stabilization effected by feedback signals from the exit slits of the analyzer magnet. We have paid particular attention to stability of the analyzer magnet, and have made some modifications of the stabilizing circuits to provide long term stability of the analyzing field to about 1 part in 10^4.

The proton beam is focussed on the sample by an electrostatic quadrupole lens which images

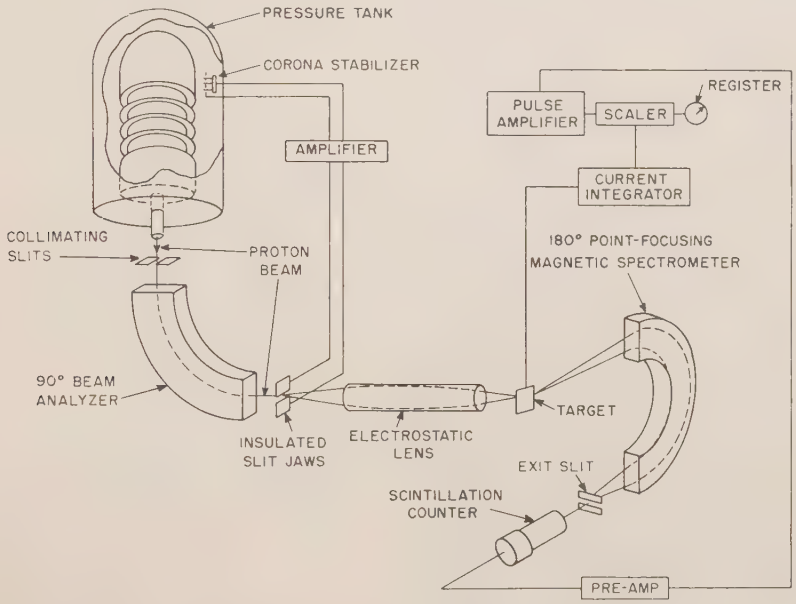

Fig. 3. Schematic drawing of apparatus used for scattering analyses.

Since the change in momentum of a proton scattered from a heavy nucleus is quite small, it is necessary to make measurements with very high precision in order to determine the mass of the scattering nucleus, and it is also necessary to have an incident proton beam with a very small spread in initial momentum. A Van de Graaff generator with a 90° magnetic analyzer is used to produce the proton beam with a momentum spread of about 0.05%. Fig. 3 shows schematically the layout of the apparatus.

For this application, the magnitude of the beam energy is not critical, as long as all the protons have the same energy. Two-MeV protons

the exit slit of the analyzer on the target surface. This makes it possible to analyze small areas of a sample, and also provides the small source dimensions needed for high resolution spectrometry of the scattered protons.

The magnetic spectrometer which we use to analyze the scattered protons is shown in fig. 4. It is a point-focusing spectrometer with 12-in. radius of central path, and has an aperture of 0.0025 steradian[3]). Particles from the scattering target are focused by the inhomogeneous field of this magnet on an exit slit, and are then counted

[3]) S. Rubin and D. C. Sachs, Rev. Sci. Instr. 26 (1955) 1029–1034.

by a scintillation detector behind the exit slit. The momentum resolution of this spectrometer is about 3000, which has been achieved by adjustment of the pole and gap geometry to minimize astigmatism and second-order aberrations. Fig. 5 shows a cross section through the spectrometer, and indicates how the adjustable poles are constructed. A very stable current supply is used for this magnet.

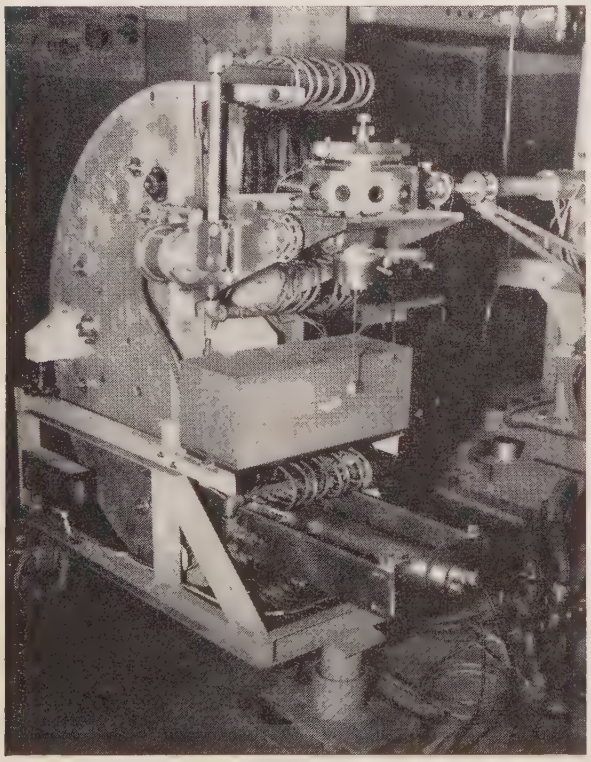

Fig. 4. Photograph of high resolution magnetic spectrograph and target chamber.

The way we usually analyze a sample is to keep the Van de Graaff voltage fixed at, say, 1.5 MeV; set the spectrometer position to detect particles scattered at 150°, and vary the spectrometer field to scan the momentum range of interest, corresponding to the range of nuclear masses we want to detect. The beam current on the sample is measured, so that the number of protons counted at each field setting of the spectrometer are quantitatively related to the concentrations of the elements scattering protons into that momentum interval. In this way, one can either use the known scattering cross sections or else the scattering yields measured on samples of known concentrations, to determine concentrations quantitatively.

We plot the counting data as a function of the ratio of the spectrometer magnetic field to the analyser magnetic field, thus giving an abscissa scale which is proportional to the ratio of the scattered to the initial momentum of the protons.

Of course, we do not observe a line spectrum, with a proton momentum group or line corresponding to each nuclear mass. The protons are slowed down by ionization in proportion to the distance they penetrate into the sample until scattered by a nucleus, and then travel out again to the surface. This produces a continuous distribution of momentum, on which we observe steps or jumps, corresponding to scattering from each different element at the surface of the sample. While this complicates the interpretation of the data, it also makes it possible to measure how thick a contaminant layer is, or how far some element or compound has diffused into a material.

Because of this ionization slowing down, protons of a particular momentum may arise either from scattering off a light element close to the surface, or from a heavier element at some greater depth in the sample. These yields are added together in the data, so the light element yield must be determined by subtraction of the heavy element yield from the total at that momentum. This is illustrated in fig. 6, which shows an analysis of an aerosol deposited on an aluminium foil. The carbon and oxygen on the surface are lighter elements than the aluminium base, so that the relative amounts of these are obtained by integrating under each peak above the aluminium background, and dividing in each case by the relative proton scattering cross section at this proton energy. The scattering yield from the heavier elements has a much smaller background, which is due to heavy element impurities in the aluminium foil.

Some idea of the sensitivity of this method can be obtained from the surface concentrations calculated from this curve. The oxygen peak is

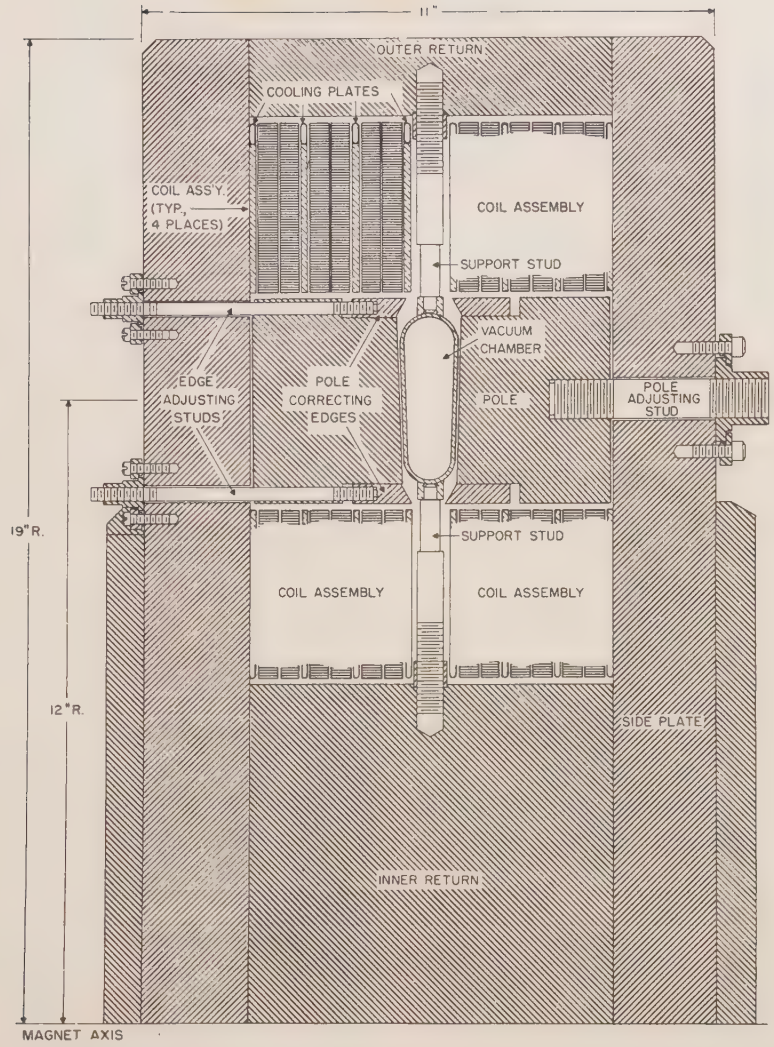

Fig. 5. Cross section drawing of magnetic spectrograph.

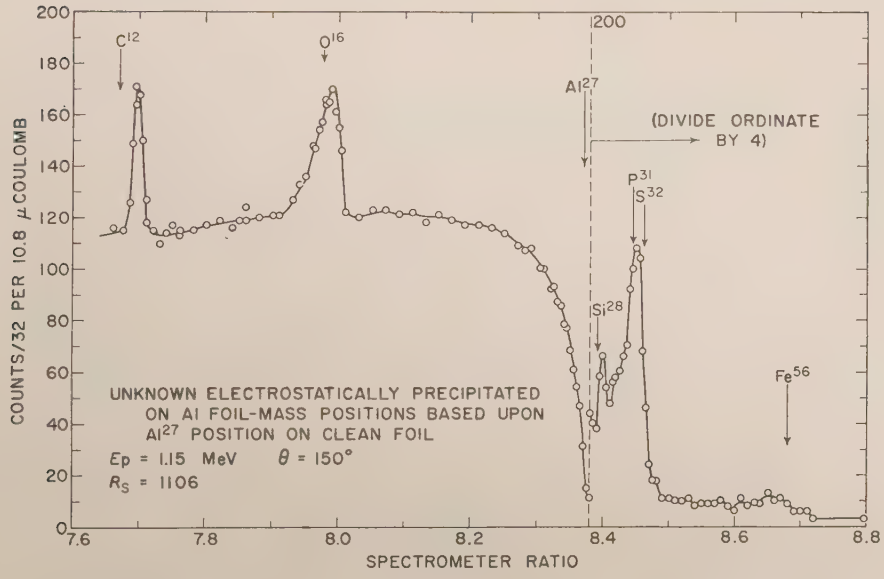

Fig. 6. Momentum distribution of protons scattered from an aerosol sample deposited on aluminium.

due to 5 micrograms per square centimeter of oxygen; and the silicon and sulfur peaks correspond to 0.13 and 0.3 micrograms per sq. cm, respectively.

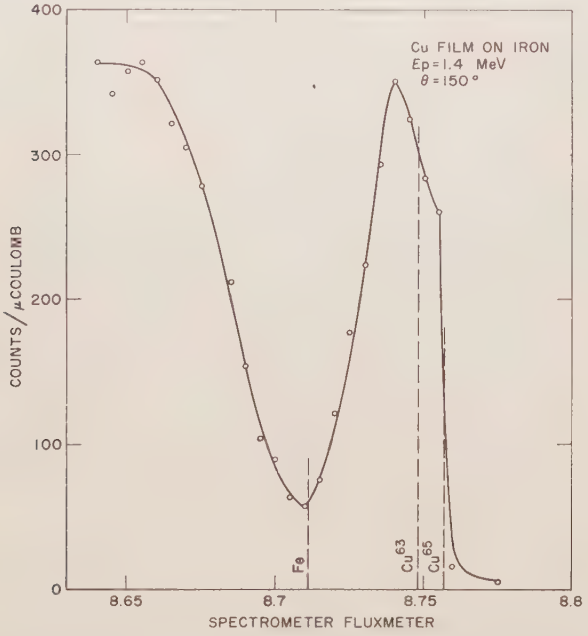

Fig. 7. Momentum distribution of scattering from thin copper film on a polished iron surface.

The resolving power for distinguishing between different nuclei is indicated in fig. 7, which was obtained with a sample consisting of a very thin copper coating electrolytically deposited on an iron surface. The scattering yields from copper and iron are well separated, but the two copper isotopes, of masses 63 and 65, are not quite resolved. This spectrum also shows how information can be obtained on the properties of thin films. Not only can the thickness of the copper film be measured, but also its variation in thickness over the area examined. Futhermore, it can be deduced that the copper coating does not entirely cover the iron, because its peak yield is smaller than that from a pure copper sample by about 20%. This curve also demonstrates that the copper lies on top of the iron, and that there has been little or no diffusion either way, because the iron edge is displaced from its computed position by just the thickness of the copper peak.

Diffusion of contaminants into a surface is displayed in fig. 8, which is a piece of steel exposed to propellant gases at high temperature and pressure. Here the diffusion into the surface of oxygen- and carbon-containing substances is shown relative to the 1-micron scale of depth on the curve. The depth scale is computed from the known stopping power of iron for 1.4-MeV protons. The concentrations of carbon, oxygen, and two heavy element groups can be interpolated with respect to the 10% points shown for each. It can be seen how we are limited by the background of scattering from the iron to

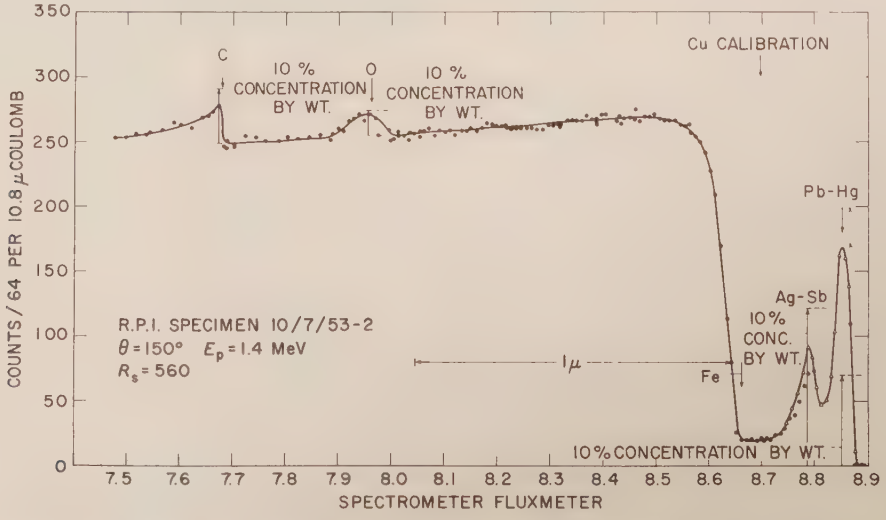

Fig. 8. Momentum distribution of scattering from a steel sample exposed to high temperature propellant gases.

measuring concentrations of light elements of 1% or greater by weight. Heavier elements than iron can be detected down to much smaller concentrations, not only because of their greater scattering cross sections, but also because of the elimination of the large background.

These few examples illustrate the types of studies and analyses which can be done by this method. The technique has particular use in three types of problems:

1. The analysis of microgram quantities of material, such as aerosol collections, which can be deposited on a carrier foil.

2. The study of the physical structure of thin films, down to 10^{-2} microns in thickness.

3. The determination of the differences in composition between the surfaces and the bulk material of all kinds of engineering materials and objects, with sensitivities to surface contaminants down to 10^{-8} grams per square centimeter.

NUCLEAR INSTRUMENTS AND METHODS 5 (1959) 184–188; NORTH-HOLLAND PUBLISHING CO.

ON THE OPTIMUM DIMENSIONS OF COLLIMATORS FOR NEUTRON DIFFRACTION

P. SZABÓ

Central Research Institute for Physics, Budapest

Received 16 July 1959

A calculation method is shown for determining the optimum dimensions of primary collimators of given collimating power for neutron diffractometers and crystal spectrometers. Exact expressions of closed form consisting of elementary functions are given for the calculation of transmitted intensity. The numerical evaluation of these expressions being rather lengthy and laborious, approximate formulae are derived too and it is shown that in cases of practical interest the use of these latter and more convenient ones is quite sufficient.

1. Introduction

The collimators used in neutron diffractometry and crystal spectrometry are in general of the Soller type[1]). Problems like the obtainable resolving power[2]) and the suitable sequence of angular divergences to be chosen in the case if three collimators are applied in a diffractometer[3]) have been discussed in the literature.

No reference is found, however, as to the optimum dimensions for ensuring maximum intensity for a given angular divergence. In the following it will be shown that for a given horizontal angular divergence there are optimum dimensions of the primary collimator dependent on the thickness of the dividing plates between the collimating channels. This optimum can be determined by calculating the intensity of the beam emerging from the collimator.

Exact expressions are derived for the calculation of the transmitted intensity, but it is more convenient and quite satisfactory to use the approximation method also given in our paper, as it will be seen in connection with the computations on the collimator designed and built in our Institute.

Above calculation methods may be applied with the necessary changes also in connection with secondary collimators, but here, as a rule, all dimensions are determined by other factors.

2. Initial Conditions and Assumptions

By horizontal and vertical angular divergence α and β, resp., we mean conveniently half the maximum angle enclosed by the directions of neutrons travelling in the horizontal and vertical plane section of the collimator, respectively. It is easy to show that while the allowed angular range of α will be close to the preset angular range of the angle of incidence on the monochromator (for $\beta = 0$ it would be exactly the same), that of β will be much higher. Thus the horizontal angular divergence α has to be preset while the vertical angular divergence of the beam is usually kept smaller than the allowed margin by the size of the reactor channel so that no presetting of β is required. β is thus determined by the collimator length l and its height h and is given as $\beta = \operatorname{arctg} h/l$.

Collimating channels of rectangular prismatic shape of the Soller collimator are lying parallel to the reactor channel assumed to be also of rectangular prismatic form and to have two equal edges, in a way that the longest edges of the prisms are parallel to each other.

The absorptive capacity of the walls of channel and collimator, and that of the dividing

[1]) W. Soller, Phys. Rev. 24 (1924) 158.

[2]) V. L. Sailor, H. L. Foote, Jr., H. H. Landon and R. E. Wood, Rev. Sci. Instr. 27 (1956) 26.

[3]) G. Caglioti, A. Paoletti and F. P. Ricci, Nuclear Instruments 3 (1958) 223.

plates (of thickness v) is assumed to be infinite. (Thus, like in [2]) and [3]) the effect of total reflection is not taken into account.) This means that the neutron radiation incident on the collimator is assumed to originate only from a plane source which is determined by the vertical cross section of square shape of the reactor channel at its end next to the reactor core, that is from the so called channel inlet surface. It is assumed further that from all points of this surface the number of neutrons emerging per cm², per sec, and per unit solid angle is the same in all directions. (Owing to the smallness of the angular range under consideration this condition can be taken generally fufilled.)

We represent by intensities I and I_m, resp., the ratio of the number of neutrons actually transmitted in a second by the collimator and the m-th collimating channel, resp., to the above number of neutrons.

The cross sections of the collimator normal to its longitudinal axis closest to and farthest from the channel inlet, resp., are called the collimator inlet and outlet surface, resp.

3. Exact Calculation

The intensity transmitted through the m-th collimating channel is given by

$$I_m = \iint F_m(\varphi,\vartheta)\cdot\sin\vartheta\cdot\mathrm{d}\varphi\,\mathrm{d}\vartheta\,, \tag{1}$$

where $F_m(\varphi,\vartheta)$ is that part of the surface area of the channel inlet which is crossed by neutrons flying in the direction characterised by polar angles φ,ϑ and actually transmitted by the m-th collimating channel. The integration has to be carried out over the angular range determined by the walls of the collimating channel and those of the reactor channel. (Outside this range $F_m = 0$.)

Conveniently let be the plane $\varphi = 0$ a vertical plane passing through the axis of the collimating channel, the axis of the cones $\vartheta = \text{const.}$ a vertical straight line lying in this plane; the origin of the coordinate system should be taken at the intersection point of the reactor channel inlet cross section and the collimating channel axis.

By substituting $\psi = \vartheta - \frac{1}{2}\pi$ we have

$$I_m = \int_{-\alpha}^{\alpha}\int_{-\beta}^{\beta} F_m(\varphi,\psi)\cdot\cos\psi\,\mathrm{d}\varphi\,\mathrm{d}\psi \tag{2}$$

where $\pm\alpha$ and $\pm\beta$ are the limits of integration with respect to φ and ψ, respectively, that is the horizontal and vertical angular divergence, resp., as they are determined by the dimensions of the collimator. (β is a function of φ.)

It is easy to see that in our case the area $F_m(\varphi,\psi)$ is of a rectangular shape. Denoting its vertical and horizontal edge length by A and B_m, respectively, we obtain

$$F_m(\varphi,\psi) = A\cdot B_m\,. \tag{3}$$

Now, A can be readily expressed by the help of fig. 1 which shows a vertical cross section of the reactor channel with $\varphi = \text{const.}\,(|\varphi| \leqslant \alpha)$ and that of one of the collimating channels, intentionally distorted.

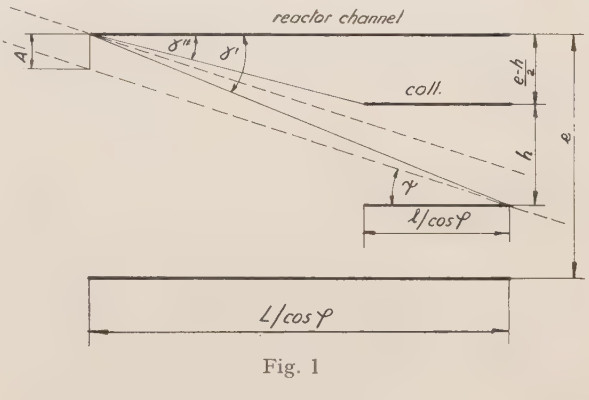

Fig. 1

Introducing the symbols

$$\gamma' = \operatorname{arctg}\left(\frac{e+h}{2L}\cos\varphi\right)$$
$$\gamma'' = \operatorname{arctg}\left(\frac{e-h}{2(L-l)}\cos\varphi\right) \tag{4}$$

A may be expressed as

$$A(\varphi,\psi) = \left[h - \frac{l}{\cos\varphi}\cdot\operatorname{tg}|\psi|\right]\cdot f(\varphi,\psi) \tag{5}$$

where

$$f(\varphi,\psi) = \begin{Bmatrix} 1 \\ \dfrac{\dfrac{e+h}{2} - \dfrac{L}{\cos\varphi}\cdot\operatorname{tg}|\psi|}{h - \dfrac{l}{\cos\varphi}\cdot\operatorname{tg}|\psi|} \\ 0 \end{Bmatrix} \text{for} \begin{Bmatrix} |\psi| \leqslant \gamma'' \\ \gamma'' \leqslant |\psi| \leqslant \gamma' \\ \gamma' \leqslant |\psi| \end{Bmatrix}. \tag{6}$$

The expression for B_m will vary in general according to the different collimating channels, otherwise it depends obviously only on φ. The expression for B_m may be found conveniently with the help of fig. 2 which shows the horizontal cross section of the reactor channel and that of the m-th collimating channel going through the collimator axis. The figure is distorted intentionally again.

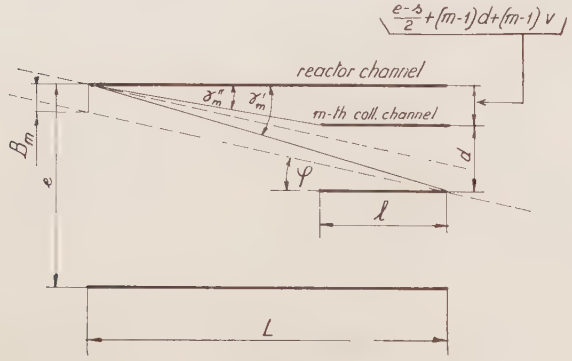

Fig. 2

Using symbols similar to (4):

$$\gamma'_m = \operatorname{arctg} \frac{\frac{1}{2}(e-s) + md + (m-1)v}{L}, \qquad \gamma''_m = \operatorname{arctg} \frac{\frac{1}{2}(e-s) + (m-1)d + (m-1)v}{L-l}, \tag{7}$$

we may write the following expression for B_m:

$$B_m(\varphi) = (d - \operatorname{tg}|\varphi|)\cdot f_m(\varphi) = d\left(1 - \frac{\operatorname{tg}|\varphi|}{\operatorname{tg}\alpha}\right)\cdot f_m(\varphi) \tag{8}$$

where

$$f_m(\varphi) = \begin{cases} 1 \\ \dfrac{d - L\cdot\operatorname{tg}|\varphi| + \frac{1}{2}(e-s) + (m-1)d + (m-1)v}{d\left(1 - \dfrac{\operatorname{tg}|\varphi|}{\operatorname{tg}\alpha}\right)} \\ 0 \end{cases} \quad \text{for} \quad \begin{cases} |\varphi| \leqslant \gamma''_m \\ \gamma''_m \leqslant |\varphi| \leqslant \gamma'_m \\ \gamma'_m \leqslant |\varphi| \end{cases}. \tag{9}$$

Hence the following sum gives the intensity transmitted by the collimator consisting of n collimating channels:

$$I = \sum_{m=1}^{n} I_m = 4q \sum_{m=1}^{n} \int_0^{\alpha}\int_0^{\beta} \left(1 - \frac{\operatorname{tg}\varphi}{\operatorname{tg}\alpha}\right)\cdot f_m(\varphi)\cdot\left(1 - \frac{\operatorname{tg}\psi}{\operatorname{tg}\beta\cos\varphi}\right)\cdot f(\varphi,\psi)\cdot\cos\psi\,\mathrm{d}\varphi\,\mathrm{d}\psi\,. \tag{10}$$

The integrals in (10) may be reduced to the following four integral types:

$$\int_0^{\gamma} \mathrm{d}\varphi \int_0^{\operatorname{arctg}(k\cos\varphi)} \mathrm{d}\psi \begin{cases} \cos\psi = \arcsin\left[\dfrac{k}{\sqrt{1+k^2}}\cdot\sin\gamma\right] \\ \dfrac{\sin\psi}{\cos\varphi} = -\frac{1}{2}\ln\dfrac{\sqrt{1-\dfrac{k^2}{1+k^2}\cdot\sin^2\gamma} + \sqrt{1-\dfrac{k^2}{1+k^2}}\cdot\sin\gamma}{\sqrt{1-\dfrac{k^2}{1+k^2}\cdot\sin^2\gamma} - \sqrt{1-\dfrac{k^2}{1+k^2}}\cdot\sin\gamma} + \ln|\operatorname{tg}(\tfrac{1}{2}\gamma + \tfrac{1}{4}\pi) \\ \operatorname{tg}\varphi\cos\psi = \operatorname{arctg}k - \operatorname{arctg}(k\cos\gamma) \\ \dfrac{\operatorname{tg}\varphi}{\cos\varphi}\sin\psi = \dfrac{1}{\cos\gamma} - 1 + \\ + \frac{1}{2}k\left[\dfrac{\sqrt{1+k^2}-1}{k} - \dfrac{\sqrt{1+k^2\cos^2\gamma}-1}{k\cos\gamma} + \dfrac{k}{\sqrt{1+k^2}-1} - \dfrac{k\cos\gamma}{\sqrt{1+k^2\cos^2\gamma}-1}\right]. \end{cases}$$

In these expressions one or other of the coefficients of $\cos\varphi$ as given in (4) is to be substituted for the constant k and γ'_m or γ''_m from (7) for γ.

Consequently from (10) we obtain an exact expression for I in closed form consisting of elementary functions.

4. Approximate Calculation

Unfortunately the evaluation of the above closed expression is rather lengthy and laborious. Considering the types of the integrals involved, it is obvious that for expressing I "low figure differences of high figure numbers" are to be dealt with. Thus we have to perform operations with high figure numbers (sixteen digit numbers among them in the case of computations the results of which will be dealt with in section 5) in order to obtain e.g. a three digit number for I. Therefore it seemed advisable to find an approximation method which in problems of practical interest would not lead to significantly different results and would be easier to be evaluated numerically. Such a suitable approximation has been found by the following considerations. (In section 5 we shall deal with the accuracy of it.)

Within the limits of integration as given in (10) only very low values of φ and ψ occur, practically they never exceed 20′ and 1.5°, respectively. Consequently the cosines in (10) may be set equal to unity and the sines and tangents to their arguments. In this way (10) becomes

$$I = 4q \sum_{m=1}^{n} \int_0^{\alpha} \int_0^{\beta} \left(1 - \frac{\varphi}{\alpha}\right) \cdot f_m(\varphi) \cdot \left(1 - \frac{\psi}{\beta}\right) \cdot f(\psi)\, \mathrm{d}\varphi\, \mathrm{d}\psi \quad (11)$$

where

$$f_m(\varphi) = \left\{ \begin{array}{c} 1 \\ \dfrac{d - L\,|\varphi| + \frac{1}{2}(e-s) + (m-1)\,d + (m-1)v}{d\left(1 - \dfrac{|\varphi|}{\alpha}\right)} \\ 0 \end{array} \right\} \quad (12)$$

for

$$\left\{ \begin{array}{c} |\varphi| \leqslant \gamma''_m \\ \gamma''_m \leqslant |\varphi| \leqslant \gamma'_m \\ \gamma'_m \leqslant |\varphi| \end{array} \right\}$$

and

$$\gamma'_m = \frac{\frac{1}{2}(e-s) + md + (m-1)\,v}{L}, \qquad \gamma''_m = \frac{\frac{1}{2}(e-s) + (m-1)\,d + (m-1)\,v}{L - l} \quad (13)$$

and further

$$f(\psi) = \left\{ \begin{array}{c} 1 \\ \dfrac{\frac{1}{2}(e+h) - L\,|\psi|}{h - l\,|\psi|} \\ 0 \end{array} \right\} \text{ for } \left\{ \begin{array}{c} |\psi| \leqslant \gamma'' \\ \gamma'' \leqslant |\psi| \leqslant \gamma' \\ \gamma' \leqslant |\psi| \end{array} \right\} \quad (14)$$

and

$$\gamma' = \frac{e+h}{2L}, \qquad \gamma'' = \frac{e-h}{2(L-l)}. \quad (15)$$

The double integral in (11) may be written as the product of two integrals:

$$I = 4q \sum_{m=1}^{n} I'_m(\varphi) \cdot I''(\psi), \quad (16)$$

where

$$I'_m(\varphi) = \int_0^{\alpha} \left(1 - \frac{\varphi}{\alpha}\right) f_m(\varphi)\, \mathrm{d}\varphi, \quad (17)$$

$$I''(\psi) = \int_0^{\beta} \left(1 - \frac{\psi}{\beta}\right) f(\psi)\, \mathrm{d}\psi. \quad (18)$$

Upon carrying out the integration we obtain for I'_m and I'', resp., the following expressions for above three and three corresponding ranges:

$$I'_m(\varphi) = \left\{ \begin{array}{c} \frac{1}{2}\alpha \\ \dfrac{\alpha}{d}\left[d + \frac{1}{2}(e-s) + (m-1)(d+v) - \frac{1}{2}L\alpha\right] \\ 0 \end{array} \right\} \quad (19)$$

$$I''(\psi) = \left\{ \begin{array}{c} \frac{1}{2}\beta \\ \dfrac{\beta}{2h}(e + h - L\beta) \\ 0 \end{array} \right\}. \quad (20)$$

5. Results Obtained for an Actual Problem. Accuracy of the Approximation

Above calculation methods were used to determine the dimensions of the primary collimator of our diffractometer. Owing to the large size of our apparatus, it may become necessary to put it sometimes a little farther from the reactor channel so as not to interfere with the experiments going on at the neighbouring reactor channels. Therefore we had to calculate and compare the transmitted intensity obtained with collimators of optimum dimensions for the original "close" as well as for the "distant" arrangement.

Computations were carried out for horizontal divergences up to 20′. It is obvious that for lower angular divergences than $\alpha = 20'$ the difference in the results obtained from the exact and the approximate expressions (10) and

(11), resp., will be relatively less. Therefore we show here some intensity values obtained for $\alpha = 20'$. The latter is higher than that generally used in diffractometry or crystal spectrometry.

The values used in this computation have been real ones: $e = 8.85$ cm, $h = 4$ cm, $s = 5$ cm; $L = 250$ cm and 495 cm, respectively, according to the "close" and the "distant" case, resp.

The maximum values of the transmitted intensity I_{max} together with the pertaining (i.e. optimum) values of the number n of collimating channels and of the collimator length l are given in the following table for some values of the dividing plate thickness v and for the two abovementioned values of L. These intensity values were computed from the approximate expression (11).

L (cm)	v (cm)	optimum n	optimum l (cm)	$I_{max}/10^{-3}$
250	0.01	21	39.3	3.83
250	0.03	12	66.9	3.62
250	0.05	9	87.8	3.47
495	0.05	7	115	1.85

It is easy to prove that the approximation leads to the worst results in the first of the cases shown in the table. Therefore for comparison we computed the transmitted intensity for this case using also the exact expression (10). Comparing the result thus obtained with that evaluated by means of (11), the error was found to be about 1 per cent. Consequently it can be said that equation (11) gives quite a good approximation (usually better than 1%) in cases of practical interest.

Symbols

A the vertical edge length of the rectangle surface denoted by F_m

B_m the horizontal edge length of the rectangle surface denoted by F_m

e the edge length of the reactor channel cross section of square shape normal to the longitudinal axis

d the inside width of the collimating channels

f see relations (6) and (14)

f_m see relations (9) and (12)

F_m the area of that part of the reactor channel inlet cross section which is crossed by neutrons flying in the direction characterised by polar angles φ, ϑ and actually transmitted by the m-th collimating channel

h the height of the collimating channels

I the intensity transmitted by the collimator

I_m the intensity transmitted by the m-th collimating channel

l the length of the collimator

L the distance of the channel inlet from the collimator outlet

m the serial number for the collimating channel in question

n the total number of the collimating channels

q the area of the internal cross section (normal to the longitudinal axes) of the collimating channels (equal to $h \cdot d$)

s the total internal width of the collimator

v the thickness of dividing plates between the collimating channels

α the preset horizontal angular divergence

β the vertical angular divergence (equal to arctg h/l)

γ' see fig. 1 and relations (4) and (15)

γ'' see fig. 1 and relations (4) and (15)

γ'_m see fig. 2 and relations (7) and (13)

γ''_m see fig. 2 and relations (7) and (13)

ϑ the polar angle

φ azimuth

ψ $= \vartheta - \frac{1}{2}\pi$.

NUCLEAR INSTRUMENTS AND METHODS 5 (1959) 189–193; NORTH-HOLLAND PUBLISHING CO.

EFFICIENT BEAM EXTRACTION FROM A SYNCHRO-CYCLOTRON AT $n = 1$

S. SUWA, J. SANADA, T. KARASAWA, A. SUZUKI, H. OGAWA, H. YAMAGUCHI, Y. SAJI, S. KIKUCHI, H. KUMAGAI, I. HAYASHI, K. MATSUDA and K. NISIMURA

Institute for Nuclear Study, University of Tokyo, Tanashi-machi, Tokyo

Received 30 May 1959

With an electrostatic deflector placed at $n = 1$ (the point of maximum Br), about 50 percent of the internal beam (inside $n = 0.2$) of the 160 cm synchro-cyclotron could be extracted, and most of the extracted beam was confined within a 2.5 cm diameter area at the tank exit by inserting a magnetic channel acting as a focusing lens. The homogeneity of the magnetic field is essential for this method of beam extraction. The configuration and position of the ion source, and the dee bias voltage were found to affect the transmission of the beam through $n = 0.2$ to $n = 1$. Under the optimum conditions, 70 to 80 percent of the beam inside $n = 0.2$ reached $n = 1$.

1. Introduction

As the most efficient method of the beam extraction, the regenerative deflector system has recently been applied to many synchro-cyclotrons[1–5]) and the maximum deflection efficiency thus far reported appears to be 10 percent or less.

The method proposed by Hamilton and Lipkin[6]), in which the ions are accelerated until the radius at which $n = -(r/B)\partial B/\partial r = 1$ (the radius of maximum Br) and there extracted by a deflector instead of spiraling out naturally, is another promising one, provided that a large fraction of the internal beam can get through $n = 0.2$ to $n = 1$. This method has further advantages that the beam can be accelerated to its full energy with a given magnet and that it is expected to be very homogeneous in energy. But it has generally been recognized that in the synchro-cyclotron a large part of the circulating beam is lost by vertical blow-up caused by the coupling between radial and vertical oscillations at $n = 0.2$ or by the resonant excitations of these oscillations at $n = 0.25$, 0.5, 0.75 and 1 due to the inhomogeneities of the magnetic field[6,7,8]).

Taking advantage of the homogeneous magnetic field[9]) of our cyclotron and eliminating other causes of loss of the beam, the method of extraction at $n = 1$ has successfully been applied to the 160 cm synchro-cyclotron[10]). Since this cyclotron can be used both as a fixed frequency variable energy cyclotron (7.5–15 MeV protons, 15–22 MeV deuterons, 30–44 MeV alpha particles) and as a synchro-cyclotron by changing the dee and oscillator systems[10]), and since intensive works on the various nuclear reactions with the former use have already started, our primary concern has been to confirm, in the short periods given for test, how much of the beam can be deflected to the prescribed exit of the vacuum tank, and thorough investigations of the beam characters has not yet been performed. Nevertheless, the fact that the remarkably large fraction, about 50 percent, of the internal beam could be extracted seems to be of sufficient interest.

[1]) A. V. Crewe and J. W. G. Gregory, Proc. Roy. Soc. A 232 (1955) 242.

[2]) A. V. Crewe and U. E. Kruse, Rev. Sci. Instr. 27 (1956) 5.

[3]) G. Calame *et al.*, Nuclear Instruments 1 (1957) 169.

[4]) S. Mago, C. A. Heras and J. Rosenblatt, Nuclear Instruments 2 (1958) 9.

[5]) H. Tyrén and Th. A. J. Maris, Nuclear Physics 3 (1957) 52.

[6]) D. R. Hamilton and H. J. Lipkin, Rev. Sci. Instr. 22 (1951) 783.

[7]) L. R. Henrich, D. C. Sewell and J. Vale, Rev. Sci. Instr. 20 (1949) 887.

[8]) T. Teichmann, J. Appl. Phys. 21 (1950) 1251.

[9]) H. Kumagai *et al.*, INSJ-2 (1957), unpublished.

[10]) S. Kikuchi *et al.*, J. Phys. Soc. Japan, to be published.

2. Causes of Loss of the Beam between $n = 0.2$ and $n = 1$

The homogeneity of the magnetic field is essential for accelerating ions until the radius of $n = 1$ efficiently. This was in fact confirmed as described below in 2.3. But even with a sufficiently homogeneous magnetic field, some further considerations were also necessary for the optimum condition.

2.1. ION SOURCE

The ion source-feeler configuration was found to be an important factor for the loss of the beam at large radii. Among the various ion source configurations tested, what is shown in fig. 1(A) yielded the most intense beam at $n = 1$ ($r = 76.6$ cm), the transmission through $n = 0.2$ being 80 percent for optimum conditions. It appears that this configuration reduces the vertical defocusing in the initial acceleration and at the same time gives a fairly definite orbit centre of the beam. The results described below were obtained with this configuration. We tried also a usually accepted type of ion source such as shown in fig. 1(B), but with this type, only about 30 percent of the beam could reach $n = 1$. Fig. 2 shows typical examples of plots of the beam intensity at large radii for the two types of ion source.

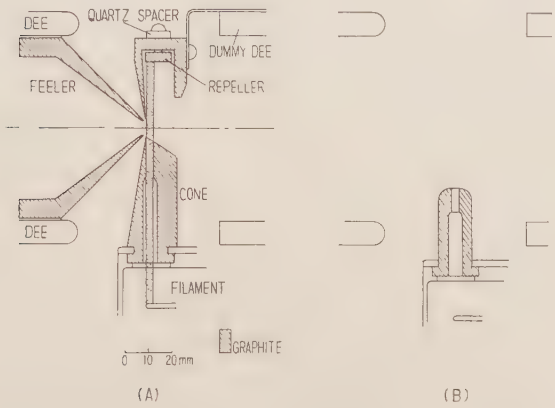

Fig. 1. Arrangement of ion source and feeler. (A) Optimum type; (B) Usually accepted type.

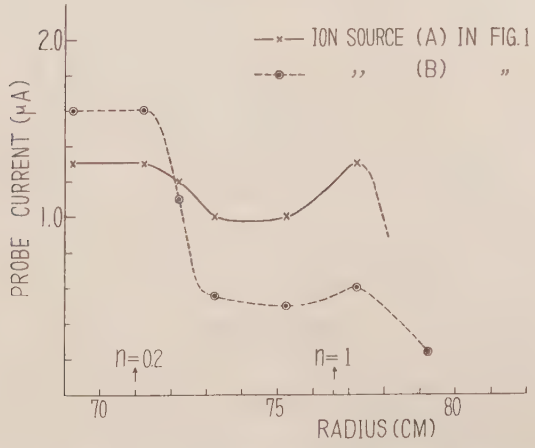

Fig. 2. Probe current at large radii. Apparent increases of the current at 77 cm are regarded as due to the fact that the front edge of the probe did not coincide exactly with the tangent of the circular orbit of the internal beam. A fraction of the ions hitting the probe at $n < 1$ could escape again with some loss of their energy, while all the ions were caught after $n = 1$ owing to the outward component of their velocity.

2.2. DEE BIAS VOLTAGE AND POSITION OF ION SOURCE

According to estimations, almost all ions suffer the complete conversion from radial to vertical oscillation somewhere near $n = 0.2$. Therefore, the amplitude of the radial oscillation inside $n = 0.2$ is desirable to be at least smaller than a quarter of the available dee height[6]), which is in our case 5 cm near $n = 0.2$. The inhomogeneities of the magnetic field in the region of small n-value which excite the radial oscillation are negligibly small for our magnet[9]).

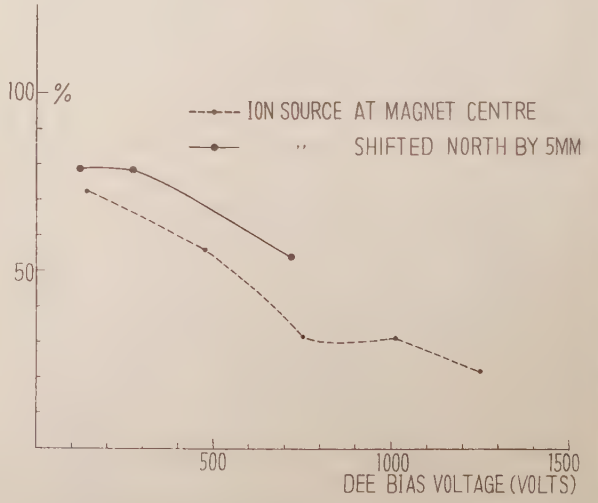

Fig. 3. Effects of dee bias voltage and ion source position. Ordinate: Ratio of the beam intensity at $n = 1$ to that at $n = 0.2$; the dee-to-ground voltage $\approx$ 7 kV.

The dee bias D. C. voltage applied to the dee system in order to suppress the multipactor action causes appreciable shifts of the orbit

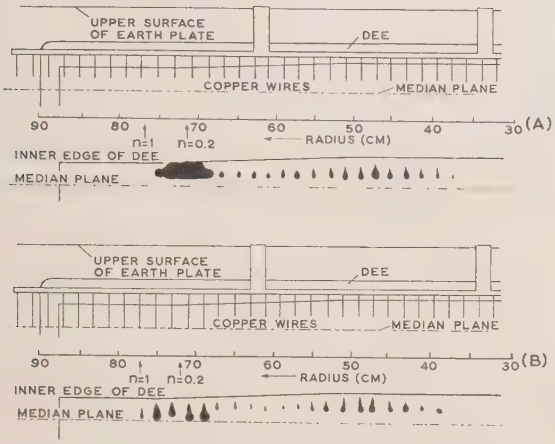

Fig. 4. Radioautographs of beam profile taken with copper wires, (A) under various not necessarily optimum conditions; (B) under the optimum condition. Note that the copper wires at radii larger than 69 cm in the case (B) are longer by 15 mm than others.

centres of the ions along the dee edge. It was found that the dee bias voltage in fact affects the beam reaching $n = 1$, as is seen in fig. 3. Fortunately, we could overcome the multipactor action with the bias voltage of as low as 100 volts and reduce its effect upon the ion orbits considerably. Fig. 3 shows also that this effect could be at least partially compensated by locating the ion source at an appropriate position. The optimum position of the ion source was found within a few mm for the given dee bias voltage.

Fig. 4 shows radioautographs taken with thin copper wires hanging along the dummy dee. Blow-ups of the beam near $n = 0.2$ (or also at $n = 0.25$) are noticiable in the case of (A), while scarcely seen in the optimum case (B).

2.3. INHOMOGENEITIES OF THE MAGNETIC FIELD AT LARGE RADII

According to the data on the magnetic field, the resonant excitation of the vertical oscillation at $n = 0.25$ is the most critical for our case among the various resonances mentioned in section 1. The coefficient of the first harmonic of the azimuthal inhomogeneity of the Z-component of the magnetic field, h_1 in

$$B_z(r,\theta) = B_z(r)\{1 + \sum_l h_l \cos(l\theta - \alpha_l)\}$$

and its derivative dh_1/dr were at $r = 71.5$ cm ($n = 0.25$) 2×10^{-4} and 3×10^{-5} cm^{-1} respectively, and α_1 was nearly constant. This is mainly due to the disturbance caused by the magnetic channel used for the external beam of the fixed frequency cyclotron case[10,11]). (See section 1 and fig. 6.)

Further, this magnet is equipped with coils wound inside the pole tips which are called the electromagnetic shims. (Details on the electromagnetic shims are described in ref.[9]).) Using these electromagnetic shims, we could compensate the above-mentioned inhomogeneity or introduce inhomogeneities up to $h_1 \approx 2 \times 10^{-3}$ deliberately. Fig. 5 shows the vital effect of the inhomogeneity upon the transmission of the beam. It is also seen that the inhomogeneity of the uncorrected field mentioned above, has a small but definite effect.

Adjusting the above-mentioned various factors so as to minimize the loss of beam, we obtained, with the dee-to-ground voltage of 7 kV, the beam intensity of about 0.8 μA at $n = 1$, which corresponds to about 80 percent of that inside $n = 0.2$.

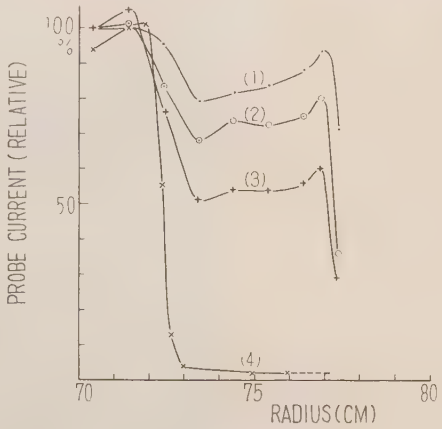

Fig. 5. Effect of azimuthal inhomogeneity of the magnetic field upon the beam. (1) corrected; (2) uncorrected; (3) and (4) are cases with inhomogeneities of $h_1 \approx 4 \times 10^{-4}$ and 1.5×10^{-3} at $r = 71$ cm, respectively. Correction or production of the inhomogeneities was made with the electromagnetic shims.

[11]) F. T. Howard, Cyclotron and High-energy Accelerators, ORNL-2644.

3. Electrostatic Deflector

After confirming the beam at $n = 1$, we installed a 65° arc electrostatic deflector channel

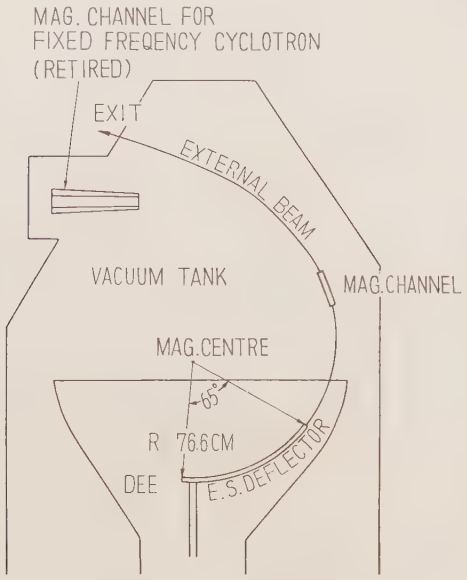

Fig. 6. Plan view of deflector system.

inside the dee, whose radius of curvature was carefully machined so as to conform to the computed paths of the ions in the channel. Each of the two parallel plates, the septum (a grounded plate) and the deflector, was pivoted about a point near the entrance end and the exit ends could be adjusted by means of lead screws without destroying the vacuum.

When the entrance end of the septum, the extraction point, was located at $r = 76.6$ to 76.9 cm with a channel width of 6 mm at the entrance, up to 80 percent of the beam arriving at $n = 1$ could be extracted by applying appropriate voltage of around 70 kV to the deflector plate and adjusting the positions of the exit ends of both plates. The deflection efficiency was found to decrease to 50 percent when the extraction point was shifted to $r = 77.2$ cm.

Thus we obtained a remarkably efficient extraction without any shimming of the magnet required by Hamilton and Lipkin's argument for a flat maximum of Br at $n = 1$. (For our magnet, the value of the parameter, $\alpha = r(dn/dr)$, at $n = 1$ is nearly 15.)

The deflected beam spot at the tank exit was 2.5 cm high by 10 cm wide (fig. 7(a)).

4. Focusing the Deflected Beam with a Magnetic Channel

By inserting a 20 cm long magnetic channel in which the vertical field strength increases with radius, and whose cross section is shown in fig. 8, most of the deflected beam could be focused within an area of 2.5 cm in diameter at the tank exit. Fig. 7 is the reproduction of the photographs obtained by exposing photographic papers at the tank exit. Horizontal divergence of the emerging beam was there 1.5° in full

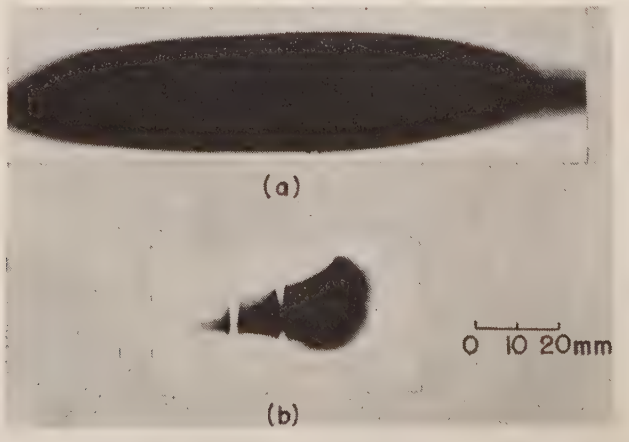

Fig. 7. Beam spot at the tank exit. (a) without magnetic channel, (b) with magnetic channel.

width. This beam will be brought into the experimental room through a pair of quadrupole magnets in the near future.

The magnetic channel mentioned above is a sort of quadrupole focusing lens. It is compact but can produce rather strong field gradient, and, in addition, its small disturbing effect upon the field outside itself reduces the correcting shims to very simple ones. A pair of such channels may have a general application e.g. for focusing the polarized beam produced by scattering in the cyclotron tank†.

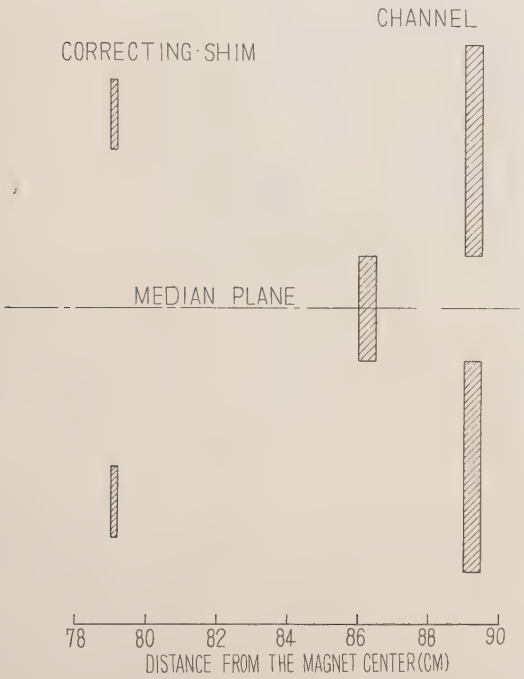

Fig. 8. Arrangement of magnetic channel.

5. Conclusion

The beam characters are summarized in table 1.

The internal beam inside $n = 0.2$ is at present limited to about 1μA for continuous operation, because the dee-to-ground voltage can not be raised over about 7 kV on account of the heat-up of the rotary condenser by rf loss, which causes temperature rise of the bearing of the rotary condenser[10]).

In conclusion it should be remarked that the success of the method of the beam extraction at $n = 1$ for our synchro-cyclotron might owe much to its rather small size, especially in that the electrostatic deflector is effective enough. But if carefully designed, the electrostatic deflector will be still applicable to larger machines.

The authors wish to acknowledge the help of the other members of the Low Energy Division of the Institute, and in particular, they wish to thank Professor I. Nonaka for his encouragement.

† *Note added in proof*: Having submitted this paper for publication, we have been aware of the report of V. I. Danilov and O. V. Savchenko (Report Laboratory of Nuclear Problems (1958)), according to which a similar device has been already applied to the 600 MeV synchro-cyclotron at Dubna.

Table 1

Beam characters

Beam energy	57 MeV (protons)		
Beam intensity	at $r = 71$ cm ($n = 0.2$)	76.6 cm ($n = 1$)	external
	1μA	0.7 to 0.8 μA	$\approx 0.5\ \mu$A

NUCLEAR INSTRUMENTS AND METHODS 5 (1959) 194–195; NORTH-HOLLAND PUBLISHING CO.

APPARATUS FOR THE DEVELOPMENT OF NUCLEAR EMULSION PLATES†

W. LOHMANN

Max Planck-Institut für Biophysik, Frankfurt/M., Germany

Received 9 July 1959

Recently we published a paper[1]) on a new mechanism for the development of nuclear emulsion plates. This included a discussion on the advantages and disadvantages of the known methods of developing[2]). The requirements which must be met by a processing apparatus have often been described and can be summarized as follows:

1. Since in some cases the time of development extends over some hours, the processing apparatus should be constructed in such a way that work in the dark is cut down to a minimum,

2. the different processing stages must be carried out without moving or touching the wet emulsions,

3. a complete control over the development-process is essential so that a result can be reproduced,

4. each grain which has been hit must also be developed,

5. the number of fog-grains must be low,

6. the degree of development must be uniform at all points of the nuclear emulsion plate, and, additionally, for temperature cycle development:

7. different variations must be possible (warm- and cold-developing etc.), and

8. abrupt changes of temperature must be avoided, to prevent distortions and loosening of the emulsion from taking place.

Bujdosó and Medveczky[3]) constructed an apparatus for the development of nuclear emulsion plates which is based on temperature cycle development. To avoid a big outlay in apparatus and possible abrupt changes of temperature when applying this method, we worked out a new development-process and described this some years ago in the paper referred to above. This present paper deals with the apparatus which was used for this purpose. In a changed form, this has been used for temperature cycle development since 1950.

A diagram of the apparatus used for the processing of the nuclear emulsion plates is shown in fig. 1. It consists of the lightproof developer tank T, in which the plates are stored horizontally on a stainless steel plate-holder Pl during the individual processing stages. This plate-holder is perforated and fixed in such a way, that the liquids will flow into the space below the holder and reach the plates through holes in it. When introducing the different liquids into the tank, an adjustable plate, fitted to a rod S which passes through the lid of the tank, is lowered in order to keep the plates in their correct position.

The developer tank is double-walled and water at a temperature of 20° C flows between the two walls to produce the correct temperature in the interior of the tank. It is made of aluminum and is covered at the inside—just as the plate-holder—with a protective paint ("Corropren") to prevent decomposition of the materials by the different processing liquids. The lid is filled with glass-wool for the purpose of heat-insulation. Between lid and tank there is a rubber-washer. By two pressure-stirrups P the lid is pressed tightly on to the tank.

The temperature of the tank-liquid is ascertained by a bent thermometer W, which is inserted into the tank through a tube at the side.

[1]) W. Lohmann, Z. Naturf. **11a** (1956) 174.

[2]) C. C. Dilworth, G. P. S. Occhialini and R. M. Payne, Nature **162** (1948) 102;
H. Yagoda, Rev. Sci. Instr. **26** (1955) 263;
A. Bernot and M. Chastel, J. Phys. Rad. **15** (1954) 781;
M. Blau and J. A. de Felice, Phys. Rev. **74** (1948) 1198;
N. W. Curtis and L. S. Osborne, Phys. Rev. **75** (1949) 1327.

[3]) E. Bujdosó and L. Medveczky, Nuclear Instruments **2** (1958) 270.

† Dedicated to Professor B. Rajewsky on the occasion of his 65th birthday.

The liquids are introduced into the tank through a tube Z fixed in the lid so that the liquids can flow beneath the plate-holder as mentioned above. The tank-liquid can be drained off through the opening H in the bottom.

The developer tank stands on the shaking-

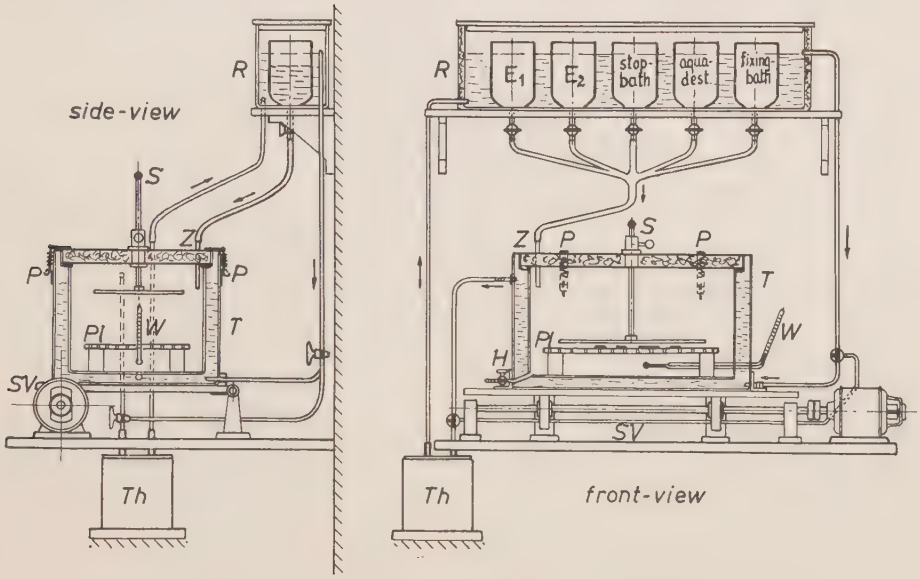

Fig. 1. Diagram of the processing apparatus for nuclear emulsion plates.

device SV, frequency of which can be changed by means of a sliding-resistance. The solution in the developer tank is kept at a laminar flow, since violent shaking may lead to increased oxidation of the developer, to a greater surface-precipitation, and to a distortion of the emulsion.

In a reservoir R there are 5 cylindrical containers with the two developer solutions E_1 and E_2 (dilution of 1:3), the stop-bath (acetic acid, CH_3COOH), aqua dest., and the fixing bath. This reservoir is rinsed with water from the thermostat Th which keeps the 5 solutions at a temperature of 20° C.

This water is pumped from the thermostat into the reservoir. From there it passes either into the developer tank or directly back into the thermostat. All connections consist only of heat-proof rubber-tubing and glass-stopcocks.

The nuclear emulsion plates are developed at first in the developer E_1 and then in the developer E_2 (time of the development s. (1)), and then the tank is washed with aqua dest. Later on acetic acid is let into the tank to interrupt the development. The stop-bath (2% acetic acid solution) is applied for about 30 min. After rinsing once more with aqua dest., the plates are fixed with a 30% fixing-solution ($Na_2S_2O_3$), the fixing-time depending on the thickness of the emulsion. When the plates have cleared the fixing is finished and they are washed with water at laminar flow. Subsequently, a 5% glicerin-bath is applied for ½ hour and this is followed by drying. Rinsing with water and glicerin-bath are both carried out in a tank made of vinidur.

The processing apparatus described here is suitable for processing emulsions of different thickness and type.

The experimental part of this work was carried out at the Institute of Physics, University of Freiburg/Brg. I am grateful to Professor Th. Schmidt, director of this institute, for his interest in, and support of, this work. I should also like to thank Professor B. Rajewsky, director of the Max Planck-Institute of Biophysics, Frankfurt/M., for his advice and for the possibility of finishing this work in his institute and Professor H. Muth, Max Planck-Institute of Biophysics for many useful discussions.

NUCLEAR INSTRUMENTS AND METHODS 5 (1959) 196–198; NORTH-HOLLAND PUBLISHING CO.

A METHOD FOR THE PREPARATION OF CYCLOTRON TARGETS OF RARE-EARTH OXIDES BY ELECTROPHORESIS

S. BJØRNHOLM, PH. DAM, H. NORDBY and N. O. ROY POULSEN

Institute for Theoretical Physics, University of Copenhagen, Denmark

Received 5 August 1958

A method for the preparation of cyclotron targets of rare-earth oxides by electrophoresis is described.

1. Introduction

In the course of a long series of bombardments in the α-beam of the Copenhagen cyclotron, made in order to produce activities of various rare-earth elements, a new technique for the preparation of targets has been developed. Rare-earth oxides in the form of a fine powder are brought to adhere on a gold plate, utilising an electrophoresis method known from the production of oxide cathodes[1,2]).

2. Apparatus

Fig. 1 shows the electrophoresis cell. The bottom and two sides of the cell are made of one piece of Teflon. The two remaining sides form the electrodes. The anode is a 0.1 cm nickel plate. The cathode is the target plate, which is a 0.1 cm gold plate hard-soldered onto a 0.5 cm copper block. The electrodes are backed up by 0.5 cm copper blocks which house the plugs for the current. A frame with a screw serves to hold the parts together. A small magnetic stirrer completes the cell.

Gold is chosen for the negative plate because this element, due to its high Z-value, has negligible cross sections for reactions with α-particles of the energies used. In addition, the fact that gold has a high thermal conductivity and does not dissolve in acids, makes it a suitable backing material for the targets.

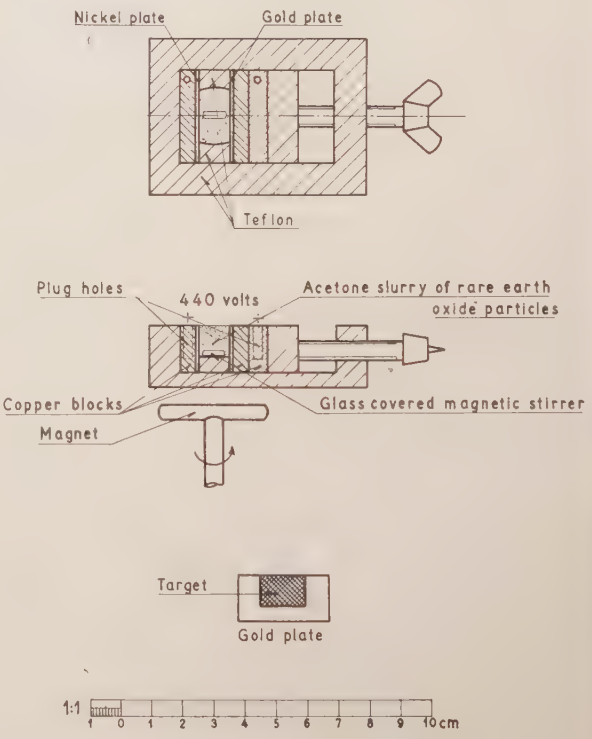

Fig. 1. Electrophoresis cell.

3. Procedure

Before assembling, the gold plate is polished with the finest grade of sand paper. A weighed amount (3–10 mg) of oxide is stirred with 1 cc of acetone and the slurry is transferred to the electrophoresis cell. The magnetic stirrer is started and acetone is added to fill the cell to

[1]) Danish Patent: 67.277, Telefunken Gesellschaft für drahtlose Telegraphie, m.b.H., Berlin-Zehlendorf, Germany, February 10, 1943.

[2]) U.S. Patent: 2.442.863, Everett I. Schneider, Emporium Pa., assignor to Sylvania Electric Products Inc., Emporium Pa., Corporation of Massachusetts. November 29, 1944.

the top. The voltage of 440 volts d.c. is switched on. In less than one minute, a uniform layer builds up on the gold plate. (The current is less than 1 mA.) The stirrer is then stopped and the acetone removed. Subsequently, the voltage can be switched off and the target taken out.

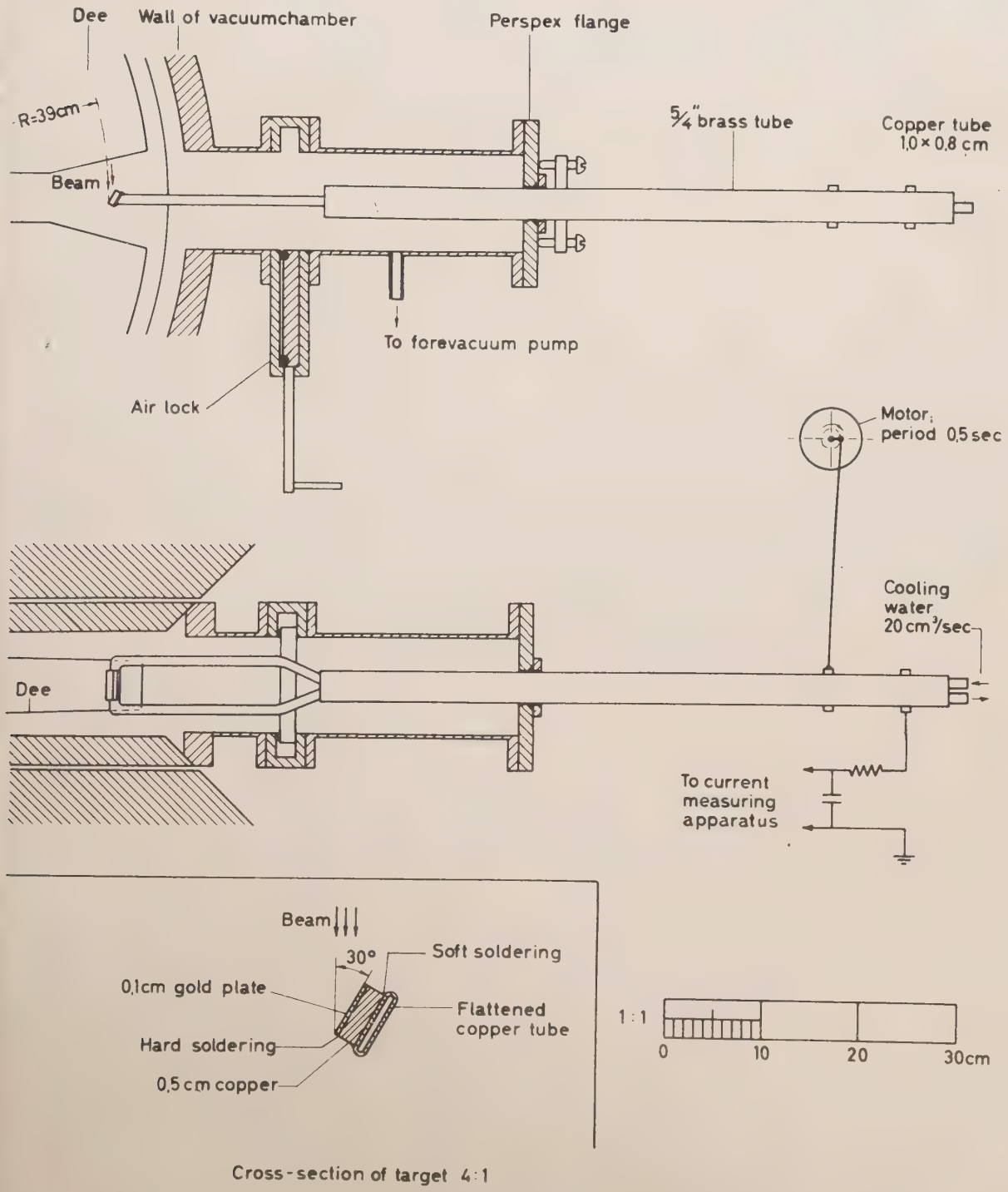

Fig. 2. Target holder with target mounted in the cyclotron.

The acetone dries quickly.

In an average case we start with 8 mg oxide. Out of this amount, 6 mg stay on the target, 1 mg is recovered from the slurry, and 1 mg of the material is lost.

The adherence of the oxide particles is found to depend strongly on their size. 30 μ ($1\mu =$ 0.001 mm) is found to be the upper limit for the diameter of the particles. In order to prepare oxide samples of sufficiently fine particles, the rare earth (usually 3–10 mg of the oxide) is dissolved in 4*N* HCl and evaporated to dryness. The residue is dissolved in 0.5 cc of water. The solution is heated almost to boiling and an oxalate precipitation is performed by adding 0.5–1 cc of boiling 0.3 *M* secondary-ammonium-oxalate solution. The sample is centrifuged and the supernatant drawn off. The precipitate is washed twice with water, dried, and finally heated for about a minute in a Bunsen burner in order to transfer the oxalate into oxide.

The target is placed on a target holder in the cyclotron, as shown in fig. 2. Most of the beam appears within a cross section of about 0.5 cm by 0.5 cm. To minimize the heat dissipation per square cm, the target is mounted at an angle of 30° to the beam and vibrating up and down about 1 cm, the period being 0.5 sec. The resolving point of the target holder is the "○"-ring in the perspex flange.

4. Discussion

Targets of oxide of Pr, Eu, Tb, Dy and Tm —in all 40 targets—have been irradiated in the α-beam of the Copenhagen cyclotron. Typical bombarding conditions are 20 MeV α-particles, 25 μA, 4 hours. It is essential that the gold plate is hard-soldered onto a rather thick copper backing plate which may then be soft-soldered to the target holder. Experience shows that, if the gold plate is soft-soldered directly to the target holder, the solder will often melt locally and the oxide layer flake off. This flaking off was also observed in bombardments in which the gold plate was screwed to the copper block. Also we have found that, to stand a strong irradiation (50 μA; 20 MeV), the layer should not be too thick.

With the above described arrangement and a target layer of less than 5 mg/cm² we have made some 35 irradiations without failure.

The procedure has the following advantages:

(1) Since the target is not covered, the full energy of the cyclotron beam can be exploited.

(2) The method is quite clean and is well suited for working with milligram quantities without noticeable loss. It has therefore been found particularly useful when working with separated isotopes.

(3) The target can in a very short time be scraped or flushed off the backing and dissolved. Activities produced in the backing material do not cause any contamination.

(4) The method should be applicable to practically all high melting metal oxides.

We want to thank Professor A. H. M. Andreasen, The Technical University of Copenhagen, who has pointed out to us the usefulness of the electrophoresis principle.

NUCLEAR INSTRUMENTS AND METHODS 5 (1959) 199; NORTH-HOLLAND PUBLISHING CO.

LETTER TO THE EDITOR

MODIFICATION TO: STATISTICAL DESIGN BASIS FOR FAST SCALING SYSTEMS (Nuclear Instruments 4 (1959) 1)

A. W. PRYOR and A. G. KLEIN

Australian Atomic Energy Commission, Sydney

Received 16 July 1959

After a careful reconsideration of our paper we agree that the modification suggested by Dr. Sanstad is necessary. Perhaps, however, our error lay rather in the phrase, "an output pulse will be missed if K or more pulses appear at the input of the scaler during the time t". This should be modified to read: "An output pulse will be missed if K or more pulses appear at the input while the main scale is dead. The main scale is dead, for a time t, N/K times per second. On each occasion there is a probability $Q_K(Nt)$ of losing a pulse. Therefore $N/K \cdot Q_K(Nt)$ output pulses are lost per second and the fraction of pulses lost is $Q_K(Nt)$". We are grateful to Dr. Sanstad in pointing out this error.

It is interesting to note that the onset of counting loss, when $K = 10$, is so sharp that even an error of 10 times in the calculation of the losses gives a comparatively small error in the estimate of the maximum input frequency.

ERRATUM

Correction to: E. Gatti, V. Svelto, Theory of time resolution in scintillation counters, Nuclear Instruments **4** (1959) 189–201.

Prof. Sands of the California Institute of Technology, reading the reprint of our paper, kindly showed us an error in our Appendix 1, p. 199.

No additional variance has to be attributed to Q electrons emitted by the photocathode beyond the usual Poisson variance and the spread in the yield of the photocathode does not add any additional variance.

Therefore, in the whole paper ε_{rr}^2 should formally be put equal to zero.

NUCLEAR INSTRUMENTS AND METHODS 5 (1959) 200–204; NORTH-HOLLAND PUBLISHING CO.

BOOK REVIEWS

Encyclopedia of Physics, Vol. 38-1, *External Properties of Atomic Nuclei* (Ed. S. FLÜGGE) Springer Verlag DM 118.—.

This volume contains six contributions which deal with nuclear masses, spins and magnetic and quadrupole moments.

A. H. Wapstra (Atomic Masses of Nucleides) presents first a survey of the various methods developed for the determination of nuclear masses. The following section contains an extensive tabulation of binding energies and atomic masses. The values have been computed from the most recent experimental data. In the third section some general trends in the variation of binding energies with mass number are discussed. Special attention is paid to the problem of adjusting the constants in the Bethe-Weizäcker formula and some interesting comments are made concerning alpha-decay energy systematics, beta-decay energy systematics and magic number effects.

The recently developed microwave methods for precise mass determinations are discussed in an interesting article by S. Geschwind (Determination of Atomic Masses by Microwave Methods). A brief survey of the theoretical fundamentals is given. The approximations that contribute to the final errors in the determination of mass ratios from the experimental data are discussed in some detail. It is shown that microwave methods can complete favourably with precision mass spectroscopy and nuclear reaction studies, at least in the light element region, provided due attention is paid to the corrections for the electronic structure. The various experimental techniques hitherto developed are briefly surveyed with an emphasize on the ultimate resolution and accuracy of each. Finally, the experimental results are summarized and compared with mass spectroscopy and nuclear reaction measurements.

F. M. Kelly has written an excellent chapter on the Determination of Nuclear Spins and Magnetic Moments by Spectroscopic Methods. It is divided into three sections: Atomic Spectra, Atomic Beams and Molecular Spectra. A simple derivation of the interval factor in hyperfine structure is given and the more exact treatment by Fermi and Segré is briefly reviewed. The various optical methods used to determine nuclear spins and magnetic methods are surveyed and the recently discovered disagreement between spectroscopic and nuclear spin resonance values of the magnetic moments is discussed. A rather short description of the atomic beam methods is given. This includes the new modification where six-pole focusing magnets are used. The latter has been found to be particularly useful for the study of radioactive isotopes. Nuclear spins and statistics as determined from molecular spectra are considered in the last section.

Isotope Shifts by L. Wilets starts with a consideration of nuclear mass effects on atomic hyperfine structure. The following section deals with field effects for spherical, incompressible nuclei. The various experimental methods available for the study of nuclear charge distributions are briefly discribed. Nuclear deformation effects are discussed in the third section. Due reference is given to nuclear spectroscopic methods for the determination of deformation parameters. Finally, nuclear compressibility and surface phenomena and the calculation of the electron density of the nucleus are considered. The last section contains a comparison with experimental results. Attention is called to the interesting even-odd staggering problem and a number of possible explanations are mentioned. Wilet's paper is an excellent survey of the subject with an emphasize on the nuclear structure part of the problem.

The chapter on Kernmagnetische Hochfrequenz-Spektroskopie by G. Lankien is in fact a complete monograph on the subject. Its 256 pages occupies more than one half of the present volume of the Encyclopedia. It is divided into three parts. The first deals with the physical fundaments, the second is devoted to the experimental techniques and the third contains an account of experimental results. In the last section the author has given an interesting review of precision absolute measurements and a discussion of the various fundamental constants that have been determined with this technique. Precision relative measurements are discussed in detail with reference to their use in molecular and solid state physics. Finally, there is a complete summary of all publications (up to January 31, 1957) on nuclear magnetic moments. This includes the known magnetic octopole moments as well as magnetic moments of excited states. This summary contains more than 1000 references. Lankien's contribution in this volume is the most complete review on this subject at present available. It will certainly remain a most valuable reference work for a long time.

Professor C. H. Townes has written the last chapter in the volume. This deals with the Determination of Nuclear Quadrupole Moments. The author has given an excellent survey of optical, radiofrequency and microwave spectroscopic methods as well as nuclear spectroscopic techniques. In the first section the atomic and molecular methods ar discussed with an emphasize on the theory of the nuclear quadrupole interaction in atomic and molecular systems. The theoretical significance of high resolution measurements is dramatically illustrated in one of the figures. The validity of the shielding and anti-shielding correction factors is considered. The second section contains a discussion of the concept "intrinsic quadrupole moment" and its relation to the "spectroscopic" quadrupole moment. The nuclear spectroscopic methods for the determination of quadrupole moments are surveyed. These include electric quadrupole transition probabilities, Coulomb excitation, scattering of high energy electrons and the study of the giant resonances. The third section deals with mesonic quadrupole effects. Finally, in the last section there is a complication of experimentally determined quadrupole moments with references to the original publications and a brief discussion of the systematics of nuclear quadrupole moments.

TOR RAGNAR GERHOLM

Review of IRE-PGNS Transactions, December 1958 Proceedings of the Sixth Scintillation Counter Symposium

Over the past ten years, physicists have gathered together biennially to discuss the developments in the uses of scintillation counters. These symposia have been extremely useful since they have served to spread the latest information on the details of the use and understanding of the scintillation counter during that period, especially, when it was developing most rapidly. The sixth such symposium was held in Washington on January 27–28, 1958, and the proceedings, which heretofore had been published, generally, only in part, have been included in a single issue of the IRE Professional Group on Nuclear Science (December 1958).

The meeting was divided into several sections. The first dealt with the scintillator itself. Papers on Čerenkov counters and noble element scintillators as well as glass, plastic and inorganic scintillators were presented. Although it is clear, that the processes involved in the light output of the inorganics are still incompletely understood (Van Scivêr and Bogart), nevertheless, new scintillators are being developed. The glass phosphors (Ginther and Schuman) and metal loaded plastics (Hyman and Ryan) clearly will have application in particular situations. The development of the noble gas scintillator has also taken great strides, particularly, in the improvement of techniques which permit their operation, stably, over long time intervals (Northrup, Gunsky and Johnsrud). An interesting paper given by Swank *et al.*, unfortunately, presented in a later session, showed the effect on rise time of various solute concentrations in liquid and plastic scintillators and their interpretation in terms of the fundamental processes in the scintillator. In particular, the pulse decays of plastics for low energy electron excitation is not exponential, implying lack of mixing of the exitation over large regions of the phosphor, as is found in liquids. Owen also reported on the decay of pulses in organics showing differences in several phosphors for different specific ionizations. He felt that this property could be used to differentiate between light and heavy radiation—in particular, gamma rays and neutrons.

The second section grouped papers on the development of photomultiplier tubes. Representatives of the two largest United States firms making these tubes reported on the current status of their photomultipliers. The beautiful work involved in the development of tubes which permit transmit time spreads of the order of 10^{-11} sec and rise times of $\approx 2 \times 10^{-11}$ sec at RCA were described (Morton, Matheson and Greenblatt) and seems to open for study a new range in time. A serious limit to precise quantitative work with scintillation spectrometers was pointed out in that the gain of photomultipliers seem to vary with time as well as with counting rate and temperature (Cathey). Of special interest was the development of a "fast" five-inch tube by RCA (Widmaier) and the interest exhibited by Dumont (Schenkel) in a low background level tube. Also interesting was the high current photomultiplier developed at Los Alamos (Glass and Rudnick) which clearly will find special application.

The third section was devoted, primarily, to the analysis and interpretation of scintillation spectrometer data. The unfolding procedure used for high energy X-ray continua was discussed by Koch and Wyckoff. For this work, the pulse height shapes were taken, primarily, from measured gamma rays in the correct energy range. The unfolding problem was reduced to a matrix inversion which could be carried out as a machine problem. The problem of unfolding was discussed by Lazar for low gamma ray energies (up to 10 MeV). The many difficulties involved in machine calculations and the desire for immediate results, led him to empirical determination of the pulse height shapes and point by point subtractions in the analysis of the data. An attempt at analytic unfolding of data was presented by Hubbell and Scofield, but only for a continuous distribution.

An interesting application of the scintillation spectrometer would be in the hundred MeV range. Knudsen and Hofstadter showed the response of a large NaI(Tl) crystal for electrons in this energy range, and pointed out the major problem is absorbing all the energy in the shower associated with such high energy electrons in order to get a meaningful peak.

The interpretation of the pulse height spectrum from Li^6 I(Eu) for neutrons was discussed by Murray and of particular interest was the improvement in "resolution" obtained by decreasing the operating temperature of the crystal.

Another section of the meeting was devoted to specific applications of the scintillation counter. Described were the first parity conservation experiment (Hayward and Hoppes), reactor applications (Managan), the several classes of experiments which may be carried out with liquid scintillators (Hayes) and the construction of a Čerenkov counter with a differential velocity response (Baldwin *et al.*). The problem of stability of spectrometers in well logging was discussed by Nelligan and Titheran and the low level problem of in vivo counting of gamma rays in humans was described by Anderson and Van Dilla. A particularly interesting device was the chronotron developed by Lefevre and Russell. Time resolution of 10^{-9} sec and a delay curve slope of 1×10^{-10} was shown for Co^{60}. Application to time of flight measurements for neutrons were given. Graveson and Sadowski discussed transistorizing linear amplifiers.

An extra evening session was devoted to developments of scintillation spectrometry in Europe. Reports from England on EMI tubes (Sharpe) and 20th Century tubes (Jennings), France (Labeyrie) and Switzerland (Maeder) clearly indicate the tremendous studies in these countries. Maeder, particularly, indicated the interesting approach to multichannel recording based on computer techniques carried out at ETH in Zurich.

The meeting clearly offered information in a wide variety of fields associated with and pertaining to scintillation counters. From the heavy attendance at the meeting (nearly 400 registrants) it is clear there is still considerable interest in such meetings. The PGNS must be accorded a vote of thanks for gathering the 33 papers and publishing them in one issue. It is only unfortunate that the large number of papers and people involved results in the long delay between the meeting and the publication. However, this is a problem which is universal in reports of this type.

N. H. LAZAR

Encyclopedia of Physics (Editor S. Flügge). Volume XLII, Nuclear Reactions III, Springer Verlag, DM 135.—.

This volume of the Encyclopedia deals mainly with the decay of energetically unstable nuclei i.e. gamma-ray emission, internal conversion and alpha-, but not beta-, decay. There are six different contributions.

D. E. Alburger (*Nuclear Isomerism*) correctly points out that "the measurement criterion for labeling a state as isomeric depends on whether or not we have the experimental techniques at our disposal for determining its lifetime". Consequently the author has adopted the definition of "isomeric" as denoting a state (except for the ground state) whose life time has been measured. Following a brief review of the historical development a survey is presented of the various methods at present available for the determination of the multipolarity and character of nuclear transitions. The following section gives an excellent summary of the experimental techniques. This includes delayed coincidence measurements, coulomb excitation, doppler shift and broadening methods as well as nuclear resonance fluorescence. Finally an extensive compliation of experimental data is presented which includes nearly 100 decay schemes and a tabulation of about 200 isomeric states.

Alpha radioactivity has been treated by I. Perlman and J. O. Rasmussen. The first section deals with alpha-disintegration energies. A table is given which contains experimental data on alpha ray spectra of the heavy elements. This table is based to a great extent on the outstanding work made in Berkeley by Professor Perlman and his co-workers. The following two sections are devoted to the kinetics of alpha decay in even-even and in odd nuclei. The one-body model decay rate theory for purely central fields is developed. Due to work by Rasmussen and others the theory has recently been extended also by taking into consideration the non-central electromagnetic field of the daughter nucleus. The problem is treated in a most interesting section and illustrative numerical examples are given for E 1 and E 2 interactions. Finally the various proposed many-body modifications of alpha decay theory are briefly surveyed. The last section contains several examples of decay schemes with due references to theoretical interpretations. The paper by Perlman and Rasmussen in the present volume of the Encyclopedia offers the most complete survey on alpha-radioactivity at present available. It is an excellent introduction to this field and will certainly for a long time remain a most valuable reference work.

The *Transuranium Elements* have been discussed by E. K. Hyde and G. T. Seaborg. After a brief discussion of the historical background the authors put forward the chemical and physical arguments for placing the elements from 83 actinium to the not yet discovered element 103, right below the lanthanides in the Periodic Table. In the following sections the individual transuranic elements are discussed. For each element there is a short historic review, a summary of known isotopes including physical data and known decay schemes and a survey of the chemical properties. The last section contains nuclear thermodynamics for the transuranium elements, alpha-decay systematics, neutron cross-sections and spontaneous fission properties. The authors have given an excellent account of the achievements obtained in the transuranium field. It is not necessary to add that this remarkable work is almost entirely due to Professor Seaborg and his co-workers at the University of California Radiation Laboratory.

The *Nuclear Photoeffect* has been reviewed by G. R. Bishop and R. Wilson. The authors first discuss the sources of gamma-rays and X-rays. In the following sections are treated theory and experiments on the photo disintegration of the deuteron and nuclear photo effect in nuclei heavier than deuterium. Special attention is given to the theories of giant resonance and in this connection compound nucleus formation versus direct interaction is discussed. Special sections are devoted to isotopic spin selection rules and to high energy photoprocesses. The last three sections deal with some special problems: the beryllium photo disintegration, elastic scattering of photons and photofission.

Angular Correlations are treated in an extensive paper by S. Devons and J. B. Goldfarb. This paper covers a wide variety of subjects which from both experimental and theoretical points of view have little in common except for the mathematical technique used for the analysis and interpretation of the experimental results. Consequently the main emphasize in this chapter is on these mathematical methods. Illustrative examples from experimental work are discussed but the reader is referred to the original publications for technical details. The authors start with some mathematical preliminaries: Clebsch-Gordon and Racah coefficients, the 9-*j* symbol as well as rotation and density matrices. In the following sections is given the general theory of directional correlation for processes involving states of well-defined symmetry. The formalism thus outlined is then applied to some particular processes like gamma-gamma and alpha gamma directional correlation, resonance reactions and directional correlations with polarized radiations. The following sections is devoted to states of not well defined symmetry. A brief chapter deals with electron-gamma angular correlations and a survey of extra-nuclei effects is also given. Finally there are some remarks concerning the applications of the angular correlation formalism to mesons, heavy mesons and hyperons. The chapter on angular correlations involving beta-decay was written before the discovery of the violation of parity conservation. In a note the authors point out that for this reason many of the statements made in this chapter need revision. With this exception, however, Devon's and Goldfarb's contribution is up to date and it presents an excellent survey of the many potentialities and applications of this powerful formalism.

The last contribution in this volume, *Oriented Nuclei*, is written by R. J. Blin-Stoyle and M. A. Grace. The two concepts polarization and alignment are first defined and a survey is given of the various methods, now available for nuclear orientation. This includes very low temperature techniques as well as optical and microwave methods. Experimental results obtained with oriented nuclei are discussed in the following section. Unfortunately the paper was written before the famous parity experiment by Dr. Wu and her co-workers. For this reason this experiment is not described in this contribution but reference to Wu's paper is given in a foot-note. Dr. Wu's experiment is certainly so far the most important application of nuclear orientation.

It is well-known that the experimental method used by Dr. Wu and her co-workers to achieve nuclear orientation was based on the pioneer work done by the groups at Oxford and Leiden. The last chapter deals with polarized nuclear reactions.

TOR RAGNAR GERHOLM

Nuclear Reactions, Editors P. M. ENDT and M. DEMEUR, Vol. I, North Holland Publish. Co., Amsterdam. Guilders 43.

This book originates from the 1956 Amsterdam Conference on Nuclear Reactions. The concept nuclear reactions is defined here as the interaction between a target nucleus and a bombarding particle or a photon. This excludes radioactive decay but a couple of nuclear decay schemes can be found nevertheless in the book and at least the contributions by A. K. Kerman (Nuclear Rotational Motion), J. P. Elliott (The Shell Model) and L. J. B. Gottfarb (Angular Correlations and Polarization) deal with problems closely related to phenomena of radioactive decay. The last two chapters duplicate to a certain extent similar contributions by the same authors recently published in the Encyclopedia of Physics.

In addition the editors have followed the police to limit the subject to the "low energy" field i.e. to bombarding energies below the threshold for strange particle production. The volume does not entirely cover the region thus defined but the editors hold out the prospect of a eecond volume.

R. J. Eden's chapter (Theory of the nucleus as a many-body system) serves as a theoretical introduction. The statistical model is considered in some detail by J. Le Couteur. J. H. Fremlin has given an interesting survey of Heavy ion reactions, and resonance reactions are considered in two chapters by E. Vogt (theoretical) and H. E. Gove (experimental). Finally, there are two chapters on neutron resonances in heavy nuclei (by D. J. Hughes and R. L. Zimmerman) and a survey of scattering and reaction experiments with medium energy nucleons and alpha-particles (by P. C. Gugelot).

The names of the contributors are among the most outstanding experts and therefore serve as garance for the highest standard. It should be added that the book is not meant for the beginning student but is directed primarily to research workers. The latter will certainly find the book as a survey and reference volume.

TOR RAGNAR GERHOLM

Internal Conversion Coefficients by M. E. ROSE, North Holland Publishing Company, Guilders 20,—

and

Nuclear Spectroscopy Tables by G. J. NIJGH, A. H. WAPSTRA and R. VAN LIESHOUT, North Holland Publishing Company, Guilders 30,—.

These two volumes contain a set of tables which are almost indispensable for the nuclear spectroscopist. Most of the material has been published elsewhere but since it has been spread out in review articles and reports it has not been readily accessible. A separate publication in two handy volumes is therefore well justified.

Dr. M. E. Rose's tables contain the theoretical K, L_I, L_{II} and L_{III} conversion coefficients with three figures for all Z between 25 and 95 and for α_1 to α_5 and β_1 to β_5 and for energy values between $k = 0.05$ and 2.0. In addition M-shell coefficients are given for $Z = 25$–65 and M subshells in the region $Z = 65$–95. In both cases the same multipolarities and energies are given as for the K and L shells. Finally the radial matrix elements are tabulated (for the K-shell). These may be used to correct for nuclear structure effects.

The Nuclear Spectroscopy Tables by Nijgh, Wapstra, and Van Lieshout are divided into 10 chapters, namely mathematical data, atomic constants, heavy particles, electrons, gamma rays, X-rays and Auger electrons, angular distributions and correlations, nuclear models and calibration standards. Each chapter is preceded by a short introduction which contains information concerning the use of the tables, interpolation procedures and estimates of the accuracy as well as references to more extensive tabulations when existing. Whenever the editors have considered it necessary, they have recalculated the original tables taking more recent data into account. It is felt that the editors have been able to make a successful compromise in the difficult choice between completeness and compactness. The present compilation of tables will be useful in all laboratories where work in nuclear spectroscopy is going on.

TOR RAGNAR GERHOLM

Proceedings of the Second United Nations International Conference on the Peaceful Uses of Atomic Energy. Vol. 31: Theoretical and Experimental Aspects of Controlled Nuclear Fusion (United Nations, Geneva 1958) (vii + 390 p.) $ 15.

This volume contains all the theoretical and some of the experimental papers presented at the fusion sessions of the conference; the main part of the experimental papers forming vol. 32. Vol. 31 also includes the general survey lectures on the subject of controlled fusion given by the leading scientists in the field at session 4. Since a vast amount of earlier classified work in this field was released at the conference, vol. 31 gives an unusually comprehensive and detailed treatment of the theoretical problems in controlled fusion research. Including vol. 32 the above statement is of course valid for the fusion field as a whole. Most likely, these volumes will form a classical source of reference.

It is an inevitable and unfortunate consequence of the previous classification that sometimes the same investigations have been carried out in parallel in different countries

and thus the same results may be given in different papers. This not being the place, however, to discuss the value of the original work presented in this volume, the following remarks will mainly concern the editorial work.

The papers are printed in an order determined by the session at which they were presented, i.e. by their subject from a very general point of view. Accordingly, papers originating from the same project, e.g. the Stellerator, may be found in several different places in the volumes 31 and 32. In at least one such case mutual references between theoretical and experimental work on the same subject are even missing. The total number of the fusion papers presented at the conference is not discouraging but—at least to the reader earlier unfamiliar with this field—some kind of author and subject index would have been valuable for each volume or for the two volumes 31 and 32 together. All readers will probably not have access to the index of the complete proceedings in vol. 33. Abstracts are unfortunately also missing. A small random test revealed a minor systematic negligence in the checking of the reference lists, as the titles of some papers have been modified since the conference and these alterations have not always been remembered when these papers are referred to.

The imperfections mentioned here are of course comparatively trifling. Some of them are presumably the result of intentional compromises in order to get the enormous material from the 1958 Geneva conference edited and printed in a few months. Thus, as a whole, the editorial staff of the conference must be complimented for outstanding work also in this volume. Finally it should be pointed out that the typographical layout is excellent.

LARS HÖGBERG

DANIEL BLANC: *Détecteur de Particules*, Masson et Cie., Paris, 1959. 324 pages, 17 × 25 cm. Prix 3.900 fr.

Ce livre a été écrit d'après un cours professé au Centre de troisième cycle de Physique nucléaire de la Faculté des Sciences de Toulouse et s'adresse à des lecteurs possédant des connaissances correspondant au grade de Licencié ès Sciences. Il donne une revue très complète du mécanisme, des propriétés et de la construction des compteurs qui fournissent un signal électrique ou lumineux en réponse au passage de la particule chargée, mais ne traite pas l'ensemble des détecteurs qui mettent en évidence les trajectoires des particules, comme les émulsions nucléaires et les chambres à bulles. La présentation générale est purement systématique et l'abondance de tables, diagrammes et références en font un ouvrage de valeur pour ceux qui cherchent quelque information détaillée sur ce sujet. D'autre part, du fait de la multitude de détails et de l'inclusion dans le sujet, de toutes les sortes imaginables de compteurs, dont certains sont tout à fait passés de mode, l'usage de ce livre peut difficilement être recommandé dans un cours de physique nucléaire.

Après une introduction élémentaire, l'auteur consacre un châpitre aux chambres d'ionisation, un second aux compteurs proportionnels et quatre châpitres aux différents types de compteurs Geiger, dont entre autres, l'important compteur autocoupeur à vapeur d'halogène. Les compteurs à étincelles et les détecteurs de neutrons sont traités chacun dans un châpitre, de même que l'intéressant détecteur à conduction électrique. Un exposé des photomultiplicateurs sert d'introduction aux compteurs de Čérenkov et aux compteurs à scintillation. Les deux derniers châpitres décrivent la réalisation technique des compteurs et leurs effets de température. Il y a certaines fautes d'impression dans le texte (par exemple: le titre des figures 11 et 97), mais les données semblent être présentées très soigneusement et le livre sera probablement utilisé souvent comme ouvrage de référence. De ce fait, il est dommage qu'il n'ait pas été relié d'une facon plus durable.

GUNNAR BÄCKSTRÖM

G. N. WALTON: *Glove Boxes and Shielded Cells* (Butterworths Scientific-Publications, London, 1958, 473 pages. 95s) (Academic Press Inc., New York, 1958, $ 16.80).

This collection of papers as presented at the Symposium on Glove Box Design and Operation, Cockroft Hall, A.E.R.E., Harwell, during the period February 19th to 21st, 1957, will form an invaluable work of reference to anyone connected with the handling of radio-active materials. The editor is to be complimented on his presentation of the subject matter which deals with the protection against, and the handling of alpha, beta and gamma activities. Using this book as a guide, no difficulty should be experienced in the selection of equipment most suitable for ones own needs. At the end of each chapter (of which there are twenty) a list of references is given. The book concludes with a comprehensive subject index, and a further list, of companies marketing accessories etc. W. PARKER

Spotlight on Industry

This section appears each month and features various happenings of interest in the nuclear industrial world and objective information on products of the nuclear manufacturers. It is offered entirely as a service and all nuclear manufacturers are cordially invited to submit clearly objective and descriptive material on their endeavours and product developments for consideration for use in this section.

PRECISION REFERENCE VOLTAGE SOURCE FEATURES LONG TERM STABILITY TO VOLTAGE OR TEMPERATURE VARIATIONS

Gyra Electronics Corporation, 518 North Spring Avenue, La Grange Park, Illinois, U.S.A.

A significant addition to the test instrumentation available for complex circuit design has been announced.

Especially useful in the design of amplifiers, the new Gyra Reference Voltage Source, Models RVS-100 and RVS-100c provide precision regulation, continuously variable from 0 to 600 in steps of 0.0001 volt. Units are used in conjunction with the Gyra Electrometer VTVM to null current.

Stability to both temperature and line voltage variations makes the units ideally suited to precision voltage reference in non-airconditioned laboratory or productions, for mobile or portable test sets and for field testing.

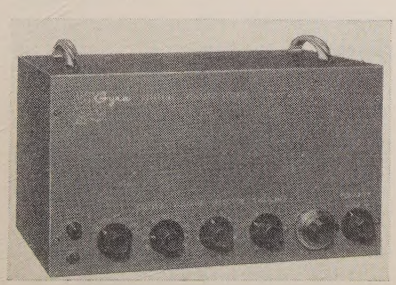

The units offer several features previously unavailable for both military and commercial test installations:

1. Fluctuations in line voltage do not affect the instrument more than 1 part in 10°.

2. Temperature fluctuations of 10° F have minimum effect on stabilty.

Exceptional long-term drift stability provided by RVS-100 allows regulation of 90–135 V, 60 cps, single phase to within $\pm$ 1 part in 10 000 per day.

Model RVS-100c incorporates a temperature regulating circuit to provide drift stability of $\pm$ 3 parts in 10^5 per day under laboratory conditions. Line voltage fluctuation is less than 2 parts in 10^6 between 90–135 V.

Simplicity of operation is suited to use by inexperienced technicians. Voltages are set by four output switches controlling 100, 10, 1 and 0.1 volts. A fine adjustment controls settings in hundreds of microvolts. Clearly marked switches provide maximum visibility.

60 W input are required for either unit.

Both models are available for rack or cabinet mounting according to the following specifications:

	Rack Mounted	Cabinet Mounted
Width	19″	$15\frac{1}{2}$
Height	$8\frac{3}{4}$″	$10\frac{1}{4}$″
Depth	10″	10″
Weight	21 pounds	

TRANSISTORIZED SWITCH

Ad. Auriema, Inc., 85 Broad Street, New York 4, N.Y.

New EECO (Engineered Electronics Co.) T-Series plug-in circuits T-120, T-121, T-122, and T-128 are transistorized plug-in circuits that will switch a 400 mA load with as little as 50 μA input current. They are normally operated directly from EECO T-Series germanium plug-in digital circuits (flip-flops, one shot, multivibrator, squaring circuit, etc.), which have standard signal levels of — 11 V for "0" and –3 V for "1". Case measures $\frac{7}{8}$″ diam. by $2\frac{3}{16}$″ seated height, weighs approximately 1 oz., and plugs into standard 9-pin miniature tube socket. Input signal frequency range 0–1 kc/s for 400 mA resistive load. In typical application (as a relay driver) circuit actuates relay at — 11 V nom.; releases at — 3 V nom. Range of operation for Model T-122 is from 400 mA max. at 6 V or less to 25 mA max. at 110 V max. Power curve for other models is identical, except T-128 has max. of 24 V, T-120 a max. of 48 V, and T-121 a max. of 84 V.

DECALCOMANIA ALPHA SCINTILLATOR

har'D'cal, Box 455, Williston, S.C., U.S.A.

ALPH-A-CAL, water-transfer ZnS(Ag) alpha scintillator permits application of uniform 15–17 mg/cm^2 of phosphor directly to phototubes, light pipes in less than two minutes.

In sheet form, ALPH-A-CAL is cut with scissors to the correct size and shape. Immersed in water for a few seconds, the scintillator may be transferred directly to the support surface and put into service immediately.

No equipment or special skills required for use of ALPH-A-CAL.

The deal is flexible, for application to inside or outside cylinders, cones, spherical surfaces, or may be used directly on the window of phototubes or on supporting light pipes.

Counting efficiency is 50% (2 pi), since the phosphor crystals are exposed and not encased in attenuating material.

Available in 12″ × 12″ sheets from stock, and up to 20″ × 30″ sheets on special order.

SIMPLIFIED SCINTILLATION TECHNIQUE FOR CARBON 14 AND TRITIUM COUNTING

Nuclear Enterprices (G.B.) Ltd., Banhead Medway, Sighthill, Edinburgh 11, Scotland

The NE 8301 System designed by Nuclear Enterprises (G.B.) Ltd. of Edinburgh affords an efficient and greatly simplified scintillation technique for the measurement of carbon 14 and tritium radioisotopes.

Among the outstanding features in the NE 8301 System are: the use of a 4″ diameter E.M.I. photomultiplier, doubly selected for lowest noise level; the new NE 5503 shielded scintillation head unit, incorporating a special rotary light locking device which permits operation of the assembly in daylight without exposure of the photomultiplier to light; silver silica counting cells; the NE 5202 Fairstein non-overloading linear pulse amplifier with high gain (5×10^4) allowing operation of the multiplier at a low voltage and improving signal to noise ratio; pulse height selector NE 5102 which optimises signal to background ratio for particular problems; and a stable source of E.H.T. the NE 5302 which has an overall stability of 0.01% per 24 hour period, and reset accuracy to 0.1 volt. Adequate temperature stabilisation is achieved by passing mains water through cooling coils round the photomultiplier tube and the use of NE 213 liquid scintillator, adjusted to produce a minimum quenching effect on the additions of samples, ensures efficient measurement of the isotopes.

Counting of two or more isotopes simultaneously can be effected with two pulse height selector units each to count a particular isotope in the most appropriate fashion, and successful routine analysis of such binary and ternary mixtures as H^3–C^{14}, H^3–Na^{22}, and H^3–C^{14}–P^{32} can be made. The NE 8301 assembly may also be applied to systems in which an insoluble sample is dispersed in a finely divided state throughout the scintillator and the Steinberg technique (Nature 182 (1958) 740 can also be used. In this technique small plastic phosphor spheres are employed as the scintillation medium, and the liquid to be investigated fills up the intervening spaces.

MODEL 201C ELECTROMETER AMPLIFIER

E-H Research Laboratories, Inc. 1922 Park Boulevard, Oakland 6, California

This device features extreme sensitivity, achieving current measurements below 3×10^{-15} amperes. It is a general purpose instrument for either AC or DC small current measurements. It combines ultra low flicker noise and excellent stability by virtue of a low grid current electrometer pentode input, single ended filamentary amplifier stages, and Zener stabilization. Fast response time is accomplished by the use of capacity neutralization, with compensation by front panel control feedback adjustment.

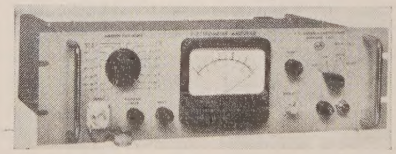

HOFMAN LIQUID HELIUM DEWAR

Hofman Laboratories, Inc. of Hillside, New Jersey

This Hofman liquid helium dewar and associated apparatus is used to observe the effect of a magnetic field on the electrical and thermal properties of semi-conductors metals and magnetic materials at low temperatures.

NEW INDOX VI PERMANENT CERAMIC MAGNETS FOR MICROWAVE EQUIPMENT

Ad. Auriema, Inc., 58 Broad Street, New York 4, N.Y.

Indox VI is the most recent permanent ceramic magnetic material developed in Indiana Steel's research laboratories.

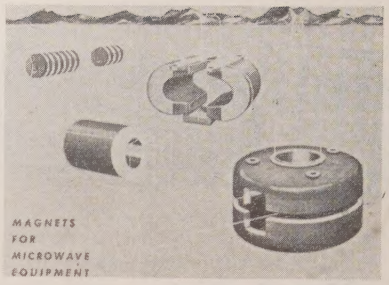

Indox VI, with an even higher coercive force than previously available Indox V, is designed for applications where greater resistance to demagnetizing fields is required, or where magnet length is limited as compared to its size. Besides, Indox VI is that is can be magnetized before assembly with results almost equal to magnetizations after assembly. Indox VI has a greater resistance to irreversible flux loss caused by exposure to low temperatures.

GELMAN AIR SAMPLING KIT

Gelman Instrument Company, Chelsea, Michigan

This instrument combines vacuum pump, flowmeter and weather proof housing and can be used to collect samples of dusts, radioactive aerosols and gases. For determining dusts in air, special filters and filter holders are available as accessories.

The Vacuum pump, used is a carbon ringed piston unit which never requires lubrication. A choice of 2 or 4 CFM air capacity is available. The flow indicating device is a tapered orifice plastic meter.